Studies on the reaction and catalyst deactivation mechanisms in the direct aromatization of methane

Submitted in partial fulfillment of the requirements for the degree of

Doctor of Philosophy

of the
Indian Institute of Technology Bombay, India
and
Monash University, Australia

by

Ponsubbiah Soundrapandian Nadar

Supervisors:

Professor Suresh K Akkihebbal (IIT Bombay)

Professor Debabrata Maiti (IIT Bombay)

Professor Alan L Chaffee (Monash University)

Dr. Sivakumar Sreeramagiri (SABIC Technical Center)

The course of study for this award was developed jointly by
Monash University, Australia and the Indian Institute of Technology Bombay, India
and was given academic recognition by each of them.
The program was administrated by the IITB-Monash Research Academy.

Year-2019

Table of Contents

Abstract

Methane direct aromatization is a non-oxidative route for converting natural gas to value-added aromatic compounds. This process can have monetary benefits and also help mitigate anthropogenic greenhouse gas emissions caused by flaring. The shortcoming with this reaction is associated with low methane conversion, poor methane activation, and rapid catalyst deactivation. These factors are major obstructions for the scaling-up and commercialization of the process. Mo/HZSM-5 catalyst has shown potential to be a catalyst for the reaction, but, insufficient detail is known about its active form for methane activation, the role of individual sites in coke formation and the impact of coking on these sites.

In this thesis, studies were conducted in a systematic way in an effort to identify the contributing roles of catalytic components in methane dimerization, aromatization, and coke formation, and also how the active components behave during the course of reaction upon treatment with nitrogen, methane, hydrogen, reaction products, coke, and oxygen. This work mainly utilized a packed bed reactor set-up coupled with spent catalysts characterization to generate information related to the physical and chemical nature of coke deposits and subsequent changes to the catalyst.

It was found that HZSM-5 (alone) catalyzed the conversion of ethylene to benzene, naphthalene, p-xylene, trimethylbenzene, methane, and coke. The coke formed has been found to increase with reaction time. The characterization tools used during the study were able to classify the amorphous and graphitic forms of coke. Most coke formed during the initial period of ethylene aromatization reaction was amorphous in nature, but this

progressively transformed with increasing reaction times to graphitic carbon in the presence of the HZSM-5 acid sites. This study suggested that ethylene is the progenitor of amorphous coke structure, but HZSM-5 acid sites are needed for the transformation process.

SiO_2 and HZSM-5 were compared as supports for molybdenum in MDA reaction. The study showed that molybdenum carbide and HZSM-5 are both needed for the catalyst to function. It was observed that the state of molybdenum transitioned from Mo-precursor → MoO_2 and MoO_3 → Mo_2C (partial) → Mo_2C (extensive) during calcination (510ºC in air), carburization and reaction, respectively, then oxidized to MoO_3 (at <600ºC in air) during regeneration. It was also found that high-temperature oxidation (600-800ºC) causes the molybdenum oxide to agglomerate and partially smear on the surface of HZSM-5, which could potentially decrease the catalyst performance upon reuse.

The investigation using methane as feed on Mo/HZSM-5 catalyst found that catalyst time-on-stream, methane feed rate, and reaction temperature all influenced both the conversion and coking reactions. At high temperatures and high methane feed rate, the coke formed was more graphitic and displayed high stability against oxidation. It is inferred that the nature of coke depends extensively on the conditions the catalyst was treated with and that therefore, the reaction conditions could be tailored to minimize the graphitic carbon build-up and design appropriate regeneration schemes. This suggests that there are advantages in conducting the reaction with 5% Mo/HZSM-5 at lower temperatures and lower methane feed rate, so as to facilitate easy regeneration.

To understand the structural dynamics of Mo/HZSM-5 catalyst during carburization, MDA reaction and regeneration, synchrotron powder X-ray diffraction analysis was

employed in conjunction with a flow reactor to monitor the structure of the catalyst and the resultant coke formed in-situ during the course of the reaction. It was observed that MoO_2 remained stable throughout, but that other states of molybdenum oxide (MoO_3 and $MoO_{2.5}$) transformed to carbides and back to oxide during the reaction and regeneration, respectively. The catalyst structure was observed to be largely unaffected by the build-up and removal of graphitic and amorphous coke during use and oxidation below 800ºC. However, it was found that the structure of molybdenum changes during high-temperature oxidation (>800ºC), which was consistent with ex-situ analysis. No dealumination of the ZSM-5 structure was found during the study, therefore, indicating that the Mo/HZSM-5 catalyst can be continuously used (recycled) if appropriately regenerated.

Overall, the work listed in this thesis adds to the existing body of scientific knowledge pertaining to MDA reaction in significant ways including elucidation of coke formation from ethylene and methane precursor, clarifying the role of HZSM-5 in methane activation and ethylene dimerization, understanding changes to the state of molybdenum in Mo/HZSM-5 during the course of reaction, and validating the structural stability of the HZSM-5 support during reaction and oxidation. This new knowledge takes the catalytic process a step closer to potential commercialization.

General Declaration

I hereby declare that this thesis contains no material which has been accepted for the award of any other degree or diploma at any university or equivalent institution and that, to the best of my knowledge and belief, this thesis contains no material previously published or written by another person, except where due reference is made in the text of the thesis.

This thesis includes no original papers published in peer-reviewed journals and four unpublished publications. The core theme of the thesis is reaction and coke formation pathway in methane aromatization reaction. The ideas, development and writing up of all the papers in the thesis were the principal responsibility of myself, the student, working within the School of Chemistry, Monash University; the Department of Chemical Engineering and Chemistry, Indian Institute of Technology Bombay, and SABIC Technical Centre under the supervision of Prof. Alan L Chaffee, Prof. Suresh A. K., Prof. D. Maiti., and Dr. S. Sivakumar. The inclusion of co-authors reflects the fact that the work came from active collaboration between researchers and acknowledges input into team-based research.

In the case of four chapters listed below, my contribution to the work involved the following:

Thesis Chapter	Publication Title	Publication status	Nature and % of student contribution	Co-author name(s), nature and % contribution	Co-author(s) Monash Student Y/N
2	Direct Aromatization of Methane: Understanding the pathways of coke formation and evolution with ethylene precursor on HZSM-5 catalyst	Submitted to I&ECR	60% Conceptualization, prepared and analyzed samples, collected data, and drafting paper.	1. Gregory Knowles: **input into manuscript 3%**, assisted in characterization, and data interpretation. 2. Timothy Williams: **input into manuscript <2%**, assisted in characterization, and data interpretation. 3. Xiya-Fang: **input into manuscript <2%**, assisted in characterization, and data interpretation. 4. Thomas Gengenbach: **input into manuscript <3%**, assisted in characterization, and data interpretation. 5. Sivakumar S: **input into manuscript 5%**, assisted in conceptualizing, supervising, manuscript reviewing, and data interpretation. 6. D Maiti: **input into manuscript 5%,** supervision	No

				7. A K Suresh: **input into manuscript 10%**, assisted in conceptualizing, supervising, data interpretation, manuscript reviewing and manuscript editing. 8. Alan Chaffee: **input into manuscript 10%**, assisted in conceptualizing, supervising, data interpretation, manuscript reviewing and manuscript editing.	
3	Changes in the catalyst state and morphology during different stages of MDA reaction	Drafted	60% Conceptualization, prepared and analyzed samples, collected data, and drafting paper.	1. Timothy Williams: **input into manuscript 3%**, assisted in characterization, and data interpretation. 2. Xiya-Fang: **input into manuscript 2%**, assisted in characterization, and data interpretation. 3. Thomas Gengenbach: **input into manuscript 3%**, assisted in characterization, and data interpretation. 4. Sivakumar S: **input into manuscript 7%**, assisted in conceptualizing, supervising, manuscript	No

				reviewing, and data interpretation. 5. <u>D Maiti:</u> **input into manuscript 5%,** supervision 6. <u>A K Suresh:</u> **input into manuscript 10%**, assisted in conceptualizing, supervising, data interpretation, manuscript reviewing and manuscript editing. 7. <u>Alan Chaffee:</u> **input into manuscript 10%**, assisted in conceptualizing, supervising, data interpretation, manuscript reviewing and manuscript editing.	
4	Coke formation mechanism and its effect on the direct aromatization reaction on 5% Mo/HZSM-5 catalyst	Drafted	60% Conceptualization, prepared and analyzed samples, collected data, and drafting paper.	1. <u>Thomas Gengenbach:</u> **input into manuscript 5%**, assisted in characterization, and data interpretation. 2. Sivakumar S: **input into manuscript 10%**, assisted in conceptualizing, supervising, manuscript reviewing, and data interpretation. 3. <u>D Maiti:</u> **input into manuscript 5%,** supervision	No

				4. A K Suresh: **input into manuscript 10%**, assisted in conceptualizing, supervising, data interpretation, manuscript reviewing and manuscript editing. 5. Alan Chaffee: **input into manuscript 10%**, assisted in conceptualizing, supervising, data interpretation manuscript reviewing and manuscript editing.	
5	Direct aromatization of methane: understanding structural changes to Mo/ HZSM5 catalyst during in-situ reaction and regeneration by synchrotron powder X-ray diffraction	Drafted	70% Conceptualization, prepared and analyzed samples, collected data, and drafting paper.	1. Sivakumar S: **input into manuscript 5%**, assisted in conceptualizing, supervising, manuscript reviewing, and data interpretation. 2. D Maiti: **input into manuscript 5%,** supervision 3. A K Suresh: **input into manuscript 10%**, assisted in conceptualizing, supervising, data interpretation manuscript reviewing and manuscript editing.	No

				4. Alan Chaffee: **input into manuscript 10%**, assisted in conceptualizing, supervising, data interpretation manuscript reviewing and manuscript editing.	

I have renumbered sections of submitted papers in order to be consistent with the thesis.

Student signature: **Date: 18.02.2020**

The undersigned hereby certify that the above declaration correctly reflects the nature and extent of the student's contributions to this work. In instances where I am not the responsible author, I have consulted with the responsible author to agree on the respective contributions of the authors.

Supervisor (IIT B): **Date:**18.02.2020

Supervisor (Monash University): **Date:** 18.02.2020

I wish to dedicate this thesis to my parents (Mr. Soundrapandian Nadar & Mrs. Ponnammal Nadar), my parents-in-laws (Mr. Subash Chandra Roy and Mrs. Uma Roy), and my wife (Mrs. Supti Roy); as their support has motivated me to undertake such a high level of study. Thank you all.

Acknowledgment

I would like to express my sincere thanks and indebtedness to my supervisors Prof. Akkihebbal K Suresh, Prof. Alan L Chaffee, Prof. Debabrata Maiti and Dr. Sivakumar Sreeramagiri for their invaluable guidance, suggestions, and support throughout the research work. I would like to thank them for inspiring me by appreciating my work, which boosted my confidence in exploring new ideas.

I wish to thank my research committee members, Prof. Sanjay Mahajani and Prof. Alison for their valuable inputs and reviews of my progress, which opened several critical opportunities that form the part of the thesis.

I express my gratitude to the IITB-Monash research academy for giving me an opportunity to work in the joint research program, which broadened my view as a researcher. I would like to thank Prof. Murali Sastry, Dr. K. S. Nagabhushana, Mrs. Nancy Sowho, Mrs. Jayasree T, Mrs. Laya Vijayan, Mrs. Kuheli Banerjee, Mrs. Beena Pillai, Mr. Kiran More, Mrs. Sheeba Sanjay, Mr. Krishna Warrier, Mr. Rahul Ingle, Mr. Bharat Ingle, Mrs. Chhaya Sonawane, and many other staff at the IITB-Monash Research Academy for their continuous support and encouragement. I would like to appreciate their assistance in all administrative related matters which smoothened the collaboration work.

I wish to thank Prof. Stuart Batten (MU), Prof. Indradev Samajdar (IIT B), Prof. Abhijit Chatterjee (IIT B), and Prof. Ateeque Malani (IIT B) for their expert opinion during the research work.

I would like to thank the School of Chemistry, Monash University, Australia and Chemical engineering department, IIT Bombay, India for providing infrastructure and laboratory facilities. I would like to acknowledge the Sophisticated Analytical Instrument Facility (SAIF), IIT Bombay and Monash Center for Electron Microscopy (MCEM) for providing access to their facility for sample characterization.

I would like to acknowledge SABIC Technical Center, Bengaluru, India for funding the study and providing access to infrastructure for reactor study and preliminary characterization.

A part of the characterization was conducted at the Australian Synchrotron PXRD beamline, I thank the facility and their staff - Dr. Qinfen Gu, Dr. Anita D'Angelo and Dr. Helen Brand for their assistance.

I acknowledge the use of facilities within the Monash Centre for Electron Microscopy, I also appreciate the assistance of Dr. Nicholas Mcdougall and Dr. Peter Miller on SEM and TEM analysis. I thank Dr. Timothy Williams and Dr. Xiya-Fang for performing SEM, EDX, and TEM analysis, its interpretation and revision of the manuscript.

I would like to acknowledge CSIRO, Manufacturing for their infrastructure. I thank Dr. Thomas Gengenbach for assistance with XPS analysis. His contribution was helpful to draw several insights into the study.

I wish to thank Dr. Gregory Knowles, Dr. Christian Vogt, Dr. Emma Qi, Dr. Marc Marshall, Mr. Romesh Wijesiri, Mrs. Dalal Alqarni, and other members of the Chaffee group at Monash University. I also like to express my thanks to Dr. Raghavendra Ragipani, Dr.

Oayes Midda, Dr. Surendra Sasikumar, Dr. Aashish Unarkar, Dr. Ratnesh Khanolkar, Dr. Karthik Manda, Dr. Ashutosh Namdeo, Mr. Abu Mohammad Khan, Mr. Jainesh Jhaveri, Mr. Nagnath Salunkhe, Mrs. Minakshee Phutke, Dr. Rucha Paranjape, Mrs. Tejaswi Ramprasad, Mrs. Ruchika Gupta, Mrs. Preeti Jha, Mrs. Shweta Negi and other members of AK Suresh Lab group at IIT Bombay.

I acknowledge the support from Dr. Vinita Dubey, Mr. Amit Kumar, Mr. Ziyad KV, Mr. Dr. Satish Angadi, Dr. Byron Rajarethnam, Dr. Suman Kumar Jha, Dr. Sreenivasa Rao, Mr. Eswara Rao, Dr. Sharan Kumar Shetty, Mr. Ganeshan and Dr. Rajeshwer Dongara and other staff at SABIC Technical Center.

I thank my friends from IIT Bombay and Monash University for supporting me through the ups and downs of my research and personal life. My joining batch, December 2014, I would like to mention a special thanks to you.

As a special mention, I would like to thank Miss Farzana Sk for being a wonderful friend, who kept motivating me. I express my thank to Mr. Sanachit Mehra, Miss Radhika Sreedevi, Mr. Jitendra Franciss Sadangi, and Mrs. Tejashree Gaidhani for supporting and mentoring me. I would also like to thank Dr. Venkatesh Radha, Mr. Neeraj Hanumante and Miss Preeti Gopal for assisting me during writing.

Lastly, I would like to express my deepest gratitude to my wife Mrs. Supti Roy for being a lovely friend and caring partner. A special thanks to her parent Mr. Subash Chandra Roy and Mrs. Uma Roy who kept believing in me at all times. I thank my parents Mr. Soundrapandian Subbiah Nadar and Mrs. Ponnammal Soundrapandian Nadar for gifting me this life, acknowledging my skills and shaping me to the respectable person I am today.

List of Figures

List of Tables

Chapter 1 Introduction

An alarming amount of natural gas (140-150 billion cubic meters) is flared every year causing a loss of potential hydrocarbon resources and increasing about 300-350 million tons of CO_2 in the earth's atmosphere [1]. Moreover, as the transportation of natural gas via pipelines is costly [2], other commercially viable options are been investigated over the last few decades for utilizing natural gas. An alternative and monetarily beneficial approach would be to use natural gas as a chemical feedstock for producing valuable aromatic compounds [3]. The methane direct aromatization (MDA) or methane to benzene (MTB) reaction (terms used interchangeably in the thesis) has therefore attracted a lot of interest over the years, but challenges remain in activating methane and minimize coke formation.

1.1 Literature review

This section provides an overview of previous work carried out related to the MDA reaction and its potential scope for development. The natural gas production, consumption, and flaring data are compared to draw a context for the challenge in the research, i.e. the need to mitigate flaring and identifying potential chemical transformation routes for natural gas utilization. The prospects of different chemical technologies for converting natural gas have been reviewed and compared to suggest interesting possibilities with MDA. A comprehensive review of the MDA process is presented which includes discussions covering thermodynamic considerations, known catalysts, the active form of catalysts, the carburization and induction periods, reaction considerations, and coke formation. Lastly, a summary of knowledge gaps in the literature is presented.

1.1.1 Natural gas status: production, usage, and flaring

Natural gas or fossil gas is a naturally occurring mixture of hydrocarbon gases rich in methane (80-85%). It is believed that the gas which is currently being consumed is a result of decomposition of plant and animal matter which has been occurring over millions of years under intense heat and pressure beneath the surface of Earth. As it is derived from fossils it is classified as a non-renewable source of energy.

As per data reported in BP statistical reviews (63-68th editions [4–8]), global energy consumption is increasing at a rate of 1.8-2% annually. Average per capita energy consumption between July 2018- June 2019 was about 76 gigajoules and was dominated by China, USA, and India [8]. A major share of this energy demand was met by oil, coal, and natural gas. The amount of natural gas produced between July 2017- June 2018 was around 3310 million tons of oil equivalent which contributed to about 40% consumption by fuel. Further, natural gas production has increased by almost 5%, reaching to about 3950 Billion cubic meters within July 2017- June 2018. This underlines the importance of natural gas as an energy source.

In petroleum refineries and natural gas processing plants, excess natural gas is flared as a primary safety protocol to protect industrial equipment from unprecedented process disruptions such as over-pressurizing. The flared gas has the composition similar to natural gas used as an energy resource, which typically comprises 80-85% methane and the remaining fraction distributed among ethane, propane, butane, and pentane [9].

Since 2011, an average of 140-150 Billion cubic meters of natural gas is flared annually which is about 4% of the total gas produced. This is a huge loss of precious hydrocarbon.

Moreover, the post-flared gases which are released in the atmosphere often contain carcinogens, heavy metals, sulfur oxides, and other toxic chemicals that are potential health hazards [2,10–12]. In addition to the loss of a valuable energy resource and potential health hazard, such a practice elevates the proportion of anthropogenic greenhouse gases in the atmosphere and contributes to global warming. Therefore, over the past few decades flaring mitigation techniques have been encouraged by the Environmental Protection Agency, the United Nations, World Bank, and several leading chemical and petrochemical industries [13].

The known strategies for natural gas utilization include pipeline transportation, liquefaction, and gas to liquid transformation (GTL). Among these, the GTL approach chemically transforms the natural gas to less volatile hydrocarbon compounds such as olefins and aromatics which are important building blocks to a wide range of compounds. Several direct and indirect catalytic routes for methane conversion have been identified and studied over the years. The indirect method involves syngas (or synthesis gas) production by steam reforming and dry reforming of methane, followed by the Fischer-Tropsch reaction to produce liquid hydrocarbon. The direct route, as the name suggests, can convert methane directly to higher hydrocarbon and therefore is a promising approach for meeting the objective. The direct method includes the oxidative coupling of methane (OCM) to ethylene and the non-oxidative methane aromatization to benzene and hydrogen. These processes are described in the following sections.

1.1.2 Indirect processes for methane conversion

Steam reforming and dry reforming methods for methane conversion are discussed in the following subsections.

1.1.2.1 Methane steam reforming

In this process, methane is reacted with steam at high temperatures to produce H_2 along with CO and CO_2 as shown by equations 1-1 and 1-2. Presently, this process is used to meet around 50% of the world hydrogen demand. The reaction is carried out at a temperature between 700-1000°C and at a pressure of 3-35 bar in the presence of a Ni-based catalyst. However, carbon formation and sintering are major challenges with this process, as they deactivate the catalyst [14]. Further, as natural gas is a potential fuel itself, alternative feedstocks such as biomass are being extensively investigated [15,16].

$$CH_4 + H_2O \rightleftarrows CO + 3H_2 \qquad \Delta H_{298K} = 206\ KJ/mol \qquad \text{1-1 [14]}$$

$$CO + H_2O \rightleftarrows CO_2 + H_2 \qquad \Delta H_{298K} = -41.2\ KJ/mol \qquad \text{1-2 [14]}$$

1.1.2.2 Methane dry reforming

The dry reforming of methane can be carried according to equation 1-3. This reaction is highly endothermic and is favored by high temperatures, between 700°C–1000°C. Low pressure favors the forward reaction, as the number of stoichiometric moles increases. This process also suffers from coke formation and subsequent catalyst deactivation [14,17].

$$CH_4 + CO_2 \rightleftarrows 2CO + 2H_2 \qquad \Delta H_{298K} = 247\ KJ/mol \qquad \text{1-3 [14,17]}$$

1.1.3 Direct processes for methane conversion

The oxidative coupling of methane and non-oxidative aromatization of methane are described in the following subsections.

1.1.3.1 Oxidative coupling of methane

The oxidative coupling of methane to ethylene has been studied since 1980, following the work by Keller and Basin [18]. In this reaction, the cyclic addition of oxygen and methane to ethylene is carried out and the reaction is known to proceed via methyl radicals [19]. Metal oxides are used as a catalyst for the reaction at temperatures between 500-1000°C under atmospheric pressure. The reaction is shown in equation 1-4. The low yield of ethylene and the oxidation of ethylene to CO_2 and H_2 are challenges in this reaction, which hinders its commercialization. However, recent studies have suggested improved schemes with better-designed catalyst and special reactors configurations which may generate interest depending upon the price dynamics of oil, natural gas and ethylene [20,21].

$$CH_4 + 0.5O_2 \rightleftarrows 0.5\,C_2H_4 + H_2O \qquad \Delta H_{298K} = 247\ KJ/mol \qquad \text{1-4 [14]}$$

1.1.3.2 Methane direct aromatization

In methane direct aromatization (MDA) reaction, the conversion of methane to ethylene, benzene**,** and hydrogen is achieved in a non-oxidative environment. The reaction is thermodynamically favorable at high temperature (> 700ºC) under atmospheric pressure conditions. The thermodynamic conversion as evaluated by using the Gibbs free energy minimization method is reported in Figure 1-1. The overall reaction from methane to benzene

is shown in equation 1-5. This reaction, however, is known to occur in stages, viz. methane activation to radicals, the coupling of the radicals to form oligomers, and aromatization or cyclization with dehydrogenation of the oligomers [22–26]. A detailed discussion on these molecular steps is discussed in detail in later sections of the thesis.

$$6CH_4 \rightleftarrows C_6H_6 + 9H_2 \qquad \Delta H_{298K} = 532\ KJ/mol \qquad \text{1-5 [27]}$$

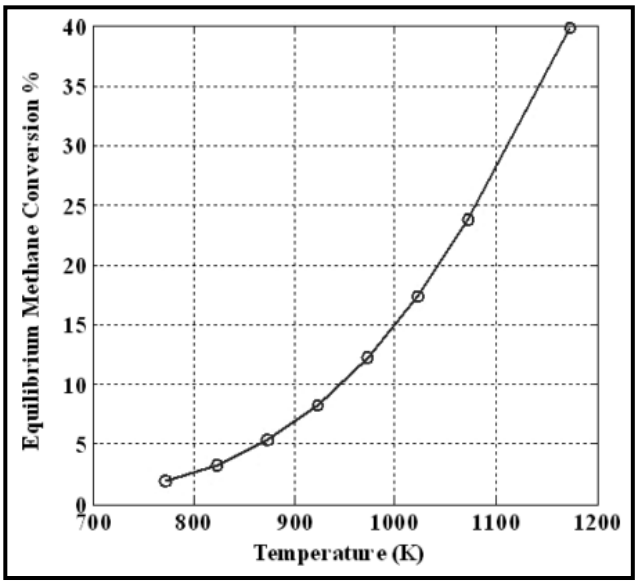

Figure 1-1 Thermodynamic equilibrium conversion of methane to aromatics with the temperature at Pressure = 1 bar [28].

1.1.3.2.1 ***The catalyst for MDA reaction***

Several catalyst**s** have been under investigation over the past few decades. Most of these catalyst**s** were transition metal supported on porous supports. Mo/HZSM-5 was introduced as the catalyst for MDA reaction by Wang et al [22] in 1993. Weckhuysen et al.[29] studied the

activity of W, Fe, V, and Cr supported on HZSM-5 and compared them with Mo/HZSM-5 to advise Mo/HZSM-5 as a better-performing catalyst. A similar conclusion was made by Yungchieh et al. [30] and Burns et al. [31] upon comparing Mo/HZSM-5 performance with Zn/HZSM-5 and Pd/HZSM-5. The Zn and Pd metals failed to activate methane and promoted methane cracking. Thus, Mo is seen as an ideal transition element for the reaction. Zhang et al. [32] tested molybdenum supported on a number of supports such as ZSM-5, ZSM-8, ZSM-11, H-β, H-MOR, H-X and H-Y, H-SAPO-5, and H-SAPO-11 and identified ZSM-5, ZSM-8, ZSM-11, H-β as suitable supports for the reaction. Shetian et al. [33] compared the performance of molybdenum supported on HZSM-5, FSM-16, mordenite, USY, SiO_2, and Al_2O_3 supports and observed that catalyst performed better with HZSM-5 support. They deduced that the support material used in MDA reaction has the following three important functions: 1. it provides support to the transition metal for anchoring by replacing acid sites, 2. it catalyzes the aromatization reaction (explained below), and 3. it acts as a molecular sieve to restrict the growth or polymerization of aromatic compounds within the pores of HZSM-5 thereby selectively producing benzene [25,34]. Therefore, the support with high microporosity, Brønsted acidic sites, and pore diameter about 5 Å is ideal for the study, and therefore, HZSM-5 is best suited.

*1.1.3.2.2 **Properties of ZSM-5 and molybdenum***

ZSM-5 or Zeolite Socony Mobil–5 or Molecular Sieve Five (MFI) is an aluminosilicate zeolite which belongs to the pentasil family of zeolites having the chemical formula as $Na_nAl_nSi_{96-n}O_{192}\cdot 16H_2O$ [35]. The Si/Al or SiO_2/ Al_2O_3 ratio defines the structure and the acidic strength of the zeolite. It is highly microporous (BET surface area about 350-400 m^2/g) and has a pore size of around 5 Å.

Molybdenum is an element in the periodic table with symbol Mo. Its atomic mass is 42 and atomic weight is 95.5. It is a d-block element which is located in group six, period five of the periodic table. Its ground state electronic configuration is given by [Kr] $4d^5$ $5s^1$. The crystal lattice of molybdenum is body-centered cubic (BCC) and its oxide forms MoO_2 and MoO_3 exist as monoclinic (PDF card 00-032-0671 [36]) and orthorhombic (PDF card 00-005-0508 [36]), respectively.

1.1.3.2.3 ***Studies on Mo/HZSM-5 catalyst synthesis***

The synthesis of Mo/HZSM-5 catalyst involves several important steps such as mixing time, pH during dispersion, and calcination temperature which decides the distribution of molybdenum, as some studies have observed molybdenum clusters on HZSM-5's surface [37,38]. Changes in these conditions can affect the active form of catalyst and lead to poor catalytic performance [39].

Ammonium heptamolybdate (AHM) is a commonly used precursor for molybdenum, but being bulky it cannot diffuse inside the zeolite pores. Therefore, during the synthesis of Mo/HZSM-5 by wet impregnation method, the heptamolybdate form of molybdenum dissociates to lower size molybdenum oxide species by maintaining a higher pH [40]. The dispersed molybdenum is strongly bonded with the Al site of HZSM-5 framework when calcined at high temperature. The reaction of AHM can be represented is shown in equations 1-6 and 1-7. These equations are interpreted from the data provided in Chithambararaj et al. [41] and Wienold et al.[42].

XPS studies on the catalyst after synthesis showed that molybdenum was present as molybdenum trioxide (Mo(VI)) [38]. It was observed that dispersed molybdenum substituted

the Brønsted acid site of HZSM-5, as the acid site's concentration decreased with impregnation [29]. Further, the impregnation of molybdenum decreases surface area and micropore volumes of ZSM-5 by occupying additional space in the channels [38,43,44]. However, there is a limited understanding of how molybdenum disperses and whether there is a clustering of molybdenum during synthesis.

$$[NH_4]_6[Mo_7O_{24}] \rightleftarrows 7\,MoO_{2.5}(OH)_{0.5} + \frac{5}{4}\,H_2O + 6\,NH_3 + \frac{7}{8}\,O_2 \qquad \text{1-6 [41,42]}$$

$$MoO_{2.5}(OH)_{0.5} + \frac{1}{8}O_2 \rightleftarrows MoO_3 + \frac{1}{4}H_2O \qquad \text{1-7 [41,42]}$$

1.1.3.2.4 ***Studies on Mo/HZSM-5 catalyst after carburization***

Studies suggest that the form of molybdenum in used Mo/HZSM-5 catalyst is carbidic, and this transformation of molybdenum oxide to molybdenum carbide happens upon contact with methane at high temperature. The carburized molybdenum, Mo_2C or β-Mo_2C, was observed from the XPS, Mo K-edge EXAFS [38], ^{13}C NMR [45] and TPSR [46] studies. However, Shu et al. [47] observed that Mo_2C formation is a gradual transition from Mo^{+6} to Mo^{+5} and Mo^{+4} to Mo_2C (Mo^{+2}). This process is referred to as carburization. Though this mechanistic route is well established, the literature reports lack clarity on the existence of particular intermediate forms.

Few other studies [45,48,49] have also suggested that some fraction of molybdenum oxide remained unaffected while some fraction got converted to molybdenum oxy-carbide and molybdenum carbide species. Thus, three forms of molybdenum coexisted in the spent catalyst, which could be potential site for methane activation. The equations 1-8 to 1-13

below highlight the possible reaction involved during carburization. However, these studies do not elaborate the extent to which Mo/HZSM-5 must be carburized for maximum activity.

A transient pulsing experiment by Vollmer et al. [45] validated that the carburization of molybdenum must happen prior to the reaction, as carburized catalyst produced benzene immediately while the non-carburized Mo/HZSM-5 catalyst underwent carburization prior to producing benzene. Due to this delay in product formation**,** there is an induction period associated with MDA reaction.

$$4MoO_3 + H_2 \rightleftarrows Mo_4O_{11} + H_2O \qquad \text{1-8 [50,51]}$$

$$Mo_4O_{11} + 3H_2 \rightleftarrows 4MoO_2 + 3H_2O \qquad \text{1-9 [50,51]}$$

$$MoO_3 + \frac{1}{2}CH_4 \rightleftarrows MoO_2 + \frac{1}{2}CO_2 \nearrow + H_2 \qquad \text{1-10 [50–52]}$$

$$MoO_2 + \frac{3}{2}CH_4 \rightleftarrows \frac{1}{2}Mo_2C + CO_2 + 3H_2 \qquad \text{1-11 [26,53,54]}$$

$$MoO_3 + \frac{5}{4}CH_4 \rightleftarrows MoC + \frac{1}{4}CO_2 + \frac{5}{2}H_2 \qquad \text{1-12 [26,53,54]}$$

$$MoO_3 + CH_4 \rightleftarrows \frac{1}{2}Mo_2C + \frac{1}{2}CO_2 + 2H_2 \qquad \text{1-13 [26,53,54]}$$

1.1.3.2.5 ***MDA reaction mechanism on Mo/HZSM-5***

Upon discovery of selective production of benzene by Wang et al. in 1993 [22], it was proposed that the reaction proceeds via a carbenium ion mechanism [22,25] and the activation of methane occurs on the carburized molybdenum sites which act as a hydride acceptor [55,56]. Yide et al. [57] proposed that it is the combination of HZSM-5 acid site and molybdenum

carbide which led to the heterolytic splitting of methane to intermediate products or active transition state such as ethylene. This suggests two stages in the MDA reaction, one which leads to ethylene from methane and other which aromatizes ethylene to benzene. The first part of the reaction can further be categorized into three stages: 1. the polarisation of the C-H bond in methane in the presence of molybdenum carbide site supported on HZSM-5 (represented as $Mo_2C_{(s)}$) (equation 1-14), 2. breaking of the polarized (equation 1-15), and 3. dimerization of the carbene to ethylene as a primary product (equation 1-16) [58–61].

$$CH_4 + Mo_2C_{(s)} \rightleftarrows CH_4 - Mo_2C_{(s)} \qquad \text{1-14 [58–61]}$$

$$CH_4 - Mo_2C_{(s)} \rightleftarrows CH_2 - Mo_2C_{(s)} + H_2 \nearrow \qquad \text{1-15 [58–61]}$$

$$CH_2 - Mo_2C_{(s)} \rightleftarrows \frac{1}{2}C_2H_4 + Mo_2C_{(s)} \qquad \text{1-16 [58–61]}$$

1.1.3.2.6 ***Kinetic modeling studies of MDA reaction***

The reaction kinetics of heterogeneously catalyzed MDA reaction has been studied by three modeling approaches; viz. power law, Langmuir-Hinshelwood-Hougen-Watson (LHHW) approach, and microkinetic modeling. The power law and the LHHW models are lump-based approaches, where the values of rate constants are estimated by minimizing one or more objective functions. Most times the parameters are estimated by regression analysis using Levenberg-Marquardt algorithms. The microkinetic model is a more detailed model, as it describes elementary reaction steps and its Arrhenius coefficients, catalytic sites densities, and sticking coefficients [62].

Iliuta et al. [63] modeled a packed bed reactor using the LHHW approach and the reaction scheme given in equations 1-17. The rate-determining step was evaluated as the surface reaction for ethylene formation (equation 1-19). Li et al. [64] and Yao et al. [65] simulated the effect of temperature, pressure and feed rate on the rate of methane aromatization to suggest that decreasing the feed rate and pressure, and increasing the temperature gave better reaction performance. A global kinetic model was developed by Zhu et al. [66] suggested that post-reactor separation and possibly CH_4 recycle would be needed in an MDA commercial scale-up,

$$r^{exp} = \frac{dX_{CH_4}}{d(\frac{W}{F_{CH_4}})} \qquad \text{1-17 [27]}$$

where, r^{exp} = rate of reaction, X_{CH_4} = methane conversion, W = weight of the catalyst, and F_{CH_4} = flow rate of methane.

$$CH_4 + S \rightleftarrows CH_2S + H_2 \qquad \text{1-18 [27]}$$

$$CH_2S \rightleftarrows \frac{1}{2}C_2H_4 + S \qquad \text{1-19 [27]}$$

$$\frac{1}{2}C_2H_4 \rightleftarrows \frac{1}{6}C_6H_6 + \frac{1}{2}H_2 \qquad \text{1-20 [27]}$$

The micro-kinetic model proposed by Bhan et al. [67] on propane aromatization using eight reaction steps *viz.* adsorption/desorption, protolytic cleavage, protolytic dehydrogenation, olefinic adsorption/desorption, β-scission, oligomerization, hydride transfer, alkylation/dealkylation, cyclization and aromatization [67], could be considered as a starting point for the MDA reaction. In this model, elementary reaction steps were categorized as

reaction families which had similar properties. Upon categorizing reactions, a systematic pathway could be established and evaluated. Other reactions with overlapping reaction steps could also serve as a valid initial guess. These other reaction studies may include autocatalytic pyrolysis of methane [68], ethene and propene aromatization [69], propane to n-hexane [70], ethane, propane and butane aromatization [71–73], cracking of C_4–C_8 hydrocarbons on HZSM-5 [74,75], and ethane and ethylene aromatization over a zinc-exchanged HZSM-5 catalyst [76].

Also, alongside the advancement in computation capability and quantum chemistry theories, theoretical chemistry calculation is considered as an advantage to understand the reaction behavior in virtual space. Specifically, quantum chemistry calculations of hydride transfer reaction [77], hexadiene cyclization via carbenium ion intermediate [78], methane dissociation on Ga/HZSM-5 [79], C-H dissociation on $Mo(CH_2)_2$, $Mo(CH_2)_2CH_3$, $Mo_2(CH_2)_4$ and $Mo_2(CH_2)_5$ supported on ZSM-5 [80], methane dehydrogenation and coupling on $Mo(CH_2)_2CH^{3+}$, $Mo_2(CH_2)_4^{2+}$ and $Mo_2(CH_2)_5^{2+}$ supported on ZSM-5 [60], ethylene dimerization, deprotonation, polymerization on the unmodified and P-modified ZSM-5 [81] have supported the earlier proposed hypothesis and have further expanded the understanding of MDA reaction. The quantum calculations also provide detailed reaction steps, the atomic configuration of the sites, and a much more authenticated value of activation energy, thus playing a vital role in developing a better kinetic model.

The first detailed reaction pathway for MDA reaction was proposed by Wong et al. [82] in 2012. This reaction model considered 50 elementary reaction steps, as described in Figure 5 of the publication [82]. Karakaya et al. [61,83] conducted a detailed parametric sensitivity analysis to show the impact of particular reaction steps on benzene formation and assist in reactor

design and process scale-up. Gerceker et al. [84] performed a microkinetic calculation to validate enhancement in the activity of Pt and Sn supported on HZSM-5.

1.1.3.2.7 Coke formation and Mo/HZSM-5 deactivation

Coke formation occurs as a parallel undesired reaction alongside MDA reaction. It deactivates the catalyst leading to decreasing the yield of benzene and hydrogen [22]. Therefore, to develop strategies in minimizing coke formation, it is necessary to understand the physical and chemical properties of coke and the routes and means by which it forms.

The coke component formed during MDA reaction, on Mo/HZSM-5 catalyst, is usually categorized as graphitic coke and as poorly developed coke or pre-graphitic coke [85–87]. These coke species form, deposit, and block catalytic active sites [88,89]. Further, coke does not form and distribute uniformly over the structure of Mo/HZSM-5 [90,91] adding to complexity in analysis. Hu et al. [92] observed that the kinetic of coking and the structure of resultant coke depends upon the temperature and pressure conditions of the reaction.

Temperature-programmed experiments (oxidation, reduction**,** and reaction) used for classifying coke species indicated that coke formed during MDA reaction has different oxidation stability. Soft natured coke has low oxidation propensity and burns at a relatively lower temperature. This consist of polyaromatic hydrocarbon (PAH) species. The hard natured coke burns at much at a higher oxidation temperature and constitute of graphite carbon [93–96].

The mechanistic pathway proposed by Dong et al. [97] suggests several routes for polyaromatic condensation and highlights the formation of planar coke structures by aryl-

aryl addition, intramolecular dehydrocyclization, and ethyne addition reaction alongside the non-planar structure of polycyclic compounds. Speybroeck et al. [98] attempted to model the coking reaction during thermal cracking and used reaction families that involved hydrogen abstraction, radical substitution, olefinic addition, β-scission**,** and cyclization reaction. Studies by Song et al. [99,100] generated further understanding of the contributing role of ethylene in coke formation. This suggested the possibility of involvement of radical species which forms during the reaction in coking as suggested by Kopinke et al. [101]. While these studies are very informative but extending them to the MDA reaction requires more experimental evidence which can elucidate the coke compounds chemical identity and its precursor.

1.2 Summary of literature review

An extensive review of fundamental aspects related to MDA reaction and coke formation is presented in a systematic way highlighting the impact on Mo/HZSM-5 catalyst. Gaps in the understanding of MDA reaction as observed in literature are summarized below:

Among tested catalyst, the combination of molybdenum impregnated on HZSM-5 has shown promise to be a commercial catalyst for MDA reaction. While literature highlights change to Mo/HZSM-5 catalyst during synthesis, several discrepancies exist in explaining the dispersion and clustering of molybdenum, a correlation between molybdenum agglomerates and synthesis conditions, crystal information of the Mo/HZSM-5 catalyst.

The literature defines that partial carburization of molybdenum in Mo/HZSM-5 is needed for reaction, however, the extent of carburization is not completely understood and remain several questions still exist to be answered. It is unclear from the literature on how

molybdenum carburizes, the existence of any intermediate forms. Further, it is reasonable to assume MoO_xC_y as oxycarbide species, but, evidence of its location, function, and changes with coking has not been studied. As the synthesis and carburization stages decide the catalyst performance, a lack of understanding of these stages is a major drawback.

Coke species formation is shown to affect the catalyst by significantly reducing the surface area and micropore volume and acid site density. Also, the reaction pathway is described as bi-functional where molybdenum sites and Brønsted acid sites play independent roles. But, there is no conclusive evidence suggesting the later, and little information related to what are the roles of these sites in coke formation.

Further, several routes for coking via polyaromatic hydrocarbon are defined in the literature, but there is no conclusive experimental evidence for any of these routes, therefore, making it less certain to be true. The biggest difficulty here is to identify the chemical form of coke and the precursor of its formation. The problem is compounded with varying reaction conditions (temperature, pressure, feed, feed rate intermediate product distribution, and reaction time-on-stream), as they may impact the coking route and surprising, no reported studies have addressed this. Moreover, the most coke characterization studies that are reported in the literature are limited to analysis coke on the surface, and missing out the coke species that is forming within the pores of the zeolite. It can be hypothesized that based on the location of the coke (surface or internal), they may play a very different role in the catalyst deactivation, as one on the surface may add to transport limitation and block pore opening, while the other inside may poison the active site.

The reaction pathway for methane conversion to benzene as suggested in literature considers ethylene as a primary product of the reaction. The detailed model also addresses several intermediate elementary steps in a format which resembles a combination of series and parallel reaction, but surprisingly, no study has validated these intermediate products by subjecting the catalyst with different reactants. The lack of experimental validation for intermediate products handicaps the progress in evaluating the reaction kinetics and make the proposed pathway vulnerable for criticism.

The coke removal by oxidation at high temperature (mostly between 400-700ºC) is repeatedly mentioned in literature for effective regeneration. While literature indicates that polyaromatic hydrocarbon burns at a lower temperature than the stable graphitic coke, this theory has less validated by experiments. Studies have also shown that this reverses carburization. But, no studies have analyzed the post-regeneration sample and compared with the fresh catalyst to ascertain the active forms are intact in terms of its physical and chemical properties. Further, the choice of regeneration conditions is obscure lacking due to the less knowledge of the coke structures. Another pitfall in the literature is the incomplete knowledge of aluminum molybdate formation which question 100% regeneration of the catalyst.

1.3 Thesis objective

The aim of this thesis is to investigate the pathways of methane conversion to ethylene, benzene and coke formations. The study is intended to further enhance the understanding of the impact to the bi-functional Mo/HZSM-5 catalyst upon usage and regeneration, and gauge its suitability for repeated use.

Specific objectives include a.) identification of active sites for the methane dimerization to ethylene and ethylene aromatization to benzene on individual site, b.) characterization of deactivated catalyst for classifying coke species with methane and ethylene as feed, c.) characterization of the resultant coke species and its dependency on methane feed rate, temperature and time-on-stream to generate a comprehensive understanding of coke development process desired for suggesting optimal reaction conditions, and d.) identification of changes to Mo/HZSM-5 catalyst upon usage and regeneration that may and comment on potential damage to Mo/HZSM-5 structure and its suitability for repeated use.

1.4 Organization of the thesis

This thesis is organized into seven chapters.

- Chapter 1 introduces literature pertaining to the field. This chapter also layouts the research problem, motivation, and objective of this work, and thesis structure.
- Chapter 2 describes ethylene aromatization on HZSM-5 catalyst to validate the second part of the MDA reaction. The routes for coking pathway with ethylene precursor is presented as a function of ethylene concentration and reaction time.
- Chapter 3 elaborates on the studies that were undertaken to identify the active form of catalyst desired for methane activation and dimerization, which forms the first part of the MDA reaction. Changes to the structural, morphological, and chemical states of molybdenum after calcination, reaction, and regeneration are detailed with the use of several analytical techniques.
- Chapter 4 discusses our experiments on identifying and classifying possible coke structures and elucidate coking mechanism during methane aromatization

reaction on Mo/HZSM-5 catalyst. Further, this chapter defines the changes to resultant coke when subjected to varying reaction temperature, catalyst time-on-stream, and methane flow rate.

- Chapter 5 of the thesis highlight the first of its kind in-situ reaction study with Mo/HZSM-5 catalyst for directly monitoring the impact of reaction on the catalyst structure. This chapter describes the novel flow capillary reactor set-up used at the Australian Synchrotron powder X-ray beamline and discusses exciting finding which validated artifacts related to MDA reaction.
- Chapter 6 summarizes the key conclusions of this thesis and their significance and outlines a few directions for future work.

Chapter 2 Direct Aromatization of Methane: Understanding the pathways of coke formation and evolution with ethylene precursor on HZSM-5 catalyst

This chapter presents results from the investigation on the nature, structure, and morphology of resultant coke formed using ethylene as a precursor on HZSM-5 at conditions similar to methane aromatization reaction. The influence of ethylene concentration and catalyst time-on-stream on coking and reaction conversion has been studied. The findings from this study will be useful in attributing the coke formed during to the second stage of the methane to benzene reaction (i.e. ethylene to benzene and hydrogen). Moreover, insights on the actual precursors and mechanism of coke formation can been elucidated upon comparison with the studies in Chapter 4.

HZSM-5 prepared by the calcination of NH_4-HZSM-5 (Si/Al = 15) and tested for its catalytic activity in a tubular packed bed reactor. The ethylene aromatization reaction was carried out with a mixture of 20% ethylene and 80% nitrogen, and with pure ethylene feed. The effect with reaction time-on-stream varied upto 120 min was studied. Fresh and used samples were characterized by N_2 adsorption, pyridine adsorbed FTIR, scanning electron microscopy and Synchrotron powder XRD studies to understand the effect of reaction on the surface area, acid site density, and structure of HZSM-5. Also, the spent samples were

analyzed with thermogravimetric analysis, CHN elemental analysis, and X-ray photoelectron spectroscopy to quantify the amount of coke species and classify them. Further characterization of the coke deposits was done by Raman spectroscopy, transmission electron microscopy, and CO_2 adsorption studies.

The study suggested a dependency on the availability of the Brønsted acidic sites for coke and aromatics formation. The nature of coke varied as the reaction progressed, from being amorphous to becoming more graphitic in the presence of the acid sites. However, a substantial increase in the coke content blocked these acid sites and also induced mechanical strain on the ZSM-5 structure. As a consequence, the conversion dropped and a slow build-up of amorphous coke took place over the already developed coke.

Declaration for Thesis Chapter 2

Declaration by candidate

In the case of chapter 2, the nature and extent of my contribution to the work was the following:

Nature of contribution	Extent of contribution
Concept development, sample preparation and analysis, data interpretation, and writing and revising manuscript	60%

The following co-authors have contributed to the work.

Name	Nature of contribution	Extent of contribution for student co-author only
Gregory Knowles	Assisted in the characterization, and data interpretation of BET studies	NA
Timothy Williams	Assisted in the characterization, and data interpretation of TEM studies.	NA
Xiya-Fang	Assisted in the characterization, and data interpretation of SEM studies.	NA
Thomas Gengenbach	Assisted in the characterization, and data interpretation of XPS studies.	NA
Sivakumar S	Assisted in conceptualizing, supervising, manuscript reviewing, and overall data interpretation.	NA

D Maiti	Supervision	NA
A K Suresh	Assisted in conceptualizing, supervising, data interpretation, manuscript reviewing and manuscript editing.	NA
Alan Chaffee	Assisted in conceptualizing, supervising, data interpretation, manuscript reviewing and manuscript editing.	NA

Student signature: Date: 18.02.2020

The undersigned hereby certify that the above declaration correctly reflects the nature and extent of the student's and co-authors' contributions to this work. In instances where I am not the responsible author I have consulted with the responsible author to agree on the respective contributions of the authors.

Supervisor signature: Date: 18.02.2020

Supervisor signature: Date: 18.02.2020

2.1 Introduction

Approximately 1–5 m^3 of natural gas (STP) are flared per barrel of oil produced. This is alarming, as it causes a loss of potential hydrocarbon resources and increases CO_2 emissions [11,12]. The utilization of this wasted resource as an alternative and cheap reactant for the production of aromatic compounds can have monetary benefits and also help mitigate greenhouse gas emissions [10]. However, the reaction for using natural gas or methane (a major component of natural gas) poses a number of challenges which have to be overcome to make it economically feasible [102-100]. Some of these challenges are the extremely low reactivity of methane and consequent difficulties in activating it, thermodynamic limitations on the extent of reaction (methane conversion to aromatics), and the rapid deactivation of the catalysts by coking ('coke' or carbonaceous deposits formation).

Following the work of Wang et al. (1993) [22], which showed selective benzene production by converting methane under non-oxidative conditions on Mo/HZSM-5 catalyst, there has been an increased interest in developing this process to utilize natural gas. In this reaction, it is generally believed that activation of methane, leading to the formation of ethylene, takes place on Mo. For this, Mo must be in carbidic form and bonded with Si-O-Al structure. The acid function of the zeolite support is believed to be important in the further conversion of ethylene to benzene and hydrogen. The coke formed during the reaction occupies the Mo and acid sites and limits the time-on-stream of the Mo/HZSM-5 catalyst. Therefore, the coked catalyst has to be regenerated and carburized frequently. Apart from being energy intensive, the conditions of regeneration make the ZSM-5 structure prone to dealumination.

Prior characterization studies have reported several forms of coke, most of them attributed to the second stage of the reaction (ethylene to benzene and hydrogen), but the actual precursors and mechanism of coke formation have not been elucidated.

In view of the generally accepted mechanism as described above, it will be interesting to observe the nature, structure, and morphology of the resultant coke formed using ethylene as a precursor on HZSM-5 at conditions similar to methane aromatization reaction. In the present work, we have studied the conversion of ethylene into aromatics on HZSM-5 catalyst at varied reaction extents (ethylene concentration and time-on-stream) followed by a comprehensive characterization of the post-reaction (spent) catalyst. This we believe, will enhance the understanding of coke formation mechanism and the role of HZSM-5 acid sites and pores.

2.2 Materials and methods

2.2.1 Catalyst preparation

Commercial NH_4-ZSM-5 (Si/Al = 11.5) powder was obtained from Zeolyst International Inc., and calcined in air at 510°C for 6 h to form HZSM-5 powder. The HZSM-5 powder was pelletized in a hydraulic press (Kimaya Engineers, Maharashtra, India) under pressure of 98 KPa, followed by crushing and sieving to obtain particles of 250 - 500 microns.

2.2.2 Set-up and catalyst testing procedure

The catalyst activity studies were carried out in a downflow packed tubular reactor made of quartz (8 mm internal diameter). The reactor was loaded with 2 g of HZSM-5 catalyst with

quartz wool on either side of the catalyst for support. The tubular reactor was positioned in the furnace so that the catalyst was in the zone of constant temperature.

Catalyst tests were conducted at 725°C and at a gas hourly space velocity (GHSV) of 6000 ml/g/h (i.e. 200 ml/min at STP for 2 g catalyst) under atmospheric pressure. The reactor bed was heated from room temperature to 725°C at 10°C/min in nitrogen flow, with a flow rate of 200 ml/min (STP). On reaching 725°C, the gas flow was switched from nitrogen to ethylene or to ethylene-nitrogen mixture. The tests were done using feed gas compositions of 100% C_2H_4 (catalyst time-on-stream of 5, 10, and 120 min) and 20% C_2H_4/ 80% N_2 (time-on-stream of 5 and 10 min).

The outlet gas products were continuously analyzed with a Varian 450-GC (Agilent Technologies, California, U.S.A) online gas chromatography system equipped with silica capillary columns viz. Petrocol-DH50 (Sigma Aldrich) and carboxen-1010PLOT (Sigma Aldrich) and both thermal conductivity (TCD) and flame ionization (FID) detectors.

At the conclusion of each test, the gas flow was switched back to nitrogen, the reactor was cooled to room temperature and the catalyst was recovered for further characterization. Table 2-1 shows the nomenclature employed for the various used catalyst samples recovered.

Secondary electron (SE) images and back-scattered electron (BSE) images of the fresh and used HZSM-5 were collected on a FEI Magellan 400 field emission gun (FEG) scanning electron microscope (SEM). Samples were coated with a thin layer of Ir (about 0.7 nm thick) to enhance conductivity. The electron current was optimized below 3 KV to avoid surface charging.

Table 2-1: Description of abbreviations for the different catalyst samples characterized

Sample name	Type	Ethylene feed (mol %)	Time-on-stream (min)
FC	Fresh HZSM-5	-	-
SC20-5	Used	20	5
SC20-10	Used	20	10
SC100-5	Used	100	5
SC100-10	Used	100	10
SC100-120	Used	100	120

2.3 Characterization techniques

Adsorption and desorption measurements on fresh and spent HZSM-5 were conducted in a Tristar II 3020 gas-sorption analyzer (Micromeritics Instruments Corporation, Georgia, U.S.A) with either liquid nitrogen (at -196°C) or gaseous CO_2 (at 0°C). Prior to the measurement, a vacuum degasser system - VacPrep-061 (Micromeritics Instruments Corporation, Georgia, U.S.A) - was used to remove moisture and adsorbed contaminants. The samples were degassed overnight in the VacPrep-061 at 120°C under vacuum (7 Pa) and backfilled with nitrogen upon cooling. Calculations of surface area and pore volume from the nitrogen isotherm data employed the Brunauer-Emmett-Teller (BET) theory [103] and Barrett-Joyner-Halenda (BJH) theories [104], respectively. The micro-pore surface area and micropore volume were calculated from the carbon dioxide adsorption data using the Dubinin-Radushkevich equation [105].

The Brønsted and Lewis acid site densities in the fresh and spent HZSM-5 were studied by FTIR spectroscopy employing a pyridine probe. 5 mg of sample was vacuum degassed in the VacPrep-061 by heating at 120°C for 2 h under vacuum (7 Pa) and was then cooled to room temperature with nitrogen backfilling. After addition of 1-3 ml of pyridine (anhydrous

99.9 %, Sigma Aldrich) to the recovered samples and sonication for 30 min, samples were heated at 120°C for 2 h and 250°C for 30 min under vacuum (13.3 Pa). The samples were recovered after cooling to room temperature and backfilling with nitrogen.

FTIR spectra in transmission mode were obtained for 1.3 cm diameter discs containing KBr and sample with adsorbed pyridine in the ratio of 75:1. A Digilab IR spectrometer was used. The analysis was conducted, with air as background, for 64 scans across the 400-4000 cm^{-1} region. The peaks of corresponding Brønsted and Lewis acid sites were identified as reported in the literature [106,107], and their respective areas were evaluated from the resolution Pro FTIR software interface (Agilent Technologies, California, U.S.A). For calculation purposes, integrated molar extinction coefficients (IMEC) of 1.67 and 2.22 cm/µmol were used for Brønsted (B) and Lewis (L) acid site respectively [107].

$$C\ (pyridine\ on\ B\ site) = \frac{IMEC_B\ IA_B\ \pi r^2}{W} \qquad 2\text{-}1$$

$$C\ (pyridine\ on\ L\ site) = \frac{IMEC_L\ IA_L\ \pi r^2}{W} \qquad 2\text{-}2$$

where W = weight of the KBr-Sample disk, r = radius of the KBr-Sample disk, and IA_B and IA_L are integrated area of peaks corresponding to Brønsted and Lewis acid sites (calculated by the resolution Pro FTIR software interface).

Transmission electron micrographs of the spent HZSM-5 were obtained with a Tecnai T20 TWIN instrument operated at 200 kV. A small amount of sample was dispersed in butanol by sonication and about 1 µl of this suspension dried on a holey carbon coated copper grid. The collected images were post-processed by the Digital Microscopy Suite (Gatan Inc.)

software interface. The post-processing included the Fourier transform (FT) and inverse Fourier transform on the selected region of the image. Data smoothing of 5 was used for FT. The d-spacing was estimated by taking the average of 5-10 values.

Raman spectra were obtained using an InVia Raman microscope (Renishaw). A blue laser (488 nm) was used to scan the region 1200-3500 cm^{-1} to classify the carbon species. 5 mg of catalyst was placed under a microscope with a lens magnification of 50X. The exposure time and laser intensity were optimized to 5-20 sec and 1-10% of maximum power respectively to prevent the destruction of the carbon on the catalyst and to minimize fluorescence. The Gaussian peak fitting was performed in OriginPro 8 applying the peak positions reported by Ferrari et al. [108].

Weight-loss profiles of the spent HZSM-5 were obtained from thermo-gravimetric analysis (TGA) using a NETZSCH 1000 TG-DSC analyzer. 15-20 mg of sample was taken in an alumina crucible and the weight loss was recorded with a heating ramp of 5°C/min, to 800°C in dry air. The sample was held at 120°C for 10 min to remove moisture [109]. The carbon formation rate on the sample recovered (time-on-stream) was estimated from the carbon that was burned.

CHN elemental analysis of the fresh and spent HZSM-5 was carried out on a Thermofinnigan-FLASH EA 1112 series. 5 mg of sample was combusted at 1800°C and the products of combustion were simultaneously analyzed using an online gas chromatograph fitted with a thermal conductivity detector (TCD). As, the coked samples were expected to adsorb moisture from the atmosphere upon storage, the hydrogen content detected from the

study was deducted by a respective amount of weight loss due to moisture calculated from TGA.

X-Ray diffraction (XRD) patterns were collected on the fresh and spent HZSM-5 using the powder diffraction beamline at the Australian Synchrotron facility. The beam with an energy of 17 keV (λ = 0.74 Å) was selected for sample capillary analysis. A borosilicate capillary (Hilgenberg GmbH, Germany) of 0.7 mm diameter was packed with approximately 5 mg of sample, mounted onto the beamline, and aligned to the beam direction using the automatic alignment system. The diffraction from a 2 theta of 2-80° was recorded using a high-resolution Mythen detector. The capillary was rotated 360 degrees, and the diffraction pattern was collected in pair to eliminate the effect of the gap in the Mythen detector. The recorded data were merged using PDViper and converted to the equivalent of λ = 1.54 Å using CMPR toolbox. The database of zeolite structures and the Inorganic Crystal Structure Database (ICSD) were used to identify the planes of different crystalline phases.

X-ray photoelectron spectroscopy (XPS) analysis of fresh and spent HZSM-5 was performed using an AXIS Nova spectrometer (Kratos Analytical Inc., Manchester, UK) with a monochromated Al Kα source at a power of 180 W (15 kV, 12 mA), a hemispherical analyzer operating in the fixed analyzer transmission mode and the standard aperture (analysis area: 0.3 mm × 0.7 mm). The total pressure in the main vacuum chamber during analysis was typically between 10-6 and 10-7 Pa. Survey spectra were acquired at a pass energy of 160 eV. To obtain more detailed information about the chemical structure, oxidation states, etc., high-resolution spectra were recorded from individual peaks at 40 eV pass energy (yielding a typical peak width for polymers of < 1.0 eV). The samples were filled into shallow wells of a custom-built sample holder and were analyzed at a nominal

photoelectron emission angle of 0° w.r.t. the surface normal. Since the actual emission angle is ill-defined in the case of particles and powders (ranging from 0° - 90°) the sampling depth may range from 0 nm to about 10 nm. The data processing was performed using CasaXPS processing software version 2.3.15 (Casa Software Ltd., Teignmouth, UK) with binding energy referenced to the C 1s peak at 284.8 eV. All elements present were identified from survey spectra. The atomic concentrations of the detected elements were calculated using integral peak intensities and the sensitivity factors supplied by the manufacturer.

2.4 Results and discussion

2.4.1 Thermodynamic analysis of ethylene to aromatics

The extent of ethylene conversion to products including benzene, methane, ethane, 1-butene, toluene, naphthalene, trimethylbenzene, p-xylene, and hydrogen was evaluated by minimizing the Gibbs free energy. An equilibrium solver tool in the CHEMKIN software was used to perform the computation. The solution is represented in Figure 2-1, which shows a near complete conversion of ethylene. Specifically, at 998 K (725°C) and 1 atm., which are the conditions of interest, ethylene converted to major products including methane, benzene, ethane, and hydrogen. A minor quantity of toluene, naphthalene, p-xylene, and trimethylbenzene were also observed, which highlights the possibility of polymerization. The selectivity of benzene was about 33% (calculated as per equation A 1-9-3 in appendix 1). The mole fraction of benzene was consistently about 0.25 till 1023 K (750°C), similar to that observed experimentally by Choudhary et al. [110], beyond which it drops exponentially to possibly form higher aromatic compounds (Figure 2-1.B). Figure 2-1 highlights that ethylene has higher tendency to crack thermally, therefore, about 75% of the product is methane,

particularly observed at temperature below 848 K (575°C). However, with increasing temperature, the amount of methane decreases to about 62% at 998 K (725°C). The methane reduction correlated with an increase in hydrogen concentration, which suggests that hydrogen might be a transient reactive component assisting methane formation at lower temperature. It is noted that these calculations were performed without considering coke (both graphite and polyaromatic hydrocarbon) formation.

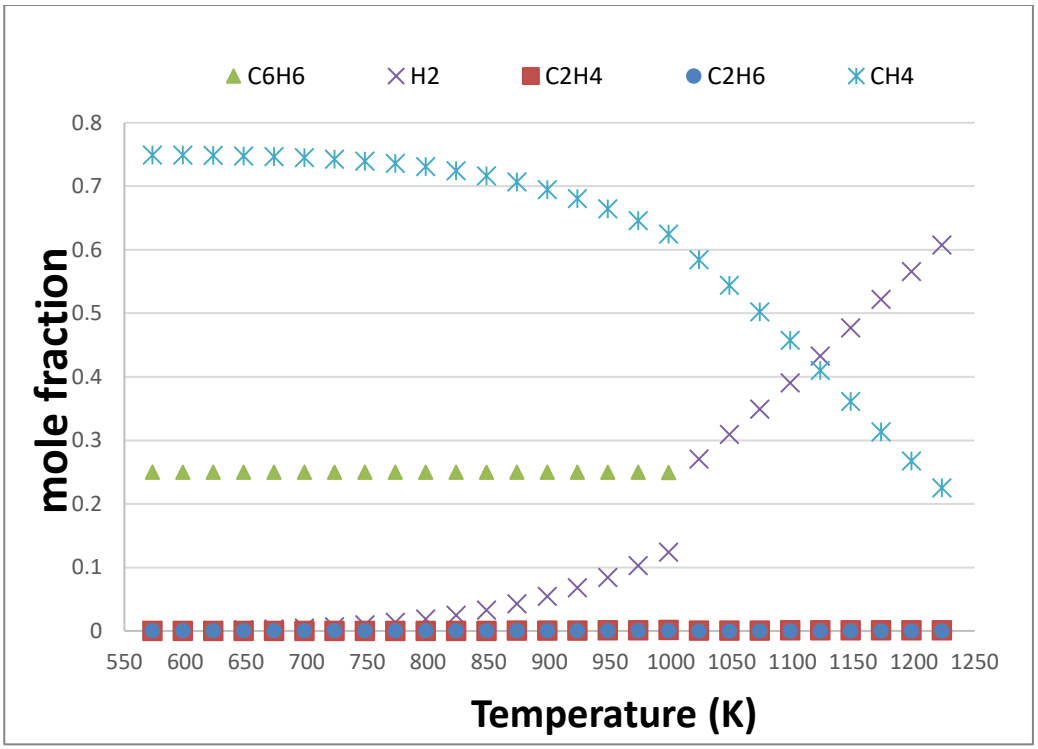

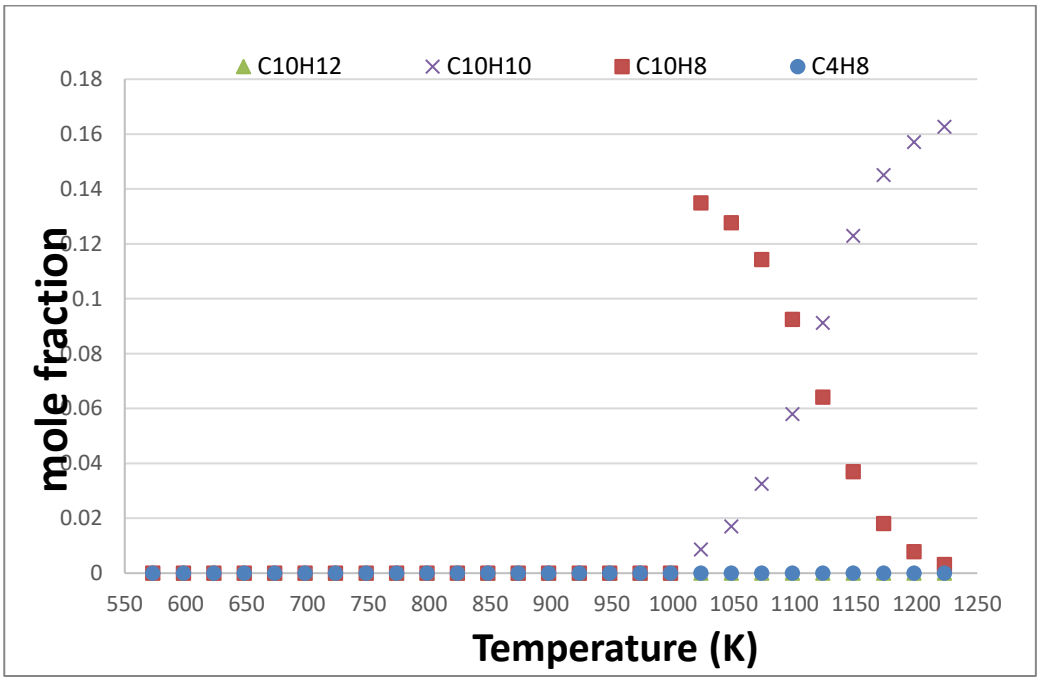

Figure 2-1: Equilibrium ethylene conversion to products as a function of temperature at 1 atm pressure.

2.4.2 Reactor studies

The major products of ethylene conversion on HZSM-5 included benzene, methane, and naphthalene, the distribution of which with time-on-stream is shown in Figure 2-2. Trace amounts of trimethylbenzene, toluene and p-xylene also formed part of the product stream, particularly at short reaction times. The order of decreasing concentration for products in the outlet gas at short reaction times was benzene > methane > naphthalene > p-xylene > toluene > trimethylbenzene (TMB). Unlike the lower selectivity towards benzene at 400ºC, reported by Choudhary et al. [110], the observed distribution implied that the formation of benzene was favored, which is possibly due to the high reaction temperature [76]. The stoichiometry of aromatic product formation from ethylene can be represented by reactions 2-3-2-6. This is, however, a simplified representation of the reactions, which have been described as having several intermediate stages in the earlier published literature [76,110]. The formation of a substantial quantity of methane indicates the possibility of a parallel reaction, 2-7 and 2-8. Interestingly, the ethylene to methane reaction path was not considered as a part of the mechanistic models of Wong et al. [82] and Karakaya et al. [61,83]. The work of Choudhary et al. [110] suggested methane formation alongside propane/propylene (at 400ºC, over Ga-modified ZSM-5) as an intermediate step in the formation of aromatics, however, as propane and propylene were not observed in the present study, indicates that propane and propylene may have reacted completely at 725ºC and methane escaped to the outlet. As HZSM-5 is a well-known dehydrogenation catalyst, it can be suggested that the hydrogen formed upon dehydrogenation of ethylene and other products would possibly take part as a reactant in methane formation [111].

Figure 2-2 shows a decrease in the concentration of the products with increasing time-on-stream, greater at high ethylene concentration, which implies a much stronger deactivation of the catalyst with pure ethylene feed as compared to diluted feed. As can be seen from Figure 2-2, the conversion was already quite small by 10 min and virtually zero by 25 min for the 100% ethylene feed, confirming the influence of feed concentration on the rate of deactivation of the catalyst.

$$3C_2H_4 \overset{HZSM-5}{\longleftrightarrow} C_6H_6 + 3H_2 \qquad \text{2-3 [76,110]}$$

$$\frac{7}{2}C_2H_4 \overset{HZSM-5}{\longleftrightarrow} C_7H_8 + 3H_2 \qquad \text{2-4 [76,110]}$$

$$4C_2H_4 \overset{HZSM-5}{\longleftrightarrow} C_8H_{10} + 3H_2 \qquad \text{2-5 [76,110]}$$

$$5C_2H_4 \overset{HZSM-5}{\longleftrightarrow} C_{10}H_8 + 6H_2 \qquad \text{2-6 [76,110]}$$

$$C_2H_4 + 2H_2 \overset{HZSM-5}{\longleftrightarrow} 2CH_4 \qquad \text{2-7 [111]}$$

$$C_2H_4 \overset{HZSM-5}{\longleftrightarrow} CH_4 + C_s \qquad \text{2-8 [111]}$$

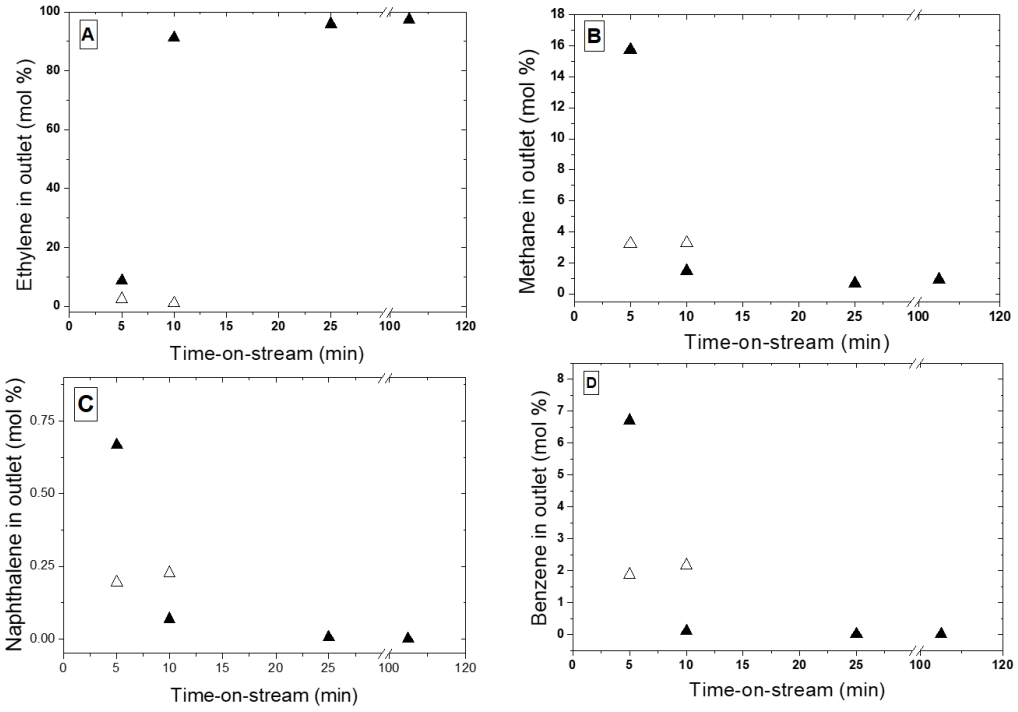

Figure 2-2: A) Ethylene, B) Methane, C) Naphthalene, and D) Benzene mole percentage during the conversion of ethylene to benzene on HZMS-5 at 725 °C under atmospheric pressure as analyzed by online GC. Filled symbols represent the value with 100% ethylene feed and open symbols represent the value with 20% ethylene feed.

2.5 Catalyst and coke characterization studies

2.5.1 Quantification of coke species:

The TGA profiles and their derivatives (dTG) during oxidation of used samples are shown in Figure 2-3, and highlight the burning of coke species. From Figure 2-3, it can be seen that the shorter reaction time spent catalyst samples (SC20-5, SC20-10, SC100-5 and SC100-10) has a single weight-loss peak, at a temperature between 585-645°C, but, the sample treated with 100% ethylene for 120 min (SC100-120) was having two weight-loss peaks at 545°C

and 580°C. This indicates that the coke formed had different oxidizing characteristics. The coke on the samples oxidized in the following order: SC100-120 < SC20-5 ≈ SC20-10 < SC100-5 < SC100-10. The rise in the oxidation temperature with the reaction time as in SC100-5 < SC100-10 and SC20-5 < SC100-5, suggests changes to the chemical form of the coke structure with reaction time and ethylene concentration [112,113]. Another possible explanation of the trend would be that increased reaction time and ethylene concentration led to blocking of zeolite micropores by coke build-up, which will vary the rate of oxygen diffusion, and hence, would increase the combustion temperature [114]. The lower coke burning temperature in the extended used sample (SC100-120) compared to those of the other used samples, could be due to increased oxygen diffusion in the extended use samples on account of the porous nature of this coke (discussed below in related to the CO_2 adsorption study).

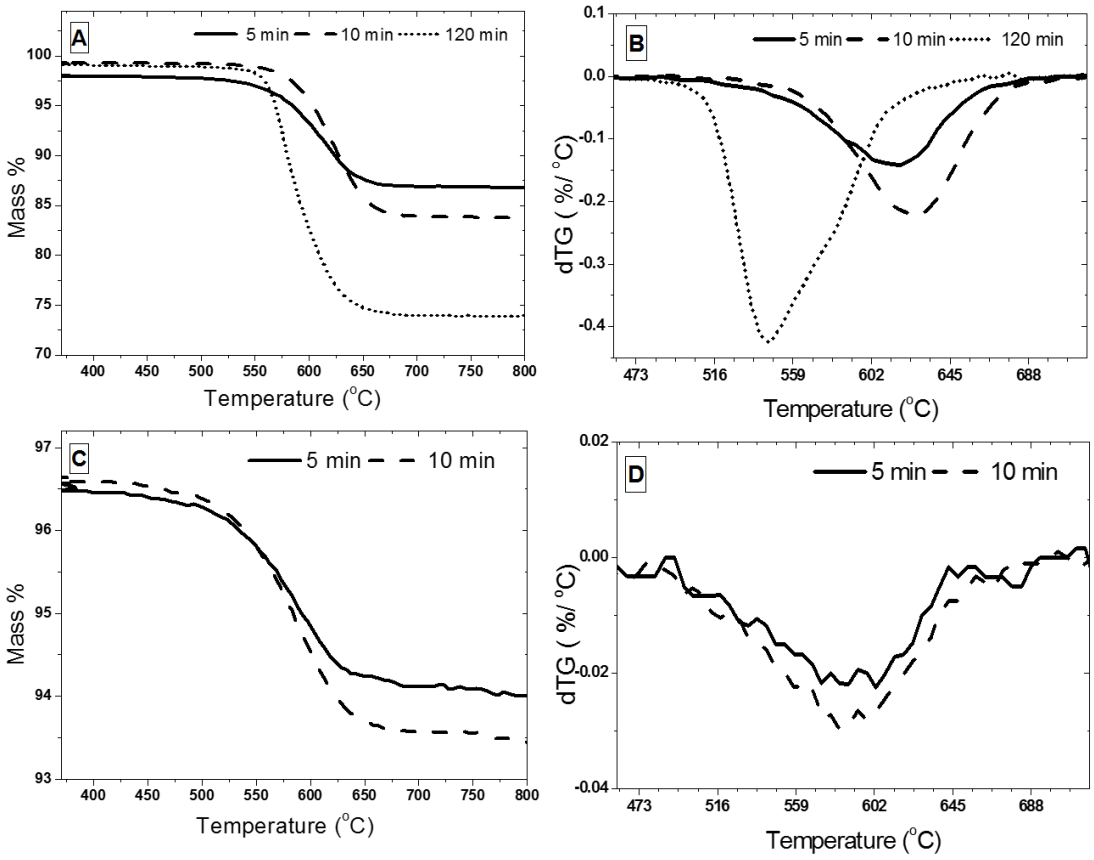

Figure 2-3: Thermo-gravimetric analysis in air up to 800°C of the spent HZSM-5 catalysts that were treated with 100% and 20% ethylene at 725°C under atmospheric pressure for the times-on-stream. A) TGA weight-loss curves of the 100% ethylene treated samples, B) Derivatives of the TGA weight-loss curves of the 100% ethylene treated samples, C) TGA weight-loss curves of the 20% ethylene treated samples, and D) Derivatives of the TGA weight-loss curves of the 20% ethylene treated samples.

Table 2-2: The amount and elemental analysis of coke deposited on the spent catalysts that were treated with 100% and 20% ethylene at 725°C under atmospheric pressure for various times-on-stream, as obtained from TGA and CHN elemental analysis.

Sample ID	TGA analysis		CHN analysis		
	Weight loss wt. %	Carbon formation rate (wt.%/min)	% C [a] wt. %	% H [a] wt. %	Atomic ratio (H/C)
SC20-5	2.22	0.45	2.14 ± 0.04	0.76 ± 0.03	4.09
SC20-10	2.88	0.29	2.54 ± 0.04	0.63 ± 0.02	2.98
SC100-5	10.79	2.15	10.55 ± 0.4	0.62 ± 0.01	0.69
SC100-10	15.27	1.53	14.62 ± 0.0	0.32 ± 0.01	0.26
SC100-120	25.02	0.21	23.6 ± 1.4	0.18 ± 0.2	0.09

[a] corrected hydrogen content by TGA

The amount of coke deposited during the reaction was determined from the TGA curves in Figure 2-3 and is summarized in Table 2-2. The value of coke content in Table 2-2 showed an increase with reaction time-on-stream (SC20-10 > SC20-5) and ethylene concentration (SC100-5 > SC20-5). The rate of coke formation was higher at short reaction time-on-stream (5 min) and decreased with increasing time. Interestingly, coke formation continued even after the catalyst lost activity towards aromatization, though at a slower rate, suggesting ethylene reaction persists with the existing coke structure, as similarly reported by Speybroeck et al. [98]. (It is a possibility that the coke formation may have ceased at some point between the time-on-stream of 10 and 120 min since no samples were taken in this interval).

The elemental carbon and hydrogen contents of the spent samples are also reported in Table 2-2. As can be seen from the data in Table 2-2, the H/C atomic ratio decreases with increasing time-on-stream, which indicates that the coke structure undergoes graphitization,

as reported previously [88]. Further, the samples treated with 100% ethylene concentration showed lower H/C ratios, strongly suggesting the increased presence of graphitic coke over the samples compared to the samples treated with 20% (SC20-5 and SC20-10). The used samples seemed to have strongly absorbed moisture, as H/C ratio was beyond 4 (max. atomic ratio by hydrocarbon).

2.6 Changes to HZSM-5 catalyst during use:

The electron microscopy images showing morphological details of the fresh and spent HZMS-5 samples are given in Figure 2-4. The ZSM-5 crystallite is a box-shaped particle with a size between 120-160 nm, similar to what is reported in the literature [115]. The sharp edges underscore the good crystallinity of the fresh catalyst, which was retained during use, over the period examined, despite the accumulation of carbon (as shown in TEM images).

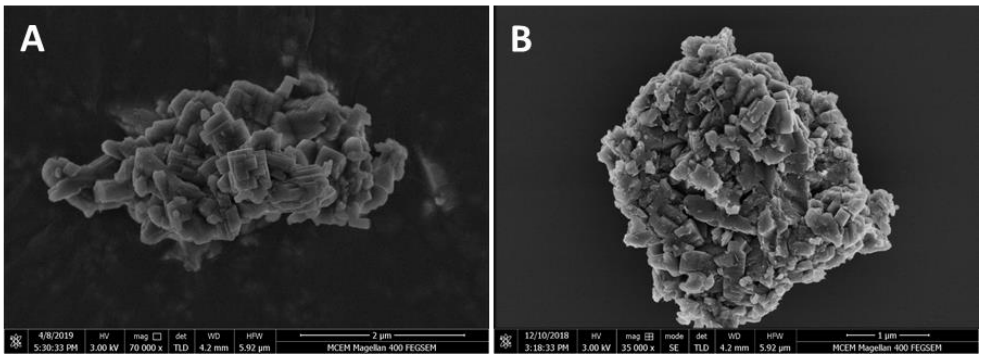

Figure 2-4: SEM images of (A) fresh HZSM-5 catalyst, and B) Spent HZSM-5 catalyst that was treated with 100% ethylene for 10 min. Sample (B) was coated with 0.7 nm of Ir.

Figure 2-5 shows the N_2 adsorption isotherm profiles of fresh and used HZSM-5 samples. For those samples exhibiting appreciable adsorption, these are type IV isotherms, confirming the presence of micropores. The hysteresis is indicative of some mesoporosity. The

micropore volume of the fresh sample was highest, and this volume progressively decreases with coke formation, indicating coke accumulation within pores.

Table **2-3** presents a summary of the surface area (calculated by BET method) and single point pore volume (obtained from isotherm data at P/P0 = 0.99), and pore volume between 17-3000 Å (calculated using BJH methods). The order of N_2 uptake is as follows: SC100-120 = SC100-10 < SC100-5 < SC20-10 = SC20-5 < FC. This indicate that coke structures occupy the micropores. The calculated BET surface area and pore volume of the fresh catalyst (303.9 m^2/g and 0.209 cm^3/g), decreased rapidly with time-on-stream for 100% ethylene feed, and at a much slower rate for the 20% ethylene feed. (The difference between the results for 5 and 10 min on stream is slight and within estimated experimental error). The near zero value of BET surface area at 10 min and above time-on-stream indicates complete pore blockage, making the catalyst useless.

Table 2-3: Summary of surface area and pore volume as calculated from the N_2 adsorption isotherms for the fresh HZSM-5 and for the spent HZSM-5 catalysts that were treated with ethylene concentrations of 100% and 20% at 725°C under atmospheric pressure for time-on-stream as noted.

Sample	SA_{BET} (m^2/g)	SPV (at P/P0 =0.99) (cm^3/g)	CPV_{BJH} (17-3000 Å) (cm^3/g)
Fresh HZSM-5	303.9 ± 7.3	0.209	0.081
SC20-5	232.1 ± 6	0.195	0.061
SC20-10	242.3 ± 6	0.197	0.062
SC100-5	67.2 ± 2	0.071	0.042
SC100-10	3.1 ± 0.2	0.028	0.029
SC100-120	1.1 ± 0.2	0.025	0.027

SA_{BET} = surface area estimated from BET theory

SPV = single point pore volume observed at P/P0 =0.99

CPV_{BJH} = cumulative pore volume estimated by BJH theory between 17-3000 Å

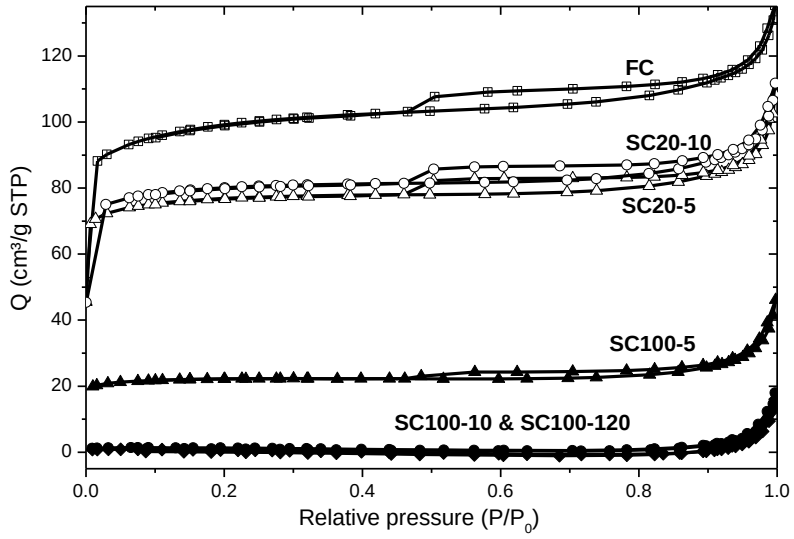

1

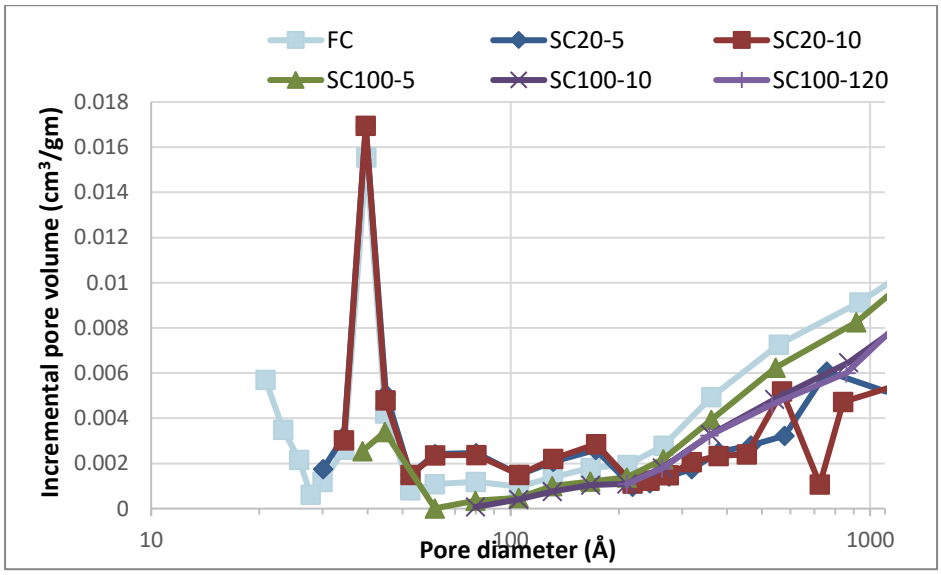

2

3 **Figure 2-5:** N_2 adsorption isotherm profile and BJH plot at 196°C for the fresh catalyst
4 (open square with cross symbol line) and spent HZSM-5 catalysts that were reacted with
5 100% ethylene (closed symbol lines) and 20% ethylene (open symbol lines) at 725°C under
6 atmospheric pressure for time-on-stream as noted.

7 The site density of Brønsted and Lewis acid sites, as calculated from equation 2-1 and 2-2,
8 is reported in Table 2-4. The calculated values suggest that maximum pyridine adsorption

was observed on the fresh HZSM-5 sample, indicating that the number of accessible acid sites for the reaction was greater for the fresh than for the used catalyst samples. The samples (SC20-5 and SC20-10) treated with 20% ethylene feed showed a 40-42% and 17-27 % decrease in the density of Brønsted and Lewis acid sites, at 5 and 10 minutes of reaction time-on-stream, respectively. A similar decrease of the acid site density due to coke deposition was reported by Lui et al. [33]. Further, for the used catalysts treated with 100% ethylene, the decrease was found to be so great that almost no pyridine was adsorbed on them (and could not be quantified).

Table 2-4: Density of Brønsted and Lewis acid sites as estimated from pyridine-adsorbed FTIR spectroscopy for the fresh HZSM-5 and the spent HZSM-5 catalysts that were treated with 20% ethylene at 725°C under atmospheric pressure for times-on-stream as noted.

Sample	Brønsted acid site (μmol/g)	Brønsted acid site (%)	Lewis acid site (μmol/g)	Lewis acid site (%)
Fresh HZSM-5	455.8	100	134.5	100
SC20-5	269.5	59.2	112.7	83.5
SC20-10	280.5	61.4	99.2	73.8

2.7 Graphitic and amorphous coke formations:

The SC20-10 and SC100-10 samples were observed under a transmission electron microscope to ascertain the changes to the coke structure (Figure 2-6). Figure 2-6 (A.1, and A.3) suggest that the coke species formed on the HZSM-5 sample treated with 100% ethylene was a combination of layered and amorphous coke. The thickness of the layered coke varies

between 3-12 nm (Figure 2-6 (A.1)). This layered coke was identified as graphitic, as the d-spacing of 0.33-0.35 nm corresponds to the (002) plane of graphite (Figure 2-6 (A.2)) [116,117]. Interestingly, it can be observed that in an instance of increased d-spacing beyond 0.38 nm, an additional layer builds-up retaining the original lattice spacing. Near the point of these dislocations, some sp3 carbon atoms (and associated additional hydrogen atoms) must exist to accommodate the irregularity and incorporation of additional carbon layers [118].

In Figure 2-6 (A.3), carbonaceous deposits lacking any obvious crystalline form can be seen; these are referred to as amorphous coke [119]. These forms of coke deposits were visible as progressive fronts and sometimes encapsulated by graphitic layers, such that they may be progressing towards further layers of graphitic coke. In contrast to the 100% ethylene treated sample, no layered graphitic coke was seen on the surface of ZSM-5 treated with 20% ethylene, in the region imaged. From Figure 2-6 (B.1 and B.2), a weak signal probably due to coke was observed on the surface, which could be a hint of coke species progressing towards graphitic coke as in the 100% ethylene treated sample.

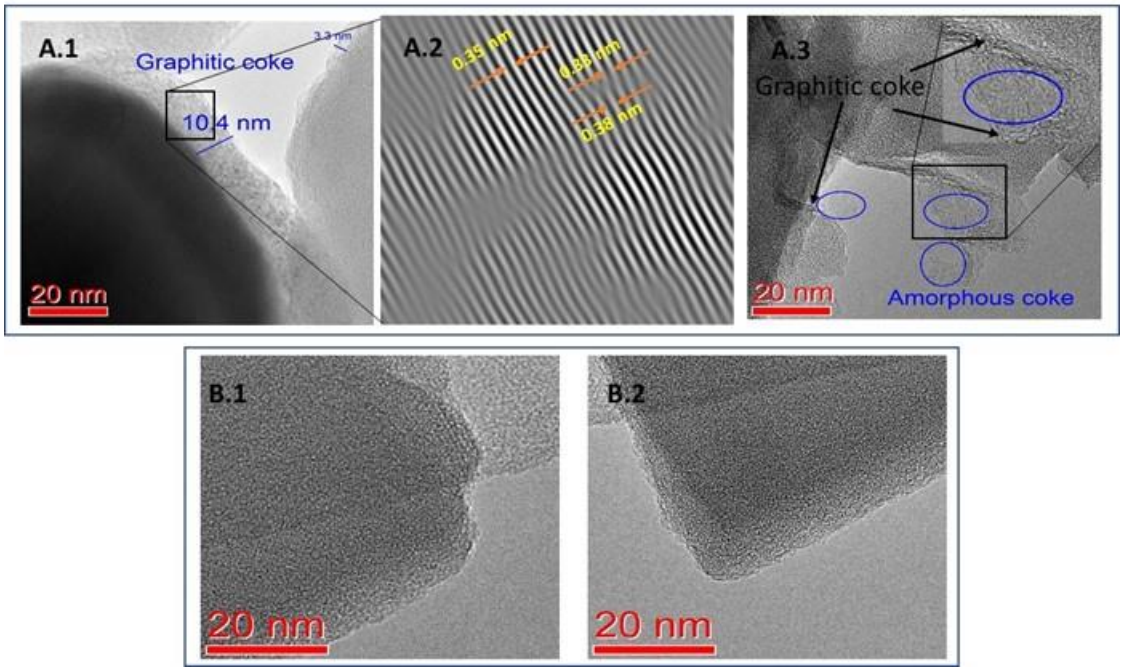

Figure 2-6: TEM of spent HZSM-5 catalyst recovered after 10 min of reaction time-on-stream (A) 100% ethylene feed [A.1: Raw image, A.2: Post-process image of the squared section in A.1, and A.3: Raw image], and B) 20% ethylene feed [B.1 and B.2 are raw images]. Amorphous coke in 100% ethylene treated samples are indicated by circles.

The chemical nature of the carbonaceous deposits on the used catalyst samples was studied by Raman spectroscopy, and the spectra are shown in Figure 2-7. Eight (8) peaks were fitted in the region of interest (1100-1700 cm^{-1}) and classified as graphitic (G), valley (V), disordered (D), and side (S) bands following previous studies [120,121]. As each of these peaks represents a different carbonaceous form, the presence of several fitted peaks highlights the chemical complexity of the coke formed during the reaction.

The peaks observed in the region between 1580-1640 cm^{-1} relate to C=C sp^2 stretch vibration in graphite, which is labeled as the 'G' (graphitic) band. As the vibration in the G band originates from condensed aromatic rings (1580-1600 cm^{-1}), as well as olefinic chains

(1600-1640 cm^{-1}), changes in the position of this maximum can provide further information on the coke structure. It can be seen from Figure 2-7 that the samples treated with 100% ethylene for short times (SC100-5 and SC100-10) had the G-band peak position at < 1600 cm^{-1} (suggesting dominance by polyaromatic hydrocarbons), whereas for other samples (SC100-120, SC20-5 and SC20-10) it was at > 1600 cm^{-1} (suggesting dominance by olefinic hydrocarbon chains that had not been able to fully aromatize).

Table 2-5: Summary of band's areas between 1100-1700 cm^{-1} as estimated by Gaussian peak fitting (R2 > 0.98) using OriginPro-8 software for the Raman spectra between of the spent HZSM-5 catalysts that were treated with ethylene concentration of 100% and 20% at 725°C under atmospheric pressure for the times-on-stream as noted.

Sample	Band				D/G ratio
	G	V	D	S	
	1580-1640 (cm^{-1})	1390-1580 (cm^{-1})	1275-1390 (cm^{-1})	1150-1250 (cm^{-1})	
SC20-5	0.58	0.13	0.15	0.15	0.25
SC20-10	0.71	0.08	0.15	0.06	0.21
SC100-5	0.56	0.21	0.13	0.1	0.23
SC100-10	0.61	0.22	0.07	0.09	0.12
SC100-120	0.48	0.2	0.25	0.07	0.52

The 1275-1390 cm^{-1} region of Raman spectra is generally referred to as the 'D' (disordered carbon) band. A standard peak position in this range, at 1310 cm^{-1}, is assigned to the alternate ring stretching vibration of benzene [122]. But, as can be seen in Figure 2-7, the

band position in the used samples was at a higher value (1364 cm^{-1}). This suggests aromatic clusters have been incorporated into hydrogenated carbon structures [120].

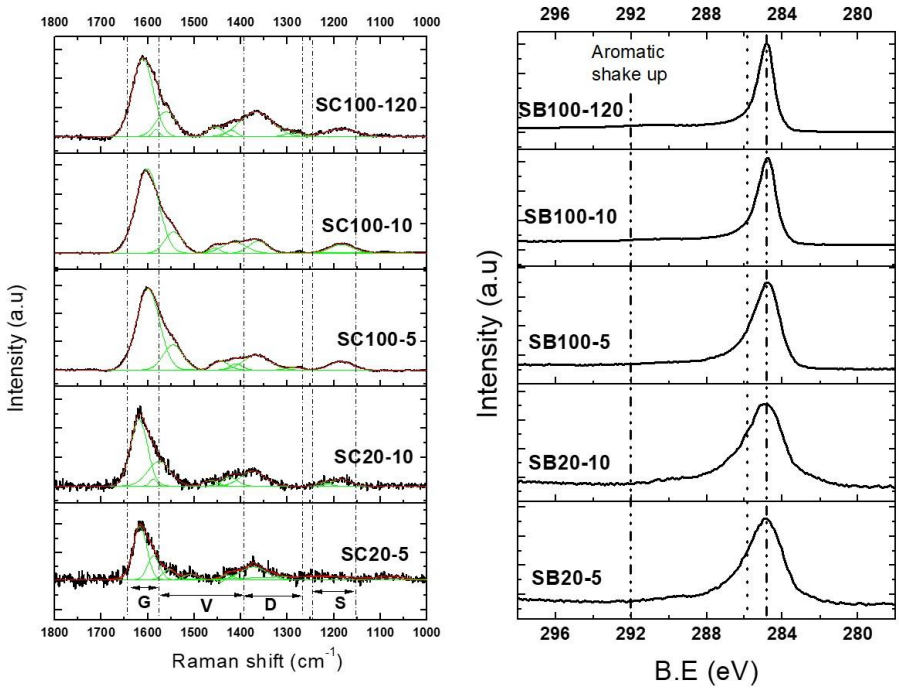

Figure 2-7: Raman (left) and X-ray photoelectron (right) spectra of the spent HZSM-5 catalysts that were treated with ethylene concentrations of 100% and 20% at 725°C under atmospheric pressure for times-on-stream as noted. Green lines within the Raman spectra indicate the Gaussian peak fitting using OriginPro-8 of the respective bands and red lines indicate the overall fitting. The vertical lines on the XPS spectra (right) highlight the sp2 graphitic carbon at 284.8 eV, oxygenated hydrocarbon C-O bonding at 286.2 eV (particularly evident in the 20% ethylene treated catalyst samples), and aromatic shake-up at 292 eV [123].

The fractional area contribution of the G and D bands and their ratio for the used samples are detailed in Table 2-5. The D/G ratio was lower in the 100% ethylene treated samples (SC100-10 < SC20-10) suggesting that coke formation was much more ordered (graphitic) [124]. Further, in the short period used samples, the ordering increased with reaction time-on-

stream due to progressive graphitization, probably facilitated by the accessibility of acid sites on the zeolite surface. However, the D/G ratio in the extended duration sample (SC100-120) was much higher, suggesting an increased contribution of the disordered coke. In this case, the acid sites are covered and hence no longer available to promote graphitization of the coke, which continued to accumulate as a consequence of ethylene addition.

Multiple (fitted) peaks were observed between 1390-1580 cm^{-1}, which are assigned to mono and di-alkylated ethylene vibrations at 1420 cm^{-1} [125], semicircle stretch of benzyl or polyaromatic structures at 1465 cm^{-1} [125], and aromatics with 3-5 rings at 1540 cm^{-1} [126]; these are collectively referred to as the 'V' (valley) band. As this band suggests a fusion of multiple benzene rings, it can be understood as an intermediate stage of graphitic coke development or pre-graphitic coke.

As can be seen from Table 2-5, the contribution of the 'V' band during initial reaction time was higher in the samples treated with pure ethylene (SC20-5 < SC100-5), which is an indication that polyaromatic formation has started and will potentially form graphitic coke with further increase in time. A stable band contribution in 100% ethylene treated samples with reaction time-on-stream (SC100-5 ≈ SC100-10 ≈ SC100-120), suggests that much of the newly formed coke had not been graphitized in these cases. The decrease in the fractional area of the 'V' band with increased reaction time-on-stream in the samples treated with 20% ethylene (SC20-10 < SC20-5), suggested a much higher rate of transformation of amorphous coke to graphite.

A weak peak at 1180 cm^{-1} was observed in Figure 2-7, which was labeled as the 'S' (side) band, and is indicative of C-C of hydroaromatic compounds, C-H in aromatic species and/or

aliphatic branched chain compounds of aromatic rings [$C_{aromatic}$-$C_{aliphatic}$] [120,121,127]. The peak areas from Table 2-5 show that the S band's contribution was significant at short reaction time (5 min) on samples treated with 20% ethylene (SC100-5), suggesting their presence as an intermediate stage in coke formation.

Table 2-6 presents the surface composition of the fresh and spent HZSM-5 catalysts as determined by XPS. The fresh HZSM-5 sample was included because it was expected that a certain level of adventitious carbon would be present on the surface prior to any reactions having taken place. The data show an increased deposition of surface carbon with time-on-stream and ethylene concentration, from a baseline level of approx. 11 % (fresh catalyst) to a maximum of 93.4% carbon in the case of the extended duration catalyst sample (SC100-120). It should be noted that, while these values show a clear trend in the amount of carbon, a direct correlation cannot be made, since the coke deposition thickness on the surface may vary to some extent accounting to a different number of atom detection in the measured layer (thickness of 10 nm)[128]. It is possible that (at least some of) the coke species formed during the reaction were within the pores or bulk of HZSM-5 (beyond 10 nm), and hence not detectable by XPS.

As the concentration of C increased the signals for the catalyst components (Si, Al, O) all decreased in intensity as the HZSM-5 surface was increasingly buried underneath a layer of deposited coke. The Si/Al ratio showed negligible change with reaction, consistent with zeolite stability. The C 1s high-resolution spectra are shown in Figure 2-7. All spectra display an asymmetry with a distinct high BE tail which confirms the presence of sp2 (graphitic) carbon. Particularly for the samples treated with 100% ethylene, the graphitic nature of the deposited coke species on the surface of HZSM-5 is evident in the sharp and narrow C 1s

core line as well as the characteristic tail up to approx. 292 eV [129] due to aromatic shake-up. The catalyst samples treated with 20% ethylene displayed a much broader core line at 284.6 eV and a less pronounced high BE tail at 292 eV, indicating a substantial fraction of aliphatic carbon (also possibly partially oxidized) and less aromatic carbon, respectively [123].

Table 2-6: Surface composition (relative atomic percent) determined by XPS analysis of the fresh HZSM-5 and the spent HZSM-5 catalysts that were treated with 100% and 20% ethylene at 725°C under atmospheric pressure for times-on-stream as noted.

Sample	Element				
	Si	Al	O	C	N
Fresh HZSM-5	26.3	2.3	60.1	10.6	0.8
SC20-5	25.8	2.3	59.1	12.2	0.6
SC20-10	25.4	2.3	58.2	13.4	0.7
SC100-5	21.2	2.1	46.6	29.6	0.4
SC100-10	13	1.3	26.8	58.6	0.3
SC100-120	1.7	0.2	4.4	93.4	0.3

A CO_2 adsorption study was performed to calculate the porosity due to coke species, as it was suspected that the coke formed in the study could have ultra-micropores which might not be detectable by the nitrogen adsorption data [130]. Table 2-7 shows the micropore surface area and the monolayer volume of the samples calculated by the Dubinin-Radushkevich (DR) theory. The sample micropore surface area decreased in the following order: Fresh HZSM-5 > SC20-5 > SC20-10 > SC100-120 > SC100-5 > SC100-10. The surface and monolayer volume of the short duration used samples decreased with reaction time. The decrease was

greater for samples treated with 100% ethylene, indicating an increased formation of condensed coke structure such as polyaromatic hydrocarbons. However, after prolonged use (SC100-120), the CO_2 surface area increased, indicating the creation of micropores, consistent with the development of disordered carbon as implied by Raman spectroscopy.

Table 2-7: Summary of estimated micropore surface area and micropore volume in the fresh HZSM-5 and spent HZSM-5 catalyst treated with 100% and 20% ethylene at 725°C under atmospheric pressure for time-on-stream as obtained from CO_2 adsorption-desorption isotherms.

Sample	Micropore surface area (m^2/g)	Micropore volume (cm^3/g)
Fresh HZSM-5	461.9	0.016
SC20-5	382.7	0.019
SC20-10	366.2	0.020
SC100-5	134.5	0.054
SC100-10	43.8	0.167
SC100-120	167.1	0.044

A powder X-ray diffraction (PXRD) study was performed to observe structural changes during the reaction and is reported in Figure 2-8. The diffraction pattern of fresh HZSM-5 was validated as that of orthorhombic ZSM-5 [131]. For HZSM-5 treated with dilute ethylene feed, the ZSM-5 structure did not show any changes, which is an indication of the structure stability. However, intense peaks at 2Θ = 26.7, 45.2, and 51.4 26.5°, 44.6º, and 50.7º (Figure 2-8.A) representing the (002), (101), and (102) planes of graphite were observed in the

catalysts treated with 100% ethylene, validating the presence of graphitic crystallites in the used samples. Interestingly, with the formation of graphitic coke, some ZSM-5 peaks disappeared (for SC100-5, SC100-10, and SC100-120), such that the resultant XRD pattern resembled Silicalite-1 [131] (Figure 2-8.B and 7.C). However, the diffraction patterns of the samples after regeneration (Figure 2-8.D, 7.E, and 7.F) confirmed the revival of ZSM-5 structure after coke removal, suggesting that the graphite formation induces mechanical strain to the zeolite cages and that this is relieved upon regeneration. The ZSM-5 the peaks at low 2theta (9.8° and 13.2°) values observed at shift of <0.1°, which could be due to manual error during analysis, retention of some strain in the ZSM-5 matrix, or minor dealumination as suggested by Hoff et al. [132].

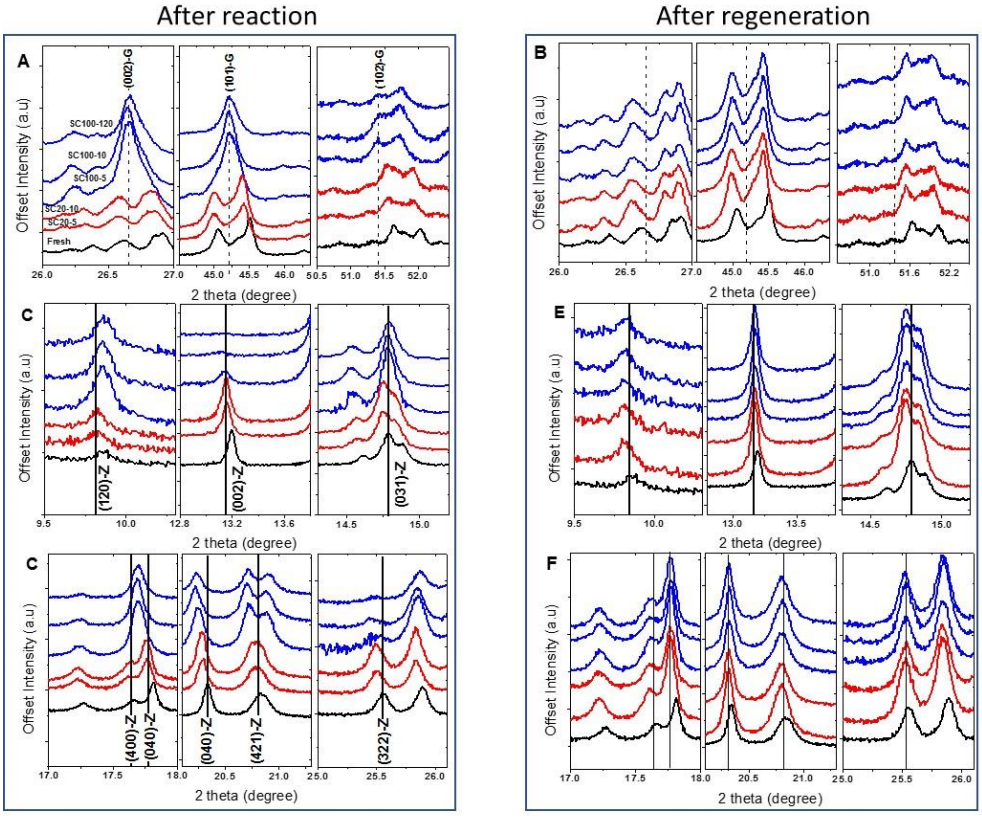

Figure 2-8: Powder XRD spectra of the fresh HZSM-5 (black line), spent HZSM-5, and HZSM-5 catalyst after regeneration. The spent catalyst had been treated with 20% (red lines) and 100% (blue lines) ethylene at 725°C under atmospheric pressure for the respective time-on-stream and regenerated with air to 650°C. The sample names are marked on the plot (A), The same order from top to bottom is repeated in (B-F). A, B, and C highlight regions of XRD for spent catalysts and D, E and F highlight the same regions for after regenerated catalysts.

2.8 Summary and Conclusion:

During short reaction times (0-10 min), aromatic hydrocarbons formed with high selectivity (selectivity to benzene > naphthalene > trimethylbenzene > p-xylene). Methane was also observed as a major product of the reaction during this period. As the reaction progressed, graphitic carbon began to build-up on the catalyst surface and the formation of these compounds waned. The rate of carbon content build-up on the surface was higher at higher concentration of ethylene in the feed. Since aromatization of methane proceeds via ethylene, this study has confirmed that ethylene does lead to the build-up of carbonaceous deposits (coke) on HZSM-5 under reaction conditions that are similar to those used for the conversion of methane to aromatics.

The TEM and XPS data, in conjunction with the Raman spectra, indicated that a relatively high proportion of amorphous coke formed at short reaction times, and that part of this coke then transforms into more condensed graphitic coke by dehydrogenation. It is surmised that the rate of carbon formation depends on the availability of coke free zeolite cages with available acid sites, and therefore, decreases as the formation of condensed coke structures

block the pores and active sites. After the zeolite pores are substantially filled and the acid sites substantially covered, the coke that continues to build-up on the surface becomes microporous in nature and tends to remain amorphous. This microporous coke is more reactive and more readily oxidized away in air, as indicated by TGA studies.

The coke accumulation beyond the zeolite pore volume, begins to induce mechanical strain on the zeolite cages, as evidenced by the disappearance of some of the characteristic ZSM-5 diffraction peaks, such that the diffraction pattern appears more like that of Silicalite-1. Regeneration (complete oxidation) restores the ZSM-5 to its original form.

Chapter 3 Changes in the catalyst state and morphology during different stages of MDA reaction

This chapter details the state of molybdenum during the course of carburization, reaction, and regeneration. The reaction performance of molybdenum supported on HZSM-5 and SiO_2 samples to dimerize methane to ethylene was studied. The effect of catalyst time-on-stream on the state of the catalyst was investigated.

Molybdenum supported on HZSM-5 was prepared by the wet impregnation method, and molybdenum on SiO_2 support was prepared by physical mixing. Both samples, however, were calcined and carburized at same conditions and tested for its catalytic performance in a quartz tubular packed bed reactor with an online gas chromatography set-up to continuously monitor the reaction product. The test was carried out at 725^{o}C under atmospheric pressure for varied reaction time-on-stream. Fresh and used samples were characterized by N_2 adsorption, scanning electron microscopy, transmission electron microscopy and synchrotron powder X-ray diffraction studies to understand the effect of reaction on the surface areas and pore volumes, morphology, and structure of HZSM-5 and Mo species. The used samples were also analyzed with thermogravimetric analysis and X-ray photoelectron spectroscopy to quantify the amount of molybdenum carbide and coke formation, and their respective oxidation states.

It was observed from the catalytic test that sample without Mo and HZSM-5 showed no activity towards the reaction, which confirmed a dependency on the availability of both, the Brønsted acidic sites of HZSM-5 and molybdenum carbide, for catalytic action. Catalyst characterization suggested that molybdenum oxide gets partially converted to molybdenum carbide during carburization, and extensively converted to molybdenum carbide during the reaction. The formation of coke during the reaction was observed to encapsulate the molybdenum particles. These coke structures were removed by oxidation at high temperature. However, it was observed that the molybdenum particles were sensitive to oxidation at high temperature as they agglomerated and smeared over the surface. Thereby, it can be interpreted that oxidizing Mo/HZSM-5 catalyst at high temperature must be avoided as it might harm the catalytic sites.

3.1 Introduction

Annually, an average of 140 billion cubic meters of natural gas is burned producing 300 million tons of CO_2 [13]. Moreover, due to technical difficulties and infrastructure at the offshore fields, excess natural gas is often vented directly to the atmosphere. If valuable aromatic intermediates can be produced from the relatively inexpensive natural gas, this would solve both the problems of natural gas utilization and carbon emissions. The direct aromatization of methane has attracted a lot of interest in this context. Molybdenum on HZSM-5 has been shown to be an effective catalyst for this reaction, but several challenges remain with respect to catalyst activation and deactivation, which are the major stumbling blocks to the commercialization of the process.

The catalyst undergoes a series of changes during the reaction, with respect to the oxidation state of Mo, conversion from oxide to carbidic form, changes in the catalyst structure and function due to coke deposition, etc. Therefore, the optimal operation of the process depends critically on identifying a suitable window in which carburization is (at least substantially) complete while carbon formation is not encouraged. For identification of this window depends on understanding the forms of Mo and mechanisms of reaction and carbon formation that gets deposited on it, their propensity of interconversion, and their relative abilities to deactivate the catalyst. The present study is a contribution to understanding these changes.

The reaction has been extensively investigated following the seminal work on the selective conversion of methane to benzene using Mo/HZSM-5 catalyst under the non-oxidative conditions by Wang et al. [133] in 1993. This reaction is believed to involve the following steps:

a carburization of the molybdenum species anchored on HZSM-5, methane adsorption and activation on the carburized molybdenum site at the high temperatures (700-900ºC) employed, leading to the formation of ethylene from methane, and aromatization with the involvement of the Brønsted acidic sites function in HZSM-5. While it is generally believed that methane dimerization happens on molybdenum carbide, there are indications that the support plays a vital role in methane activation, as molybdenum carbide by itself, seems to have poor methane conversion ability [48]. However, the dispersion of molybdenum carbide within the zeolite channels, the many changes that the catalyst undergoes during the reaction, and rapid coke deposition over the catalyst during reaction make it difficult to gain insights into the catalytic mechanism.

In the present study, molybdenum supported on HZSM-5 and on SiO_2 were compared for their catalytic behavior. SiO_2, which has virtually no Brønsted acidity, was chosen as a relatively inert support for molybdenum, for comparison with HZSM-5, the proven support. Extensive characterization of samples recovered after calcination, carburization, reaction, and regeneration stages has been carried out to study changes in the structural, morphological, and chemical state of molybdenum during the course of the reaction.

3.2 Materials and methods

3.2.1 Catalyst preparation

3.2.1.1 Synthesis of 5%Mo/H-ZSM5 (MoZ) catalyst

The synthesis of 5%Mo/H-ZSM5 was carried out using the wet impregnation method as detailed in the literature [22,26,38,55,56,134]. Firstly, NH_4-ZSM-5 (Si/Al = 11.5) obtained from

Zeolyst International Inc. was calcined at 510°C in a flow of air for 6 h to remove NH_3 and form HZSM-5. A calculated quantity of 83.3 % ammonium heptamolybdate (AHM) $[[NH_4]_6[Mo_7O_{24}].4H_2O]$, obtained from Sigma Aldrich, was dissolved in a measured quantity of water. The HZMS-5 powder was slowly added to the AHM solution to form a paste while stirring at 300 rpm for 2 h. The pH of the paste was maintained at 4-5 by adding ammonia as a buffer. The excess water was removed by evaporation in a hot bath maintained at 95°C for 3 h, at a stirring speed of 300 rpm. The dried mixture was calcined in a flow of air at 510°C for 16 hours to form 5% Mo/HZSM-5 or MoZ which was pelletized by application of a pressure of 98 KPa using a hydraulic press (Kimaya engineers, India). These pellets were crushed and sieved to obtain particles of 250-500 micron.

3.2.1.2 Synthesis of molybdenum supported on SiO_2 samples (SiMo3, SiMo2, and SiMoAHM)

A calculated quantity of the precursor (MoO_3, MoO_2, and AHM obtained from Sigma Aldrich), corresponding to the desired molybdenum loading of 5%, was mechanically mixed with the SiO_2 support obtained from Evonik Industries, AEROSIL®, using a mortar-and-pestle. The mixed sample was calcined in the flow of air at 510°C for 16 hours to obtain *SiMo3, SiMo2, and SiMoAHM*. The calcined powder was pelletized, crushed and sieved accordingly, to obtain particles of 250-500 micron.

3.2.2 Reactor set-up, gas analysis, and catalyst testing

The catalyst activity test was carried out in a quartz tubular reactor (8 mm diameter). The schematic of the set-up is shown in Figure 3-1. The tubular reactor was loaded with 2 g of the required catalyst sample to form a catalyst bed. Quartz wool was placed on either side of

the catalyst bed for supporting the sample's weight. The sample-loaded reactor was placed in the known constant heating zone of a furnace.

The sample was preheated from room temperature to 725°C at 10°C/min under atmospheric pressure in a nitrogen flow of 200 ml/min (STP). The flow was then switched to a 1: 9 mixture of methane and hydrogen for 1 h for carburization of the molybdenum. Following the carburization, the flow was switched to 100% methane gas for the reaction. The feed gas hourly space velocity (GHSV) during the reaction was 6000 ml/g/h.

A Varian 450-GC (Agilent Technologies, California, U.S.A) online gas chromatography system equipped with silica capillary columns (*Petrocol-DH50 (Sigma Aldrich) and carboxen-1010PLOT (Sigma Aldrich))* was used to continuously analyze the products in outlet. The system was equipped with a thermal conductivity detector (TCD) and a flame ionization detector (FID). The overall methane conversion and products selectivity were calculated from equation described in Appendix A (Equation A.1.1 and A.1.2).

All synthesized samples (MoZ, SiMo3, SiMo2, and SiMoAHM) were tested for a reaction time-on-stream of 65 min. Additionally, the MoZ sample was tested for a reaction time-on-stream of 15, 25, and 45 min to understand the progressive change to the state and function of the catalyst. Also, SiO_2 and HZSM-5 supports were tested in blank experiments.

After the respective reaction time-on-stream, the reactor was cooled to room temperature in a minimal flow of nitrogen (20 ml/min @STP), and the catalyst sample was recovered for further characterization. Also, samples were cooled and recovered in nitrogen following to carburization stage for further characterization and comparison.

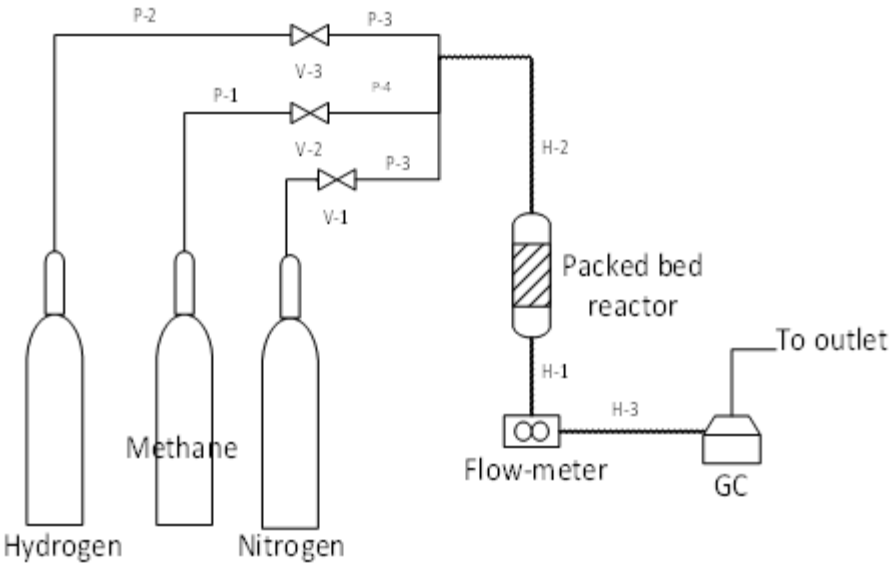

Figure 3-1: Schematic of the experimental set up used for the catalytic test.

3.2.3 Catalyst regeneration:

About 30-50 gm of the spent MoZ sample was taken in an alumina crucible and oxidized in a furnace (CM Rapid Temp Box Furnace, Bloomfield, New Jersey, USA) in air at 400ºC, 600ºC, and 800ºC, respectively. The heating sequence was: ramp heating at 5ºC/min from room temperature to the required temperature (400ºC, 600ºC, or 800ºC), followed by an isothermal hold for 10 min, and ramp cooling from the respective temperature to the room temperature at 10ºC/min.

The following nomenclature scheme was used for the catalyst samples analyzed: F, C, and U are used to indicate fresh, carburized, and used samples, respectively and the others are indicated as follows: R600-U-MoZ-XX: 600 represents the temperature of regeneration to which the 5% Mo/HZSM-5 sample used for XX min was treated.

3.3 Characterization techniques

The high-resolution X-Ray diffraction (XRD) pattern of the fresh and used samples was collected using the powder X-Ray diffraction beamline at the Australian Synchrotron. The analysis was carried out in a borosilicate capillary (Hilgenberg GmbH, Germany) of 0.7 mm diameter containing 2-5 mg sample. The X-ray beam with an energy of 17 keV (λ = 0.74 Å) was targeted on the sample during the analysis, while the capillary was rotated from 0-360º. The diffraction pattern between a 2theta of 2-80° was recorded using a high-resolution Mythen detector [135]. The pattern was collected in pair at an offset of 0.5° to eliminate the gap in the Mythen detector. The recorded pair of diffraction patterns were merged using PDViper software and converted to the equivalent of Cu Kα wavelength (λ = 1.54 Å) using CMPR toolbox software [136]. The database of zeolite structures [131] and the Inorganic Crystal Structure Database (ICSD) [137] was used to identify the planes of different crystalline phases within the sample.

A NETZSCH 1000 TG-DSC analyzer was used to study the oxidation behavior of the samples recovered after use by thermogravimetric analysis (TGA). About 15-20 mg of sample was taken in an alumina crucible for the analysis. For the used molybdenum on SiO_2 samples, the analysis was done by heating from room temperature to 350ºC at 20ºC/min, and from 350-1100°C at 10ºC/min in air. For the used MoZ samples, the analysis was done by heating from room temperature to 700ºC at a rate of 5°C/min in air with 10 isothermal periods of 10 min each. An isothermal period at 120 °C was used to achieve moisture removal; subsequent isothermal periods at 300°C, 350°C, 400°C, 450°C, 500°C, 550°C, 600°C, 650°C, and 700°C were used to study the oxidation of the molybdenum species and coke.

An AXIS Nova spectrometer (Kratos Analytical Inc., Manchester, UK) was used to perform X-ray photoelectron spectroscopy (XPS) analysis of the fresh and the recovered MoZ sample after reaction and regeneration. A monochromated Al Kα source at a power of 180 W (15 kV, 12 mA) was employed. The hemispherical analyzer operating in the fixed analyzer transmission mode at a standard aperture of analysis area 0.3 mm x 0.7 mm was used and the survey spectra were acquired at pass energy of 160 eV. The total pressure in the main vacuum chamber was typically between 10^{-7} and 10^{-6} Pa. The high-resolution spectra were recorded from individual peaks at 40 eV pass energy (yielding a typical peak width for polymers of < 1.0 eV). The samples were filled into the shallow wells of a custom-built sample holder and analyzed at a nominal photoelectron emission angle of 0º w.r.t. the surface normal. The sampling depth may range from 0-10 nm, as the actual emission angle is ill-defined for particles and powders (ranging from 0º to 90º). The CasaXPS processing software version 2.3.15 (Casa Software Ltd., Teignmouth, UK) was used to identify the elements from the survey spectra, and calculate their atomic concentrations using the integral peak intensities and the manufacturer supplied sensitivity factors.

A Tecnai T20 TWIN instrument was operated at 200 kV to obtain transmission electron micrographs of the MoZ samples recovered after carburization, reaction, and regeneration. About 5 mg of the sample was dispersed in butanol, sonicated, and dried on a holey carbon-coated copper grid. The post-processing on the selected region of the image was done by using Fourier transform (FT) and inverse FT with a data smoothing of 5. The Digital Microscopy suite (Gatan Inc) software interface was used for this purpose. The identity of the element in the sample was confirmed by energy dispersive X-ray analysis (EDX).

The back-scattered electron (BSE) image of the recovered MoZ samples after carburization, reaction, and regeneration was collected on a FEI Magellan 400 field emission gun (FEG) scanning electron microscope (SEM). The imaging was conducted at BSE mode with 0.5 kV landing energy without stage bias. The size distribution of the molybdenum particles on the sample's surface was estimated by recording the size of several particles and performing a Gaussian distribution fitting using ImageJ and OriginPro 8 software, respectively.

The N_2 adsorption isotherms of the fresh and the used samples (SiMo3, SiMo2, SiMoAHM, and MoZ) were collected using a Tristar II 3020 gas-sorption analyzer (Micromeritics Instruments Corporation, Georgia, U.S.A) with liquid nitrogen at -196°C. A vacuum degasser system VacPrep-061 (Micromeritics Instruments Corporation, Georgia, U.S.A) was used to remove moisture and adsorbed contaminants from the sample by degassing overnight at 120 °C under vacuum (7 Pa) and backfilling with nitrogen gas (STP) upon cooling. Calculation of surface area was accomplished using the Brunauer-Emmett-Teller (BET) theory [103]. The cumulative pore volume between 17-3000 Å contributed by mesopores was calculated by using Barrett-Joyner-Halenda (BJH) theory [104], the total volume was estimated directly from the desorption data, and the difference between the two is estimated micropore volume.

3.4 Results and Discussion

3.4.1 Catalyst activity studies: role of support in the methane dimerization step

The activity tests on the supports (SiO_2 and HZSM-5) and on the molybdenum supported on the SiO_2 and HZSM-5 supports (SiMo3, SiMo2, SiMoAHM, and MoZ) were conducted in a tubular packed bed reactor. Figure 3-2 shows the results. It was observed that the support materials alone (SiO_2 and HZSM-5) failed to activate and dimerize methane to ethylene, as previously reported in the literature [138]. Molybdenum supported on SiO_2 samples (SiMo3, SiMo2, and SiMoAHM) also failed to convert methane at the conditions tested, also consistent with literature reports [139,140]. The MoZ sample, however, did convert methane under the same reaction conditions and following the same pretreatment. This suggests that methane activation requires the presence of both HZSM-5 and molybdenum carbide sites.

The maximum methane conversion on the MoZ sample was about 11% (which may be compared with the thermodynamic equilibrium conversion of 15% at this temperature [19]) and was achieved only at the beginning of the reaction time-on-stream. This indicates that enough molybdenum carbide sites were present at the start of reaction or within a short time of reaction. The decreasing conversion with increasing reaction time-on-stream suggests rapid deactivation of the catalyst due to coke formation. It was observed that the methane conversion falls to about 8% in a short while (25 min), and keeps progressive decreasing. In addition to decreasing conversion, the catalyst deactivation also affected the products selectivity, as the selectivity of benzene decreases. However, the selectivity towards ethylene

seemed to increase slightly similar to what is reported in the literature[25,34,48], which highlights that ethylene to aromatic formation slowed with ZSM-5 pores blocked by coke species.

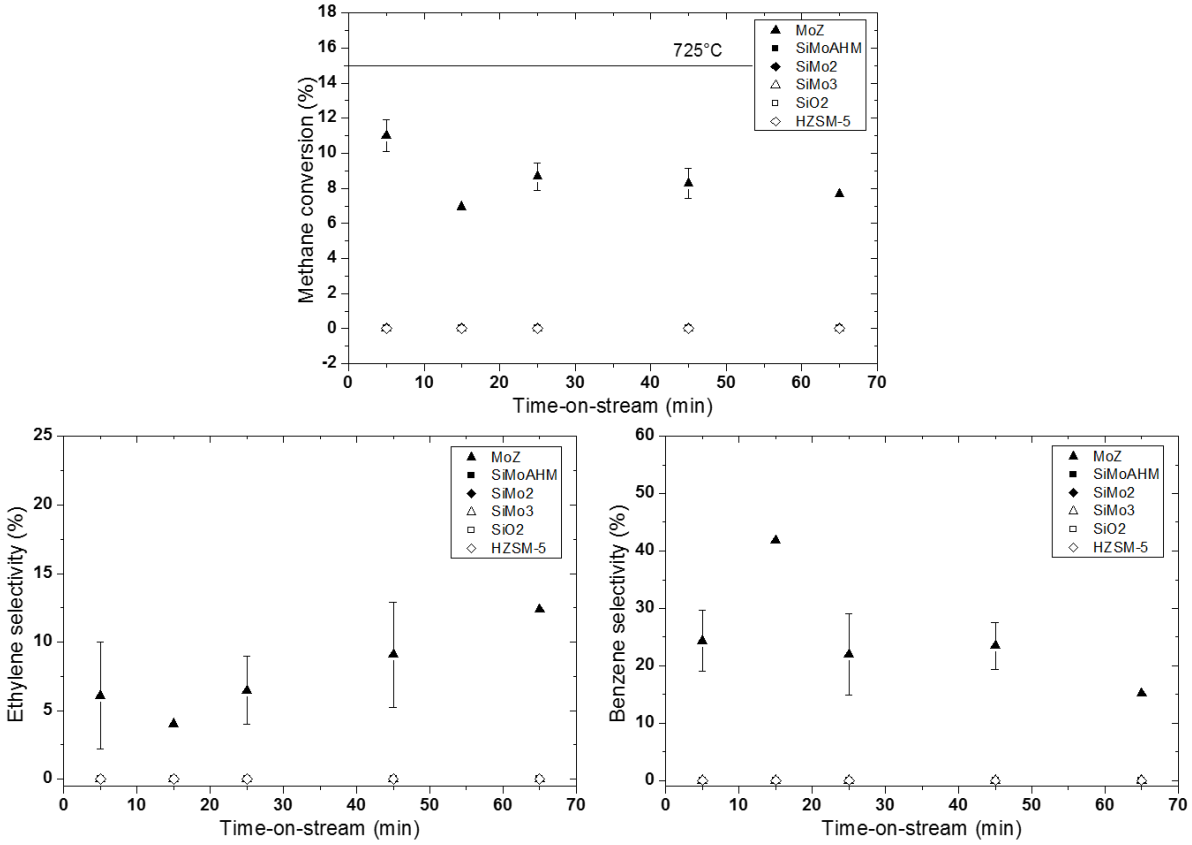

Figure 3-2: Catalyst activity study for methane direct aromatization to ethylene and benzene on the sample as marked. (A) Overall methane conversion, (B) ethylene selectivity, and C) benzene selectivity. Error bars represent the standard error (Se) of multiple data points estimated by $s_e = \frac{\sigma}{N^{0.5}}$ where, N = sample size, σ = standard deviation. Data without error bars were single data. The line represents the maximum equilibrium conversion at the respective temperature [28].

3.4.2 Changes experienced by the catalyst during reaction

3.4.2.1 Effects on the pores and surface area of the samples after use:

Table 3-1 compares the surface area and micropore volume of the different catalysts before and after reaction. It was observed that fresh MoZ sample was highly microporous, whereas SiMo3, SiMo2, and SiMoAHM samples were mesoporous. The data showed that the fresh samples had much higher BET surface areas and micropore volumes than the samples after use, which indicated that pore filling occurred during use. A decrease in the surface area of 85 m^2/g and micropore volume of 0.5 cm^3/g was observed for MoZ sample, could be due to the effects of coke formation and/or molybdenum carburization.

Table 3-1: Summary of estimated micropore surface area and micropore volume in the fresh and the used molybdenum supported samples treated with a methane flow of 6000 ml/g/h at 725°C under atmospheric pressure for 65 min time-on-stream as obtained from N_2 adsorption-desorption isotherms.

Sample	BET Surface area (m^2/g)		Total pore volume (at P/P0 =0.99) (cm^3/g)		BJH cumulative pore volume (between 17-3000 Å) (cm^3/g)		micropore volume (cm^3/g)	
	F	U [a]	F	U [a]	F	U [a]	F	U [a]
MoZ	252.5 ± 6.1	167.2 ± 4	0.17	0.13	0.05	0.06	0.12	0.07
SiMo3	111.8 ± 1.3	27 ± 0.5	0.74	0.18	0.74	0.14	0.01	0.04
SiMo2	115.5 ± 1.3	34.9 ± 0.5	0.74	0.35	0.74	0.32	0.01	0.03
SiMoAHM	114 ± 1.4	40.7 ± 0.7	0.66	0.34	0.66	0.31	0.00	0.03

[a] 65 min of reaction time-on-stream

For the SiMo3, SiMo2, and SiMoAHM samples, the decrease in the surface area was 75-85 m^2/g, despite the fact that hardly any methane conversion or coke formation occurred. Further, the mesopore volume was affected with use, probably indicating a rearrangement of the SiO_2 structure upon treatment at the high temperature of reaction in addition to the carburization of molybdenum.

3.4.3 Structural changes in the catalyst due to reaction

The powder X-ray diffraction (XRD) technique was employed to probe the structural details and the state of molybdenum on HZSM-5 and SiO_2 supports after use. The XRD pattern of fresh SiO_2 and HZSM-5 supports are shown in Figure 3-3.A and 3.B (blue lines) for reference. The pattern for HZSM5 matches that of orthorhombic ZSM-5 (Database of Zeolite structures [141]) indicating that the HZSM-5 support was highly crystalline. Also, it was observed that the crystallinity of HZSM-5 was retained throughout molybdenum impregnation and reaction, as its diffraction peaks were unaffected. The SiO_2 support, however, was amorphous.

The fresh samples (F-MoZ, F-SiMo3, F-SiMo2, and F-SiMoAHM) in Figure 3-3 show diffraction peaks related to molybdenum oxides (MoO_2 and MoO_3), which is an indication of phase transformation from the molybdenum precursors (MoO_3, MoO_2 or AHM). The respective reactions are given in equations 3-1-3-4 [41,50,51]. Interestingly, the intermediate phases ($MoO_{2.5}$ and Mo_4O_{11}) were not observed in the diffraction patterns possibly due to their short-life. The diffractograms of the used samples (U-MoZ, U-SiMo3, U-SiMo2, and U-SiMoAHM) in Figure 3-3 show that the peak intensity of the MoO_3 phase decreases during the reaction, and concurrently, the peak intensity of the Mo_2C species which is weak seems

increases. The weak peak corresponds to the fact that the concentration of Mo_2C species is very low (about 3-3.5%, from XPS analysis). The carburization of molybdenum species, and the associated reaction is given in 3-5 and 3-6 [52]. Again, as for the calcination step, the extent of carburization of molybdenum does not seem to be significantly affected by the precursors and supports.

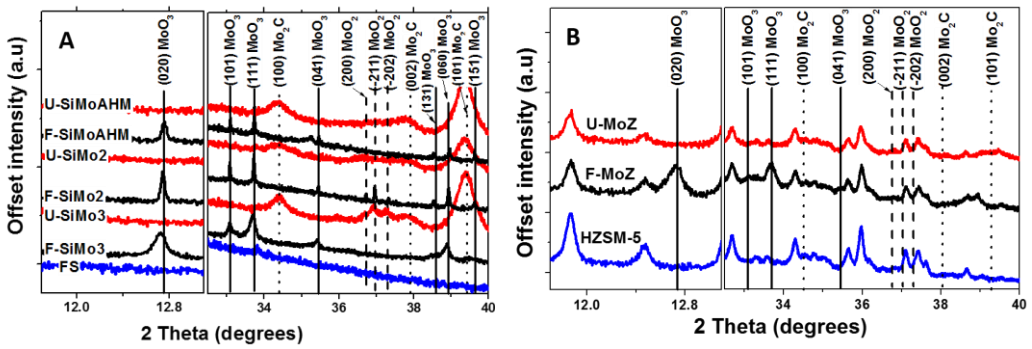

Figure 3-3: Powder X-ray diffraction patterns of the fresh (black) and used (red) molybdenum supported on SiO_2 (A) and molybdenum supported on HZSM-5 (B) as marked. The used samples were treated with a methane flow rate of 6000 ml/g/h for 65 min at 725°C under atmospheric pressure. The patterns for fresh SiO_2 and HZSM-5 (blue lines) were collected for reference. (Planes representing MoO_3, MoO_2, and Mo_2C are highlighted by solid, dash, and dotted lines, respectively).

$$[NH_4]_6[Mo_7O_{24}] \rightleftarrows 7\,MoO_{2.5}(OH)_{0.5} + \frac{5}{4}\,H_2O + 6\,NH_3 + \frac{7}{8}\,O_2 \qquad \text{3-1 [41]}$$

$$MoO_{2.5}(OH)_{0.5} + \frac{1}{8}O_2 \rightleftarrows MoO_3 + \frac{1}{4}H_2O \uparrow \qquad \text{3-2 [41]}$$

$$4MoO_3 + H_2 \rightleftarrows Mo_4O_{11} + H_2O \uparrow \qquad \text{3-3 [50,51]}$$

$$Mo_4O_{11} + 3H_2 \rightleftarrows 4MoO_2 + 3H_2O \nearrow \quad \text{3-4}$$

$$MoO_3 + \frac{1}{2}CH_4 \rightleftarrows MoO_2 + \frac{1}{2}CO_2 \nearrow + H_2 \nearrow \quad \text{3-5 [52]}$$

$$MoO_2 + \frac{3}{2}CH_4 \rightleftarrows \frac{1}{2}Mo_2C + CO_2 \nearrow + 3H_2 \nearrow \quad \text{3-6 [52]}$$

3.4.4 Chemical changes to molybdenum species during calcination, carburization, reaction, and regeneration:

The X-ray photoelectron spectra of the fresh and recovered (after carburization, reaction, and regeneration) MoZ samples were collected to identify the relative surface concentrations of the elements as well as their chemical states. The Mo 3d region of the spectra is shown in Figure 3-4, which highlights three oxidation states of molybdenum (+2, +4, and +6). Figure 3-4 shows there is a gradual shift in the molybdenum oxidation state, from high to low with carburization and reaction, and from low to high with regeneration. The relative atomic composition and the relative molybdenum distribution were estimated by curve-fitting the spectra. The values from the curve-fitting are presented in

Table 3-2, which suggests a dominant presence of MoO_3 species (about 70%) and MoO_2 species (30%) in the fresh sample. This molybdenum distribution is however near the catalyst's surface (up to 10 nm). The presence of MoO_2 species in the fresh catalyst was surprisingly not reported in the earlier studies [48,142,143], but possible upon calcination, as molybdenum species diffuse within the ZSM-5 structure while interacting and occupying Bronsted acid sites[134]. It was also observed that adventitious carbon played no role in carburizing molybdenum, as the fresh sample had no carburized molybdenum phase.

Table 3-2: Summary of estimated atomic composition and molybdenum relative distribution of the fresh and recovered MoZ samples with the course of the reaction.

	Relative Mo atomic %			Atomic %				
	Mo^{+2}	Mo^{+4}	Mo^{+6}	Mo	Si	Al	O	C
Sample	228.3 eV	231 eV	232.8 eV	3d	2p	2p	1s	1s
F-MoZ	0.1	29.7	70.2	3.0	22.0	2.2	57.4	15.4
C-MoZ	20.5	25.7	53.8	2.0	24.4	2.7	59.3	11.6
U-MoZ-15	69.8	16.2	14.0	1.4	23.3	2.5	54.0	18.7
U-MoZ-25	61.1	19.7	19.2	0.9	23.6	2.2	56.3	17.0
U-MoZ-45	68.2	12.9	18.8	1.3	23.2	2.4	53.1	20.1
U-MoZ-65	71.3	11.6	17.1	1.5	22.3	2.6	52.0	21.7
R600-U-MoZ-15	0.1	19.3	80.5	4.1	20.5	2.3	53.2	19.9
R600-U-MoZ-25	0.0	13.9	86.1	2.2	25.3	1.8	59.6	11.1
R600-U-MoZ-45	0.0	16.7	83.3	2.5	23.6	2.1	57.5	14.3
R600-U-MoZ-65	0.1	17.2	82.8	3.7	21.6	2.1	56.4	16.2
R800-U-MoZ-65	0.0	17.4	82.6	1.5	25.8	2.0	60.4	10.3

A partial (about 20%) and gradual reduction of MoO_3 to Mo(+4) and Mo(+2) species occurred during the carburization stage. The Mo(+4) species present on this sample are possibly MoO_2 and molybdenum oxy-carbide, and the Mo(+2) species is Mo_2C as suggested in the literature [144]. Upon reaction, MoO_3 reduces more extensively (about 70%) to Mo_2C. It must also be noted here that, such an extensive reduction in the state of molybdenum occurred within a short span of 15 min reaction in 100% methane (U-MoZ-15) as compared to the 1 h of carburization (C-MoZ), which suggests that methane and hydrogen partial pressures are important factors in carburizing molybdenum. Also, at large times-on-stream, the content of carburized molybdenum was the same, suggesting that the maximum or complete carburization of molybdenum happened within the initial 15 min. Upon heating at 600ºC in

air, these molybdenum carbides oxidize back to Mo (6+) and Mo (+4) species alongside the removal of the carbon deposited.

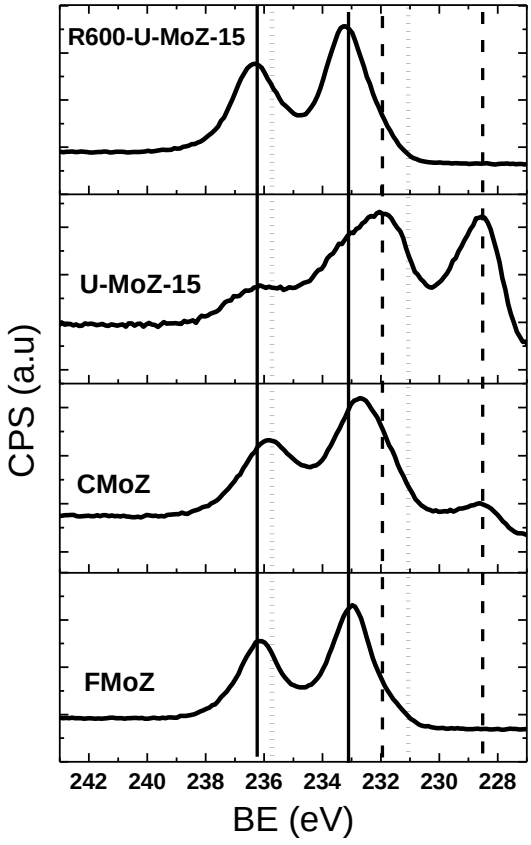

Figure 3-4: Mo 3d region of the X-ray photoelectron spectra of the MoZ samples during the course of reaction as indicated.

3.4.5 Thermogravimetric study to quantify molybdenum oxide and carbide species formed during reaction:

The oxidation behavior of the molybdenum carbide in the used SiMo3, SiMo2, SiMoAHM, and MoZ samples was studied by thermogravimetric analysis. The percentage weight gain between 300-400ºC, representing oxidation of Mo_2C to MoO_3 species [91,145], is

reported in Figure 3-5. The percentage increase in the weight of MoZ sample during oxidation was around 0.6-1.1% and for SiMo3, SiMo2, and SiMoAHM samples was around 1.1-1.25%. This weight increase was less than the estimated weight gain from the XPS data (1.6%), which suggests that coke species have been simultaneous removed by combustion.

$$Mo_2C + 4\,O_2 \rightleftarrows 2\,MoO_3 + CO_2 \nearrow$$ 3-7 [49,146,147]

$$C_xH_y + \left(\frac{y}{4} + x\right) O_2 \rightleftarrows \frac{y}{2}\,H_2O + x\,CO_2 \nearrow$$ 3-8 [49,146,147]

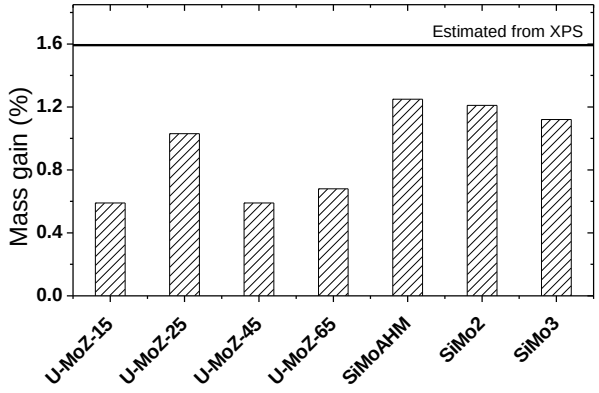

Figure 3-5: Summary of % mass gain observed during thermogravimetric analysis (<400ºC) of used 5% Mo/HZMS-5, SiMo3, SiMo2, and SiMoAHM samples that was recovered at respective time-on-stream of reaction after methane to benzene reaction at 6000 ml/g/h, 725°C, and under atmospheric pressure.

Lazlo et al [146] suggested that Mo_2C oxidizes by 1.) O_2 adsorption and dissociation on the respective Mo and C sites of Mo_2C ii.) oxidation of the top most carbide layer, and iii.) oxidation of layers within the bulk of the catalyst. CO, CO_2 and H_2O are observed as the reaction products [49]. Additionally, the formation of MoO_xC_y (molybdenum oxy-carbide)

species was found to be thermodynamically favorable by Likith et al. [147]. So, the reaction routes for Mo_2C oxidation can be described by Eq. 3-7 and 3-8.

3.4.6 Understanding the morphological changes to molybdenum species with carburization, reaction, and regeneration by electron microscopy (SEM and TEM) and energy dispersive X-ray (EDX) studies:

The recovered MoZ sample after carburization, reaction, and regeneration were studied by SEM analysis, and the respective micrographs are reported in Figure 3-6. The morphology of HZSM-5 crystallite as seen from these micrographs was box-shaped with a size of 100-160 nm, similar to a previous report (our studies, [148]). The crystallite's sharp edges, which reflect the crystallinity of HZSM-5, were retained during the course of the reaction, indicating that the structure was stable.

Over the HZSM-5 surface, several spherical particles were observed which were distributed evenly. These particles were relatively denser, and therefore, could be related to molybdenum. The size of molybdenum particles over the carburized MoZ sample was between 12-14 nm which was several times larger than its unit cell dimension of 0.3-0.47 nm (from XRD pattern PDF-card 00-035 0787 [149]), and therefore represents a cluster. The size of the cluster was not affected as the reaction progressed, indicating the stability of the carbide species. However, the molybdenum cluster did increase in size during oxidation at 600ºC in air, resulting into particles with an average size of 40-50 nm (nearly 2.5 times). An extended effect of this agglomeration was observed with the progressive oxidation at 800ºC (Figure 3-6). It can be seen that the molybdenum cluster no longer retained its spherical

morphology and has tended to ‘smear’ over the zeolite surface. Such a behavior could be due to the lack of binding or anchoring site which led to the spread of the molybdenum species over the surface.

Energy dispersive X-ray (EDX) spectrum images are shown in Figure 3-7 which highlights the distribution of Mo, C, Al, and Si on the carburized MoZ sample. The images reveal that Mo is distributed uniformly up to 400 nm thickness within the HZSM-5 structure, therefore, providing supporting evidence to the atomic distribution observed by XPS analysis (discussed above). Whilst it can be seen that Si, Al, and Mo were uniformly distributed throughout the sample, the elemental carbon seemed to be more concentrated near the edges or surface of the catalyst which are submerged below the cluster of molybdenum carbide particles. This indicates progressive molybdenum carburization and coke formation starting from the near-surface region of ZSM-5.

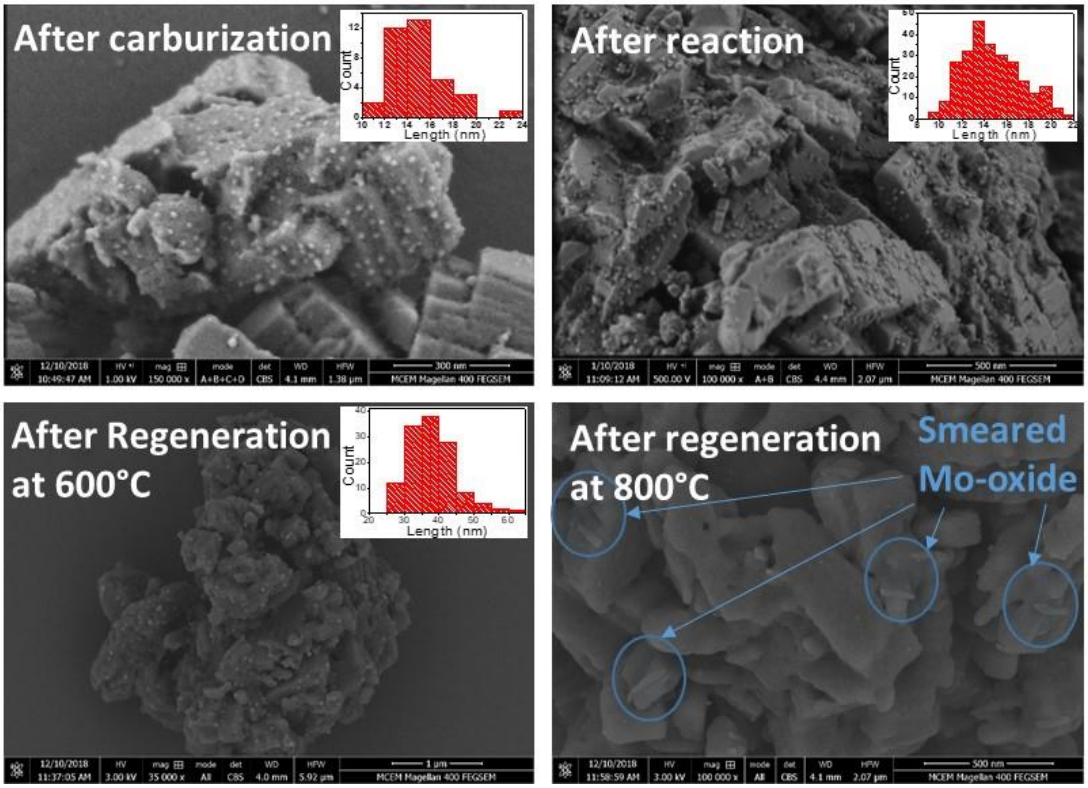

Figure 3-6: FEG-SEM image of the MoZ sample recovered after 1. carburization for 1 hr, 2. reaction for 1 h, at 725ºC, 6000GHSV, 3. Regeneration in oxygen at 600ºC, and 4. Regeneration in oxygen at 800ºC. Embedded within the images are the size distribution of the molybdenum particles that were present on the catalyst surface. Region highlighted by circles represent smeared molybdenum particles.

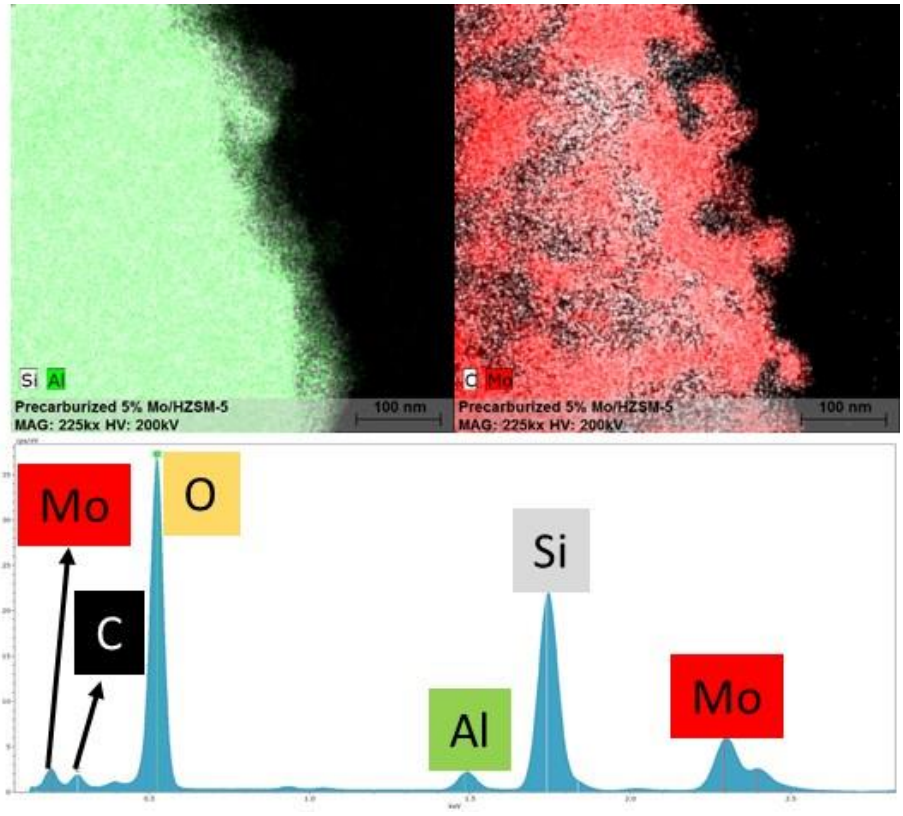

Figure 3-7: Elemental mapping and spectrum of the elements in the MoZ sample after carburization for 1 h at 725ºC under atmospheric pressure.

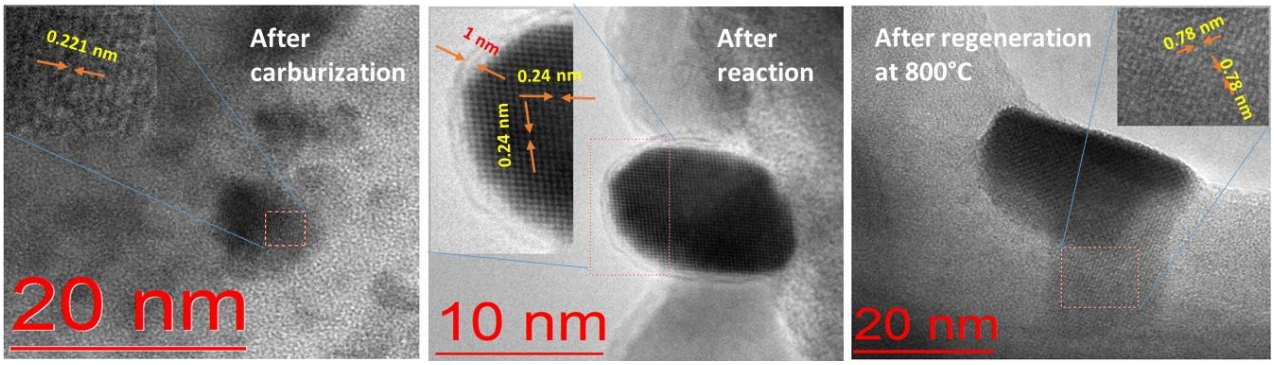

Figure 3-8: TEM images of 5% Mo/HZSM5 sample recovered after a particular stage of reaction as marked.

The transmission electron microscopy images of the carburized, used and regenerated MoZ samples are presented in Figure 3-8. The carburized (Figure 3-8) and used (Figure 3-8) samples showed a spherical to oval-shaped molybdenum cluster of size between 12-14 nm (similar to observed by SEM). The d-spacing of 0.21 nm and 0.24 nm associated with the (101) and (020) planes of orthorhombic molybdenum carbide (β-Mo2C) were observed [150–152]. Further, carbon depositions with a thickness of 1 nm were observed on the used sample, particularly around the neighborhood of the molybdenum cluster, which could be a possible reason for the catalyst deactivation [87]. The layered coke represents graphitic carbon, as the d-spacing of 0.36 nm corresponded to the (002) plane of graphite. The TEM image of the sample regenerated at 800ºC (Figure 3-8), confirmed the smearing of the molybdenum cluster over the surface of HZSM-5. However, though the morphology of the molybdenum cluster changed its crystallinity was retained, as the structure showed clear lattice spacing. The d-spacing of 0.78 nm was observed, which represented the (200) plane of MoO_3.

3.5 Conclusion:

The form of molybdenum in the fresh catalyst (after calcination) synthesized with MoO_3, MoO_2 and AHM precursors was mainly MoO_3 and MoO_2, which was distributed uniformly over the HZSM-5 support. A fraction of this (about 20%) MoO_3 carburized to Mo_2C during the carburization stage and participated in the reaction.

The study confirmed that molybdenum, by itself, cannot activate methane, and requires the participation of the acidic HZSM-5 support for MTB reaction. This activation process on Mo/HZSM-5 catalyst can be schematized in two stages: 1. Formation of an oxidic complex between molybdenum oxide and HZSM-5 structure during calcination 2. Transformation of the oxidic complex to carbidic complex upon contact with methane during carburization. As SiO_2 lacked the Brønsted acidic sites, methane dimerization was not possible on molybdenum supported on SiO_2.

The molybdenum carbide and coke contents increased with the reaction time-on-stream, thereby, leveraging the formation and consumption of the active sites. However, following complete carburization of the molybdenum species, the reaction conversion decreased monotonously as more and more active sites were surrounded by the increasing coke build-up.

The removal of coke by oxidizing in air simultaneously oxidized the molybdenum carbide species, therefore, to re-use the catalyst another carburization cycle would be needed to activate the catalyst. The oxidation at high temperature causes agglomeration and smearing of the molybdenum particles over the surface of HZSM-5.

The above conclusions were made based upon the average and macro changes to the supported molybdenum which are close to the surface. However, a fraction of the catalytically active Mo sites can be present inside the bulk of zeolite, which must be considered while correlating the catalyst's performance.

Chapter 4 Coke formation mechanism and its effect on the direct aromatization reaction on 5% Mo/HZSM-5 catalyst

This chapter presents an investigation on the nature, structure, and morphology of the resultant coke formed using methane as feed on Mo/HZSM-5 catalyst during MTB reaction. Three parameters *viz.* catalyst time-on-stream, space velocity, and reaction temperature were studied and their influence on coking and reaction conversion was observed.

The Mo/HZSM-5 catalyst was prepared by wet impregnating AHM on HZSM-5 support as described in the section 3.2 of Chapter 3. The prepared catalyst was tested for its catalytic activity in a tubular packed bed reactor. The catalyst was carburized for 65 min at 725ºC in a 1:9 mixture of methane and hydrogen prior to the reaction. The activity test was conducted at three temperatures *viz.* 725, 750, and 775ºC each at a methane gas hourly space velocity of 6000 and 9000 ml/g/h. 100% methane was used as feed and the used catalyst was recovered after a time-on-stream of 15, 25, 45, and 65 min, respectively. The spent Mo/HZSM-5 catalyst was recovered and characterized by N_2 adsorption, thermogravimetric analysis, X-ray photoelectron spectroscopy, Raman spectroscopy, transmission electron microscopy studies to understand the effect of reaction condition on the nature and characteristics of the coke species.

The study suggested that the nature of coke formed depended on the reaction condition. Also, the yield of ethylene and higher aromatic compounds played a vital role in the coke

formation. The nature of coke varied across the series of catalytic test and showed a trend in the formation of more graphitic coke with decreasing higher aromatics and more aromatic coke with decreasing ethylene yield fraction.

It was concluded that pure methane feed did not generate the complex nature of coke structures that were found using pure ethylene feed (Chapter 2), however, there was an indication of the coke being dependent on ethylene availability. The study advises that performing MTB reaction at lower reaction temperature and lower methane flow rate could be beneficial for the catalyst due to the ease of regeneration.

4.1 Introduction:

Natural gas is abundantly available, of which, an average of 140 billion cubic meters (bcm) is flared annually. This presents an opportunity to use natural gas as a chemical feedstock while minimizing the impact of flaring on the atmosphere. Methane to benzene (MTB) reaction via the non-oxidative route has gained attraction as a single step process to convert natural gas to aromatic compounds [1,153]. However, the reaction poses a number of challenges such as difficulty in activating the methane, thermodynamically limited reaction conversion [28], and rapid catalyst deactivation due to carbonaceous deposit formation. These difficulties need to be overcome to make this process technically feasible and commercially viable [102-100].

Molybdenum supported on HZSM-5, which was introduced by Wang et al. [133] in 1993, has been widely investigated for this reaction as a potential catalyst. But, this catalyst like all known catalyst studied to date, is prone to deactivation due to coke formation. It is generally considered that the activation of methane to ethylene occurs on molybdenum carbide

supported HZSM-5 and that the subsequent aromatization of ethylene utilizes the Brønsted acid sites of HZSM-5 (shown in chapters 1 and 2). Therefore, as the reaction progresses, the formation of coke structures covers or blocks these active sites, making them unavailable for further reaction unless they can be regenerated. A conventional approach to remove the coke and reactivate the catalyst is by subjecting the coked catalyst to oxidation at high temperatures. However, the conditions of regeneration must be wisely selected to avoid the concurrent destruction of the active sites. Thus, a better understanding of the coke that forms and its development when subjected to varied reaction conditions should be beneficial.

Earlier studies (shown in chapter 2, [99]) established that ethylene acts as a precursor for coke formation, and implied the importance of ethylene concentration and fresh Brønsted acid sites in coking. It was also suggested that the structure of the coke can be complex depending upon the ethylene concentration, as it may have variable fractions of hydrocarbon species (aliphatic and ring compounds, polyaromatics hydrocarbons (PAH), and graphitic). Further, prior studies which investigated coke formation during the direct aromatization reaction did not consider the transitory nature and evolutionary behavior of the coke and the precursors for its formation. Therefore, it was of interest to schematize the coke formation mechanism with reaction progression. Upon considering the aspects of scaling-up of the process such insights on coking would be a valuable piece in the overall process development.

This study attempted to understand the coking mechanism during methane aromatization reaction with pure methane as feed on the Mo/HZSM-5 catalyst. The reaction and coking experiments were trialed at varied reaction temperatures, catalyst time-on-stream, and methane flow rates to comprehend the coking mechanism and identify potential precursors.

Comprehensive post-reaction catalyst characterization was carried out to identify changes to the physical and chemical nature of the resultant coke and its impact on the reaction and catalyst.

4.2 Materials and methods:

4.2.1 Catalyst preparation

4.2.1.1 Synthesis of 5%Mo/H-ZSM5 catalyst:

The wet impregnation method was used to synthesis the 5%Mo/H-ZSM-5. The method employed was based on previous reports [22,26,38,55,56,134]. Specifically, the support was prepared by calcining NH_4-ZSM-5 (Si/Al = 11.5) (from Zeolyst International Inc.) in air at 510°C for 6 h. A calculated quantity of ammonium heptamolybdate (AHM) $[[NH_4]_6[Mo_7O_{24}].4H_2O]$ (from Sigma Aldrich) (corresponding to 5% by the weight of molybdenum) was dissolved in water and the solution was mixed with the after calcined NH_4-ZSM-5 to form a paste. The paste was maintained at a pH of 4-5. The excess water was then evaporated using a hot bath at 95°C for 3 h while stirring the solution at 300 rpm. Upon drying, the sample was calcined at 510°C for 16 h in air to result in 5% Mo/HZSM-5. This powder was recovered and pelletized at 98 KPa using a hydraulic press (from Kimaya engineers, India). The pellets were crushed and sieved to obtain particles of 250-500 micron.

4.2.2 Catalytic testing and reactor set-up

A downflow packed tubular reactor made of quartz was used to conduct the catalyst activity tests. 2 g of catalyst was loaded into the reactor and supported by quartz wool on

both ends. The sample-loaded reactor was then placed in the known heating zone of the furnace. A Varian 450-GC online gas chromatography system (Agilent Technologies, California, U.S.A) equipped with silica capillary columns (Petrocol-DH50 and Carboxen-1010PLOT, from Sigma Aldrich) and fitted with both a thermal conductivity detector (TCD) and a flame ionization detector (FID) was used to analyze the product gaseous stream. The schematic of the set-up is shown in Figure 3-1 (in chapter 3).

A nitrogen flow rate of 200 ml/min (at STP) was maintained while preheating the sample containing reactor from RT to 725°C. A heating ramp of 10°C/min was used. The gas flow was switched to a mixture of methane and hydrogen in a 1:9 ratio. This was continued for 1 h to enable carburization of the molybdenum oxide. Following carburization, the reactor was heated to the respective reaction temperatures (725ºC, 750ºC or 775ºC). The gas mixture was then substituted by 100% methane at a gas hourly space velocity (GHSV) of 6000 or 9000 ml/g/h, respectively. The catalyst testing was performed for a reaction times-on-stream of 15, 25, 45, and 65 min, following to which the reactor was cooled to RT in a minimal flow of nitrogen and the spent sample was recovered for further characterization. The overall methane conversion, products selectivity, and benzene aromatic selectivity were calculated from equation described in Appendix A (Equation A.1.1, A.1.2, and A.1.3). The samples recovered were named based on the following nomenclature scheme: F, C, and U were used to indicate fresh, carburized, and used samples, respectively. U-MoZ6: represents the sample treated with a methane feed rate of 6000 ml/g/h, and U-MoZ9: represents sample treated with a methane feed rate of 9000 ml/g/h.

4.2.3 Generating post-regeneration samples for ex-situ characterization:

The oxidation of used catalyst samples recovered after the catalytic study was carried out in a furnace (CM Rapid Temp Box Furnace, Bloomfield, New Jersey, USA) in air at 400ºC, 600ºC, and 800ºC, respectively. About 30-50 gm of the spent catalyst was taken in an alumina crucible and the furnace was operated in the following heating-cooling sequence: heating from room temperature to respective temperature (400ºC, 600ºC, and 800ºC) at 5ºC/min, isothermal heating for 10 min at the respective temperature, and cooling from the respective temperature to room temperature at 10ºC/min. For characterization purposes, these samples were named as RYYY-U-MoZ-XX to represent regeneration at YYYºC of the used 5% Mo/HZSM-5 reacted for XX time-on-stream.

4.3 Characterization techniques

A NETZSCH 1000 TG-DSC analyzer was used to study the oxidation behavior of the resultant coke on the used 5% Mo/HZSM-5 sample. 15-20 mg of the sample was taken in an alumina crucible and weight changes were recorded. The sample was ramp heated at 5°C/min from RT to 700ºC, but with intermittent isothermal periods of 10 min at each of 120 °C, 300°C, 350°C, 400°C, 450°C, 500°C, 550°C, 600°C, 650°C, and 700°C. This procedure was employed to better distinguish the oxidation propensity of molybdenum carbide and deposited coke species in various temperature regimes.

A Tristar II 3020 gas-sorption analyzer (Micromeritics Instruments Corporation) with liquid nitrogen at -196°C was used to estimate the surface area and micropore volume of the

fresh and used samples. Each sample was pretreated by heating at 120 °C under vacuum (7 Pa) for 8 h in a vacuum degasser system - VacPrep-061 (Micromeritics Instruments Corporation) to remove moisture and adsorbed species. Calculations of the surface area and cumulative micropore volume between 17-3000 Å were done on the collected isotherm data with the use of Brunauer-Emmett-Teller (BET) [103] and Barrett-Joyner-Halenda (BJH) theories [104], respectively. The total volume was estimated directly from the desorption data, and the difference in both is estimated micropore volume.

Raman spectroscopy study was conducted using an InVia Raman microscope (Renishaw) with a blue laser (488 nm) to obtain characteristic information of the carbon built on the used samples. 2-5 mg of catalyst was placed under the Raman microscope and observed at 50X lens magnification. The exposure time of 5-20 sec and the laser intensity power between 1-10% of maximum power were optimized and used to collect good quality Raman spectrum. The characteristic peaks associated with graphitic and disordered carbon structures were assigned with reference to an earlier published study [108]. These peaks were fitted using the OriginPro 8 software package and applying Gaussian peak shape distributions.

An AXIS Nova spectrometer (Kratos Analytical Inc., Manchester, UK) with a monochromated Al Kα source at a power of 180 W (15 kV, 12 mA), a hemispherical analyzer operating in the fixed analyzer transmission mode and the standard aperture (analysis area: 0.3 mm × 0.7 mm) was used to perform X-ray photoelectron spectroscopy (XPS) analysis of fresh, used and regenerated samples. The total pressure in the main vacuum chamber during analysis was between 10^{-7} and 10^{-6} Pa. Survey spectra were acquired at pass energy of 160 eV, and high-resolution spectra were recorded from individual peaks at 40 eV (yielding a typical peak width for polymers of < 1.0 eV). The samples were filled into shallow wells of

a custom-built sample holder and were analyzed at a nominal photoelectron emission angle of 0° to the surface normal. Since the actual emission angle is ill-defined in the case of particles and powders (ranging from 0° - 90°) the sampling depth may range from 0 nm to about 10 nm. The data processing was performed using CasaXPS processing software version 2.3.15 (Casa Software Ltd., Teignmouth, UK) with binding energy referenced to the C 1s peak at 284.8 eV. All elements present in the sample were identified from the survey spectra. The atomic concentrations of the detected elements were calculated using integral peak intensities and the sensitivity factors supplied by the manufacturer.

4.4 Results and Discussion

4.4.1 Catalyst activity studies

The conversion of methane versus reaction time-on-stream, methane flow rate and reaction temperature were evaluated and is reported in Figure 4-1. A maximum conversion of 11±0.8% was achieved at 725ºC and 6000 ml/g/h at short reaction times (15 min). This value is, however, less than the calculated maximum thermodynamic conversion (14.5% at 725ºC) [28]. The methane conversion increased a little with reaction temperature but was much farther from their respective thermodynamic conversions (horizontal lines in Figure 4-1.A), as around 13% maximum conversion was achieved upon reaction at 750ºC and at 775ºC.

Upon comparing the methane conversion with the methane flow rates of 6000 and 9000 ml/g/h, it was observed that the conversion value decreases with increasing methane feed rate, which suggests a possibility that the reaction might be limited by residence time to reach thermodynamic equilibrium or maybe prone for much more rapid coking. But, as shown by

Karakaya et al. [83], the residence times operated were sufficient for achieving thermodynamic conversion value.

The reaction products include ethylene, benzene, naphthalene, p-xylene, and hydrogen. The selectivity of ethylene, benzene, naphthalene and p-xylene, and the aromatic selectivity of benzene were calculated and presented in Figure 4-1. The selectivity of products included benzene > ethylene, naphthalene > p-xylene. The aromatic selectivity of benzene was generally between 85-92% (in one case 100%).

It can be observed from Figure 4-1 that benzene, naphthalene, and p-xylene selectivity was highest during short reaction times and decreases as the reaction progresses due to catalyst deactivation. The ethylene selectivity, on the other hand, increases a little with reaction time-on-stream validating that the pore and sites are partly available for it to move in and out, as suggested in the literature [82,83]. Therefore, it can be concluded that ethylene as a primary product, benzene as a secondary product, and higher aromatic compounds such as naphthalene and p-xylene as tertiary products of the reaction (methane→ ethylene →benzene →naphthalene, p-xylene).

Increasing the reaction temperature resulted in increased product selectivity as evidenced from Figure 4-1 which shows products selectivity increase with the increase of reaction temperature from 725ºC to 750ºC and 775ºC. Further, the products selectivity seems to increase a little (prominent at short reaction times) but fluctuates in some cases with increasing methane feed rate. Such a fluctuation in the product selectivity could be due to the due to different extent of coke formation and subsequent catalyst deactivation.

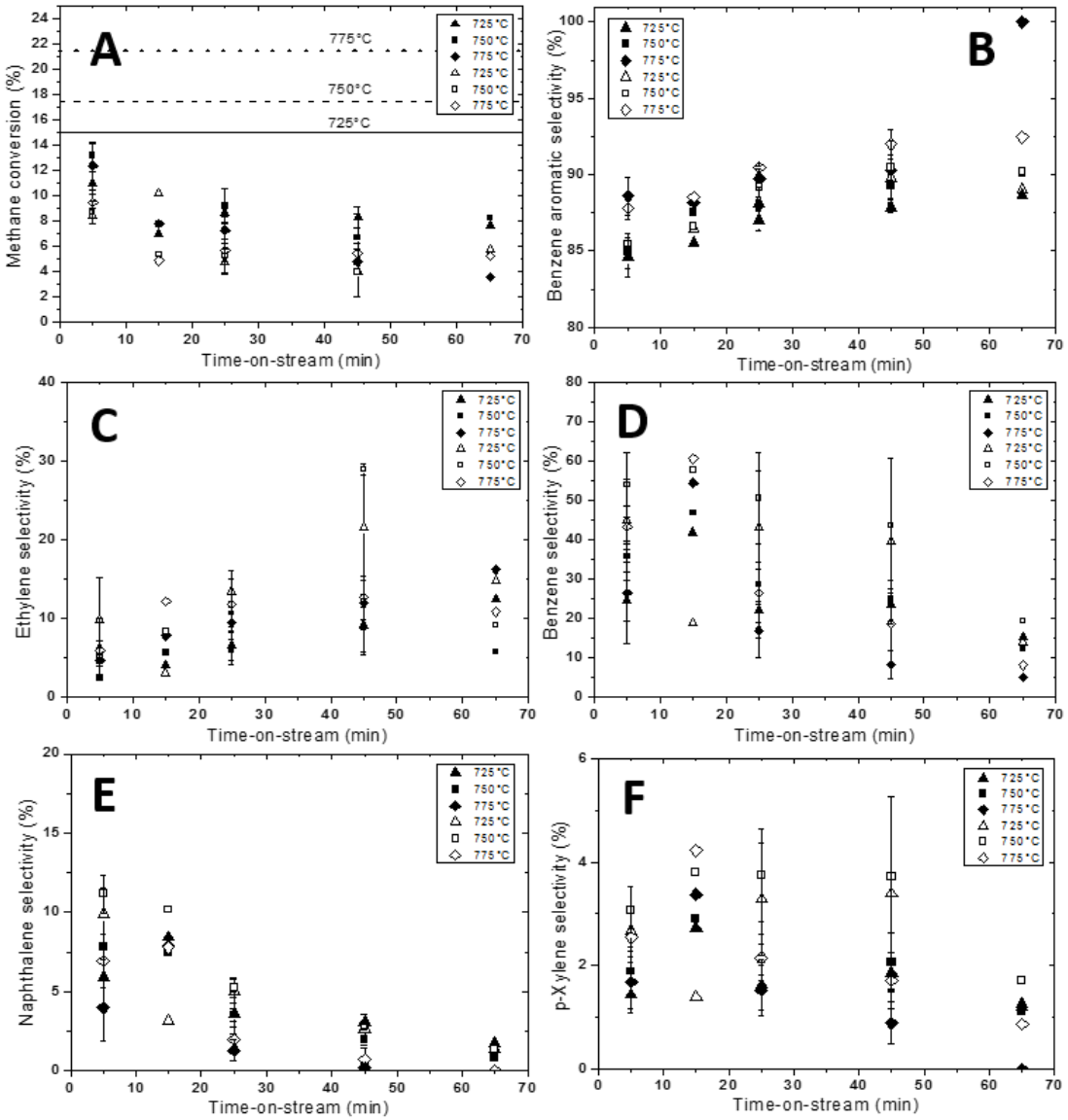

Figure 4-1: Catalyst activity study on 5% Mo/HZSM-5 during methane conversion to benzene. (A) Overall methane conversion and (B) aromatic selectivity of benzene, (C) ethylene selectivity, (D) benzene selectivity, (E) naphthalene selectivity, and (F) p-xylene selectivity. [Filled and open symbols represent data at a methane feed rate of 6000 and 9000 ml/g/h, respectively. Error bars represent the standard error (Se) of multiple data points estimated by $s_e = \frac{\sigma}{N^{0.5}}$ where, N = sample size, σ = standard deviation. Data without error

bars were single data. The line represents the maximum equilibrium conversion at the respective temperature [28].

4.4.2 Catalyst characterization

4.4.2.1 Nitrogen adsorption study:

Figure 2-5 compares the nitrogen adsorption isotherm of the fresh and the used 5%Mo/HZSM-5 catalyst samples. The isotherm profile was of type IV, which confirmed the presence of micropores.

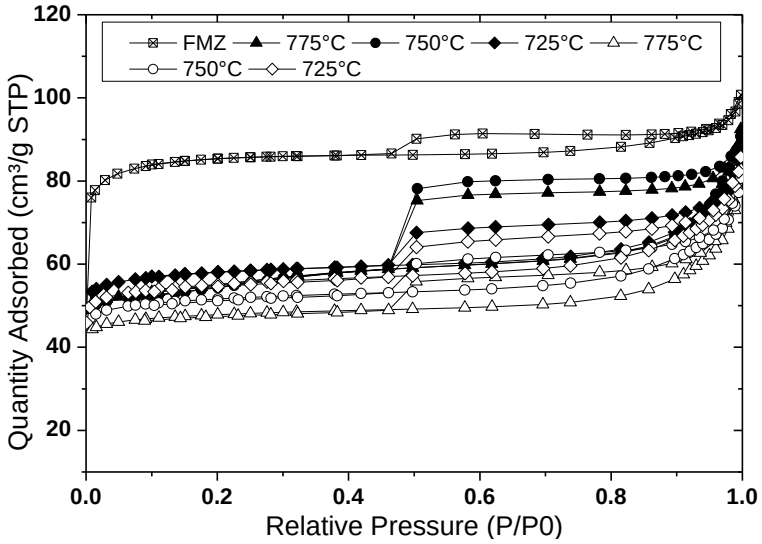

Figure 4-2: N_2 adsorption-desorption isotherm at -196°C on fresh and spent 5%Mo/HZSM-5 catalyst after treatment for 65 min at varied temperatures under atmospheric pressure during methane direct aromatization to benzene. (filled symbol- treated with 6000 GHSV and open symbols- treated with 9000 GHSV of methane, crossed open square- fresh 5% Mo/HZSM-5)

Also, as can be seen from Figure 4-2, the fresh catalyst had the highest micropore volume of 80 (cm^3/g STP) which decreases to a value about 60 (cm^3/g STP) after use due to the build-

up of coke [105,154,155]. The surface area and micropore volume of the samples were estimated from the isotherm data by using BET and BJH theories, and are reported in Table 4-1.

Table 4-1: BET surface area and micropore volume evaluated using N_2 adsorption isotherm data of the fresh and used 5% Mo/HZSM-5 catalyst treated with 100% methane for 65 min at flow rates and reaction temperatures as indicated.

Sample	BET Surface area (m^2/g)	Total pore volume (at P/P0 =0.99) (mm^3/g)	BJH cumulative pore volume (between 17-3000 Å) (mm^3/g)	micropore volume (mm^3/g)
F-MoZ	252.5	165.2	53.5	111.7
U-MoZ6-725	176.6	137.4	64.9	72.5
U-MoZ6-750	169	140.4	92.1	48.3
U-MoZ6-775	170.2	143	89	54
U-MoZ9-725	167.2	132.7	64.8	67.9
U-MoZ9-750	156.4	124.7	61.5	63.2
U-MoZ9-775	145.4	128.1	70.6	57.5

The fresh catalyst was observed to have a BET surface area of 252.5 m^2/gm and a total pore volume of 165.2 mm^3/gm, respectively, which confirmed that the catalyst sample is microporous. The BJH cumulative pore volume which indicates the mesopore volume of the sample was affected little with catalytic use. Also, it was observed that the sample's BET surface area and the micropore volume decrease extensively but not completely as coke formed. Further, the samples treated with higher methane feed rate and at high reaction temperature showed much more extensive decreases in the surface area and micropore volume, which is an indication of increased formation of condensed coke structures.

4.4.3 Thermo-gravimetric analysis:

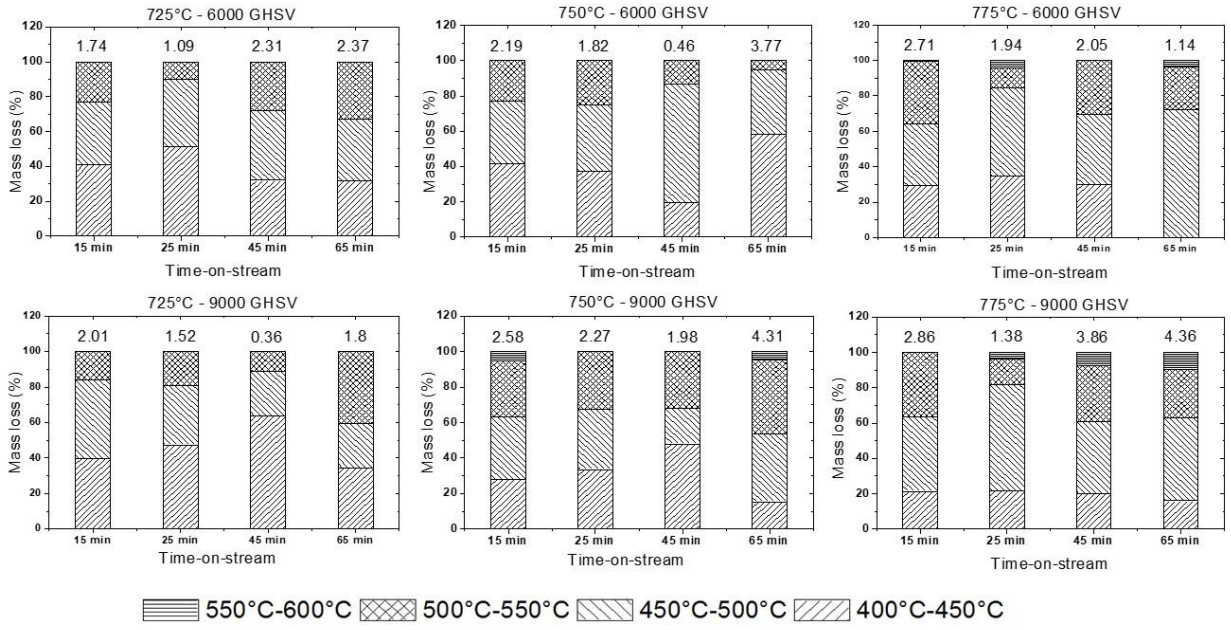

Figure 4-3: TGA study for the quantifying and classifying the coke deposits formed during methane direct aromatization to benzene on 5% Mo/HZMS-5 at 6000 GHSV and 9000 GHSV after respective reaction time-on-stream for 725°C, 750°C, and 775°C. (400°C-450°C, 450°C-500°C, 500°C-550°C, 550°C-600°C)

The oxidation behavior of the coke formed during the reaction was studied by thermogravimetric analysis.

The weight loss due to coke combustion between 400-600ºC is reported in the form of a normalized stacked bar plot in Figure 4-3. The coke contents were classified at an interval of 50ºC as highlighted in the figure. As can be seen from Figure 4-3, nearly 70-90% of the coke content was readily oxidized, as it burned below 500ºC. Coke with greater stability to oxidation was observed on the samples treated at higher reaction temperatures and higher methane flow rates. These more stable coke structures are likely to be graphitic carbon as

indicated by Raman and XPS studies (see below). It was observed that the samples treated at higher temperatures and higher flowrates were extensively coked.

Though, TGA has been repeatedly mentioned in the literature as a technique to quantify carbon content on the catalyst, locally non-uniform coke formation (as can be seen from TEM images in Figure 3-8 of Chapter 3) impacts the precision of the technique. This is evident in Figure 4-3, where it can be seen that the total amount of coke (labelled numerically over the top of each bar) that was removed upon oxidation varied across the sample in series. Moreover, a few earlier studies [91,100] divided the reactor into sections and performed post-reaction catalyst characterization to correlate the dependency of coking on reactor length. These studies directly suggest that coke formation on the catalyst depends upon reaction residence time. Another reason for inhomogeneous coke formation can be the evolutionary nature of the coke itself, which depends upon the coking pathway to graphite and PAH coke from the reaction products. Thus, it is challenging to correlate coke content with time on stream of reaction.

4.4.4 Raman spectroscopy:

The Raman spectra of the used catalysts in the region between 1200-1700 cm^{-1} are reported in Figure 4-4. As can be seen from Figure 4-4, two intense peaks were observed in the spectrum, at 1364 cm^{-1} and 1600 cm^{-1}, which corresponded to sp^2 carbon's D (disordered coke) and G (graphitic coke) bands, respectively [88,156157]. The disordered coke is amorphous in nature and highlights coke which is in transition and has not yet fully evolved into graphitic coke [121126]. Therefore, the relative graphitic ordering of the coke structure can be understood from the area ratio of the D and G bands. This coke formed has less complex structure when

compared with the coke formed during the reaction of pure ethylene (Chapter 2), which is possibly due to the increased hydrogen presence (C/H ratio of 1:4 in methane compared to 1:2 in ethylene).

The ratio estimated by the curve-fitting of these peaks is marked on the respective spectra in Figure 4-4. It can be seen that the estimated D/G ratio of the coked samples treated at high methane feed rate was much lower than the samples reacted at low methane feed, which is an indication of increased graphitization with increased methane feed rate. Upon considering the products formed during the reaction, it can be inferred that either benzene or higher aromatics might have polymerized to become a part of the graphitic content (benzene or higher aromatics → PAH→ graphite). Moreover, the estimated D/G ratio of the resultant coke at higher reaction temperatures was higher compared to the ratio at lower reaction temperatures, which emphasizes that high temperatures assist in the formation of disordered coke structures possibly from ethylene or intermediate oligomers as precursors, as suggested from our studies (chapter 2).

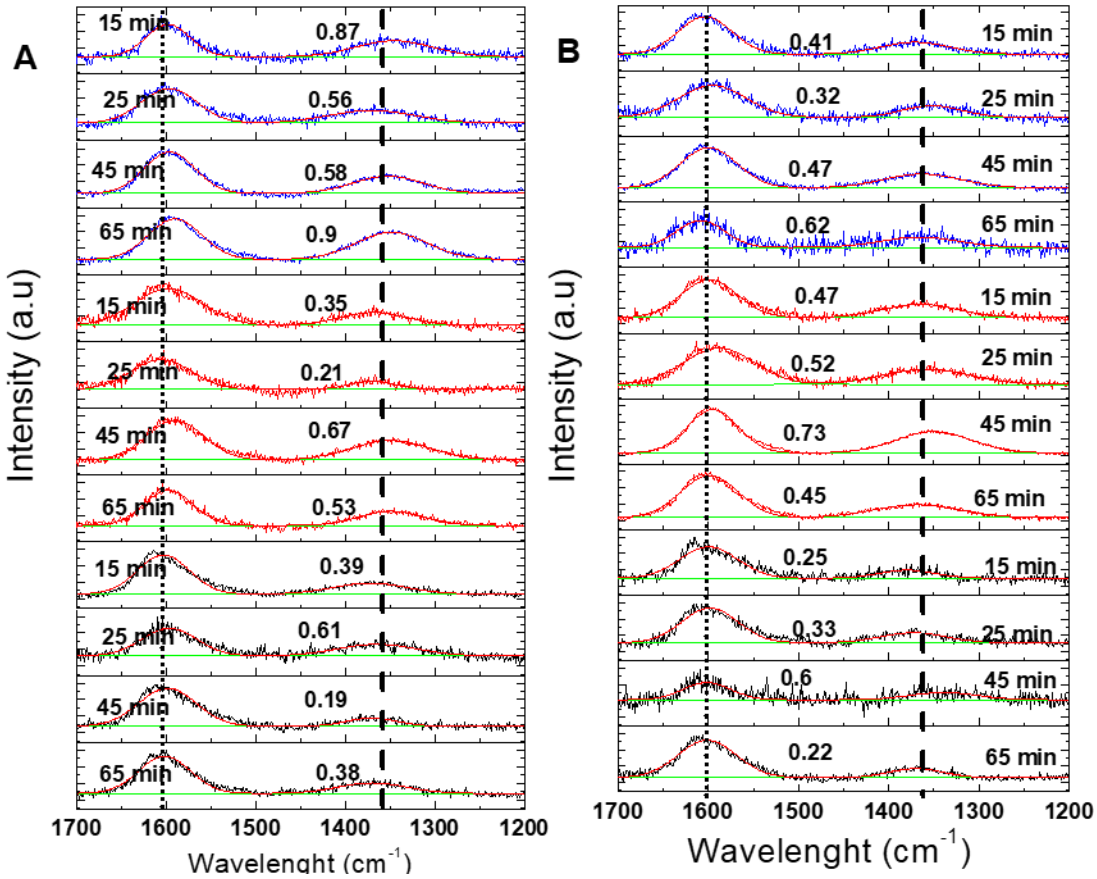

Figure 4-4: Raman spectra of spent 5% Mo/HZMS-5 after methane direct aromatization to benzene at A) 6000 GHSV of methane and B) 9000 GHSV of methane. [Spectrum of the sample treated at 725°C, 750°C, and 775°C is indicated by black, red, and blue lines. The respective time-on-stream and estimated D/G ratio are as marked. The vertical dash and dotted lines highlight the position of the D and G bands, and green lines indicate the fitted curves.]

4.4.5 X-ray photoelectron spectroscopy:

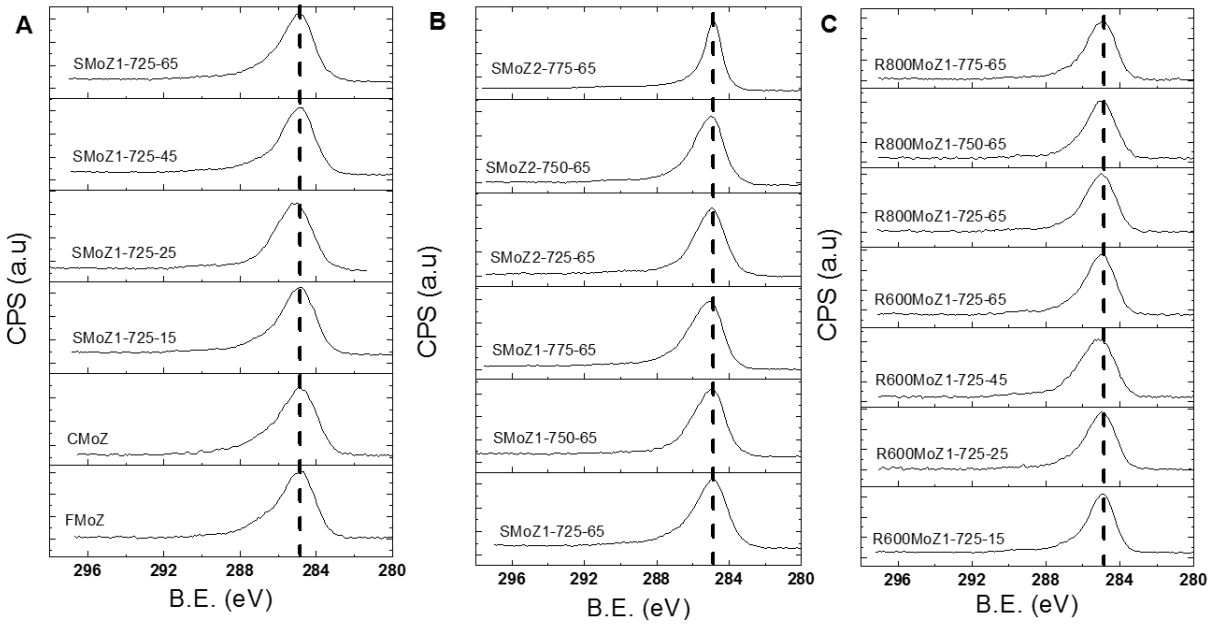

Figure 4-5: C 1s spectra obtained by XPS analysis on fresh, carburized, spent, and regenerated 5% Mo/HZSM-5 catalyst. (A) Changes with carburization and reaction time-on-stream, (B) Changes with temperature and methane flow rate during the reaction, and (C) Changes with regeneration temperature. (Dash line at BE 284.4 eV)

Table 4-2: Summarized values of elemental composition and relative atomic carbon by XPS analysis on 5%Mo/HZSM-5 treated at a different stage of experiments during methane direct aromatization reaction.

	Atomic %					Relative C atomic %			
						C-C, C-H	C-O	C=O, O-C-O	O-C=O
Sample	Si 2p	Al 2p	O 1s	Mo 3d	C 1s	284.6	286.4	287.8	289.1
F-MoZ	22.0	2.2	57.4	3.0	15.4	72.4	17.9	6.0	3.7
C-MoZ	24.4	2.7	59.3	2.0	11.6	71.4	17.9	6.9	3.8
U-MoZ6-725-15	23.3	2.5	54.0	1.4	18.7	73.4	15.4	7.4	3.8
U-MoZ6-725-25	23.6	2.2	56.2	0.9	17.0	74.1	19.5	3.7	2.8
U-MoZ6-725-45	23.2	2.4	53.1	1.2	20.1	72.4	16.3	7.5	3.7
U-MoZ6-725-65	22.3	2.6	52.0	1.5	21.7	72.8	16.2	7.3	3.7
U-MoZ6-750-65	23.7	2.0	53.2	1.1	20.1	70.5	24.2	3.6	1.8
U-MoZ6-775-65	22.5	2.0	49.2	1.0	25.4	65.6	27.9	6.3	0.3
U-MoZ9-725-65	22.3	2.4	50.2	1.4	23.8	80.1	14.9	4.1	1.0
U-MoZ9-750-65	21.3	2.4	47.5	1.3	27.5	76.6	18.4	3.7	1.3
U-MoZ9-775-65	18.2	2.0	38.5	1.1	40.2	81.6	13.7	2.7	2.0
R600-U-MoZ6-725-15	20.5	2.3	53.2	4.1	19.9	77.4	16.8	0.8	5.0
R600-U-MoZ6-725-25	25.3	1.8	59.6	2.2	11.1	77.9	16.9	1.1	4.0
R600-U-MoZ6-725-45	23.6	2.1	57.5	2.5	14.3	73.7	19.8	2.3	4.2
R600-U-MoZ6-725-65	21.6	2.1	56.4	3.7	16.2	75.3	18.8	1.3	4.7
R800-U-MoZ6-725-65	25.8	2.0	60.4	1.5	10.2	76.0	18.0	1.8	4.2
R800-U-MoZ6-750-65	26.7	2.0	60.6	1.3	9.4	79.5	15.4	1.4	3.6
R800-U-MoZ6-775-65	26.8	1.9	60.7	1.3	9.3	77.1	17.5	1.8	3.6

The C 1s high-resolution XPS spectra of the fresh, used, and regenerated 5% Mo/HZSM-5 catalysts were collected and reported in Figure 4-5. These spectra highlighted the change in the nature of coke formed with reaction time-on-stream (A), reaction temperature and methane flow rate (B), and regeneration temperature (C). The fresh catalyst was studied as a blank standard to understand the interference by adventitious carbon. As can be seen from Figure 4-5, all spectra displayed the presence of an asymmetry peak at 284.6 eV, and a narrow C 1s core line with a distinct high BE tail at approx. 292 eV (related to aromatic shake-up), confirming the presence of sp^2 carbon (graphitic) [85,129,158].

The elemental composition and the carbon distribution are summarized in Table 4-2. The value suggests that the adventitious carbon over the fresh sample was about 15%. Considering this to be a base value, the quantity of coke formed on the used catalyst was estimated and was found to generally increase. The increase in the amount of coke with the reaction time-on-stream decreased the signal from other elements (Si, Al, O, Mo), correspondingly. This was expected, as the Mo/HZSM-5 surface would be increasingly buried underneath the layer of coke and beyond the analysis depth of about 10 nm. The Si/Al ratio (equivalent to SiO_2 and Al_2O_3), however, remained approximately constant as a function of reaction conditions and regeneration, which suggests that the composition of the catalyst support has remained stable.

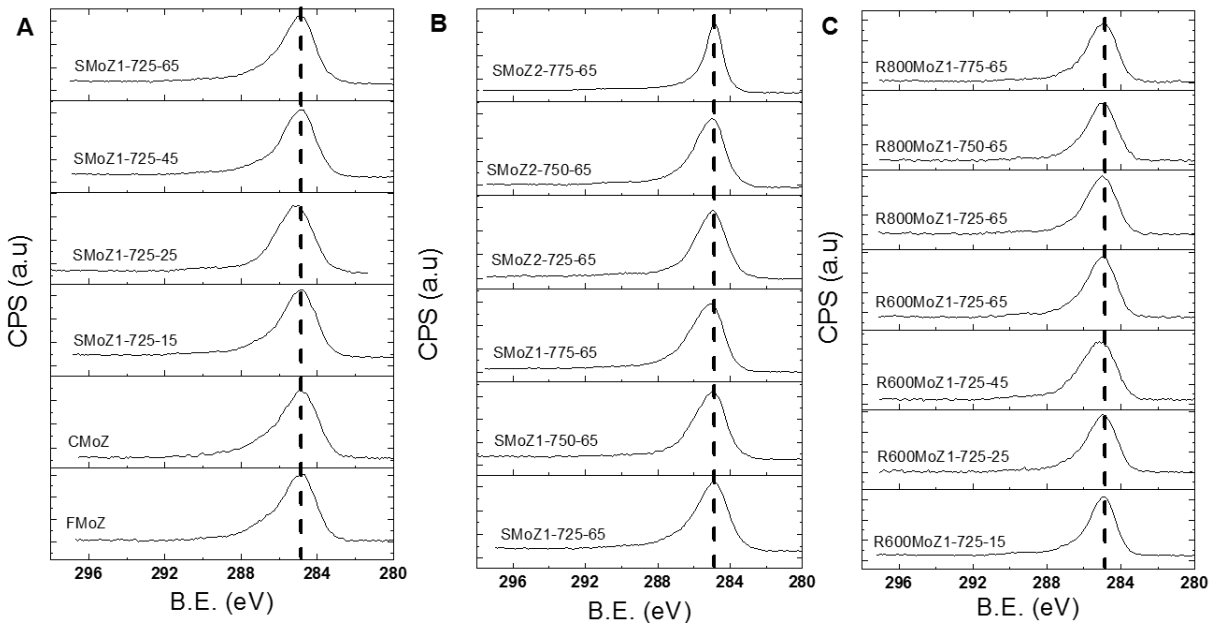

Figure 4-5: C 1s spectra obtained by XPS analysis on fresh, carburized, spent, and regenerated 5% Mo/HZSM-5 catalyst. (A) Changes with carburization and reaction time-on-stream, (B) Changes with temperature and methane flow rate during the reaction, and (C) Changes with regeneration temperature. (Dash line at BE 284.4 eV)

Table 4-2

The carbon distribution suggests that a major fraction (about 73%) of the carbon structures was dominated by C-C and C-H species, which could be graphitic coke along with a minor fraction of allied hydrocarbon phases such as polyaromatics, aliphatic and ring compounds. A part of the coke structure was oxy-carbidic, suggesting possible bonding with oxygen in the Si-Al framework. This dominance by graphitic coke was similar and varied a little with reaction temperature. However, the amount of coke and dominance by graphitic carbon increased with treatment at higher methane feed rate, which complemented the results from the Raman spectroscopy study. As can be seen from Table 4-2, the quantity of coke was around 40% (U-MoZ2-775-65) and its respective graphitic peak was narrower and more intense than for the other samples. While these values show a clear trend in the amount of surface carbon, the surface detection depth (10 nm) must be considered before comparing them directly, as carbon within the catalyst's pores may be inaccessible. The XPS spectra of the regenerated samples were identical to the fresh samples, and the amount of adventitious carbon was similar, indicating that the samples were successfully oxidized and the carbon was effectively burned and removed in air at 600°C and 800ºC.

4.5 Conclusion:

The methane conversion to benzene on 5% Mo/HZSM-5 was conducted and achieved a near thermodynamic value of conversion, especially at low reaction temperature and low methane feed rate. The reaction products included ethylene as a primary product, benzene as a secondary product, and higher aromatic compounds such as naphthalene and p-xylene as tertiary products, indicating a serial reaction path. The overall conversion of methane and the

formation of aromatic products were highest on the freshly carburized catalyst but decreased with reaction progression due to coke build-up.

In comparison to the coke formed with ethylene feed at similar reaction conditions (Chapter-2), the coke structure build-up with pure methane feed was less severe and complex, yet its Raman spectra showed a significant contribution by graphitic and disordered carbon.

The coke structure formed at low methane feed rate was relatively amorphous, compared the coke build-up at a high methane flow rate. This can be inferred due to increasing ethylene and aromatic compounds formations which assisted graphite formation via the intermediary of polyaromatic hydrocarbon. TGA studies suggested that coke structures dominated by graphitic carbon were much more stable to oxidation, and therefore, it would be advisable to conduct the reaction at lower reaction temperatures and lower feed rate of methane for the ease of regenerating the coked catalyst.

Little advantage of methane conversion was achieved at a higher reaction temperature. This is because at high reaction temperatures, a substantial amount of coke was formed with a simultaneous increase in the products. Further, as gleaned from the Raman study, the coke structure formed at high temperature had an increased contribution of disordered carbon species. Therefore, this implies that the products (preferentially ethylene) act as precursors to amorphous coke formation.

Therefore, in summary, the present results, taken together with those of our earlier study, implicate that ethylene is the responsible compound for the catalyst deactivation.

Chapter 5 Direct aromatization of methane: understanding structural changes to Mo/ HZSM5 catalyst during in-situ reaction and regeneration by synchrotron powder X-ray diffraction

This chapter describes an in-situ investigation that was conducted to identify possible transformation routes for molybdenum carburization, coke formation, coke removal, molybdenum oxidation, and HZSM-5 dealumination. The effect of carburization and reaction time and oxidation temperature was studied.

Mo/HZSM-5 catalyst which was prepared by wet impregnation method was tested in an in-situ capillary flow reactor set-up with simultaneously recording powder X-ray diffraction patterns. The changes to the catalyst during heating in nitrogen, carburization with a mixture of methane and hydrogen, reaction with pure methane, and regeneration with air was monitored.

This study is a first of its kind which attempted to directly compare the impact of reaction on the catalyst. The study observed that MoO_2 and ZSM-5 phases were stable at the reaction and regeneration conditions, however, the MoO_3 phase transformed throughout the reaction. The MoO_3 dissociates to $MoO_{2.5}$ phase upon heating in nitrogen, carburizes to molybdenum

oxy-carbide and Mo_2C during treatment with CH_4/H_2 (1/9), and transforms back to MoO_3 via $MoO_{2.5}$ phase during regeneration in air. The MoO_3 phase was also observed to be sensitive to high oxidation temperatures. Amorphous and graphitic coke species were observed to form during carburization and reaction, but were then removed completely upon regeneration.

Thus, this study implies that the form of molybdenum will be the deciding factor for effective re-use of Mo/HZSM-5 catalyst in the MDA reaction.

5.1 Introduction:

Natural gas is a valuable hydrocarbon resource which has been underused and excessively flared over the years [3,10,12]. This has been causing an increase in carbon footprint [1]. Therefore, identifying processes to fully and efficiently utilize natural gas is the need of the hour.

The direct aromatization of methane is a promising route for converting methane-containing natural gas to petrochemical products [159]. However, the lack of understanding of the active form of catalyst and the impact on it with reaction, coke formation, and regenerative oxidation has hindered the commercialization of this process.

Molybdenum supported on HZSM-5 support was introduced as a catalyst for selectively converting methane to benzene by Wang et al. [133] in 1993. For the catalytic action, molybdenum carbide must function in conjunction with the Brønsted acidic sites of HZSM-5 to activate and convert methane to ethylene and benzene. For the transformation of molybdenum oxide (MoO_2, MoO_3) in fresh Mo/HZSM-5 catalyst to molybdenum carbide (Mo_2C), a carburization stage is needed before the reaction stage [52,89,160,161]. But, the exact transformation route during carburization has not been elucidated.

During the MDA reaction on Mo/HZSM-5, coke formation occurs as a parallel undesired reaction, which deposits on the surface of the catalyst and deactivates it. Therefore, studies to understand coke structure and minimize its formation have gained interest [100,162–165]. The coke structure comprises different chemical species including polycyclic and polyaromatic, amorphous and graphitic species (our studies). In previous studies, these forms of coke were observed to vary with reaction conditions (our studies, [91,100]). However, their direct

observation under reac tion conditions, such as can be achieved with in-situ studies, would enhance understanding of the coke formation process.

The coke formed during the reaction can be removed by oxidizing the spent catalyst. Oxidation above 400ºC transforms the molybdenum carbide back to molybdenum oxide (our studies, [160]). Oxidation below 700ºC is effective in removing most coke species without damaging the catalytic active sites, and therefore, it is expected that the regenerated catalyst should be reusable. However, some coke species have very high oxidation stability and require high-temperature oxidation (>700ºC) for removal. Further, the bonding between molybdenum oxide and HZSM-5 support weakens upon oxidation at a high temperature causing agglomeration and smearing of the molybdenum oxide species on the surface of HZSM-5 (our studies). High-temperature oxidation can also dealuminate HZSM-5 and form aluminum molybdate by reacting with molybdenum oxide(s) [166–168]. However, these effects are not understood very well, thereby, limiting the regeneration process and potential use of the catalyst.

This study is the first attempt to generate evidence for catalyst structure changes during in-situ reaction and regeneration via an in-situ approach. For this purpose, the catalyst was exposed to the various stages in the reaction in a quartz capillary flow reactor and was simultaneously monitored by synchrotron X-ray beam. It was hypothesized that any impact to the structure will reflect on its respective diffraction pattern, thus, serving as a tool to identify and interpret pathways for transformation during the course of the reaction.

5.2 Methodology:

5.2.1 Catalyst preparation

5.2.1.1 Synthesis of 5%Mo/H-ZSM5 catalyst:

The catalyst was synthesized by wet impregnating the molybdenum precursor (ammonium heptamolybdate (AHM) $[[NH_4]_6[Mo_7O_{24}].4H_2O]$ (from Sigma Aldrich)) on the HZSM-5 (Si/Al = 11.5) support. NH_4-ZSM-5 (Zeolyst International Inc.) was calcined in air at 510°C for 6 h to obtain HZSM-5 powder. This HZSM-5 was then mixed with a solution of water and calculated quantity of AHM, and the mixture was maintained at a pH of 4-5 for 2 h with stirring at 200 rpm. The mixture was then dried in a hot bath at 95°C for 3 h at a stirring speed of 300 rpm. The dried sample was recovered and calcined at 510°C for 16 h in the flow of air to form the fresh catalyst. This powder was pelletized at a pressure of 98 KPa by using a hydraulic press (from Kimaya engineers, India). The pellet was size-reduced to about 50-100 micron.

5.2.1.2 Capillary flow reactor set-up, reaction sequences, and X-ray diffraction analysis:

A quartz capillary tube (from Hilgenberg GmbH, Germany) with a diameter of 1 mm was packed with the catalyst (about 2-5 mg). The sample-packed capillary was mounted to the beamline and aligned along the direction of the X-ray beam, collinear with the detector. The inlet of the capillary was connected to the gas manifold from which streams of nitrogen and compressed air, and a mixture of methane and hydrogen could be selected. The flow ratio of methane and hydrogen gas was maintained as desired with the use of a mass flow controller

Brooks model 5850i (Brooks Instrument, Hatfield, PA, USA). The outlet stream was connected to a water reservoir and the rate of the gas bubbles formed was monitored by high-resolution cameras as the indication of gas flowing through the capillary. An air blower was placed under the capillary to heat and cool the sample to the desired temperature.

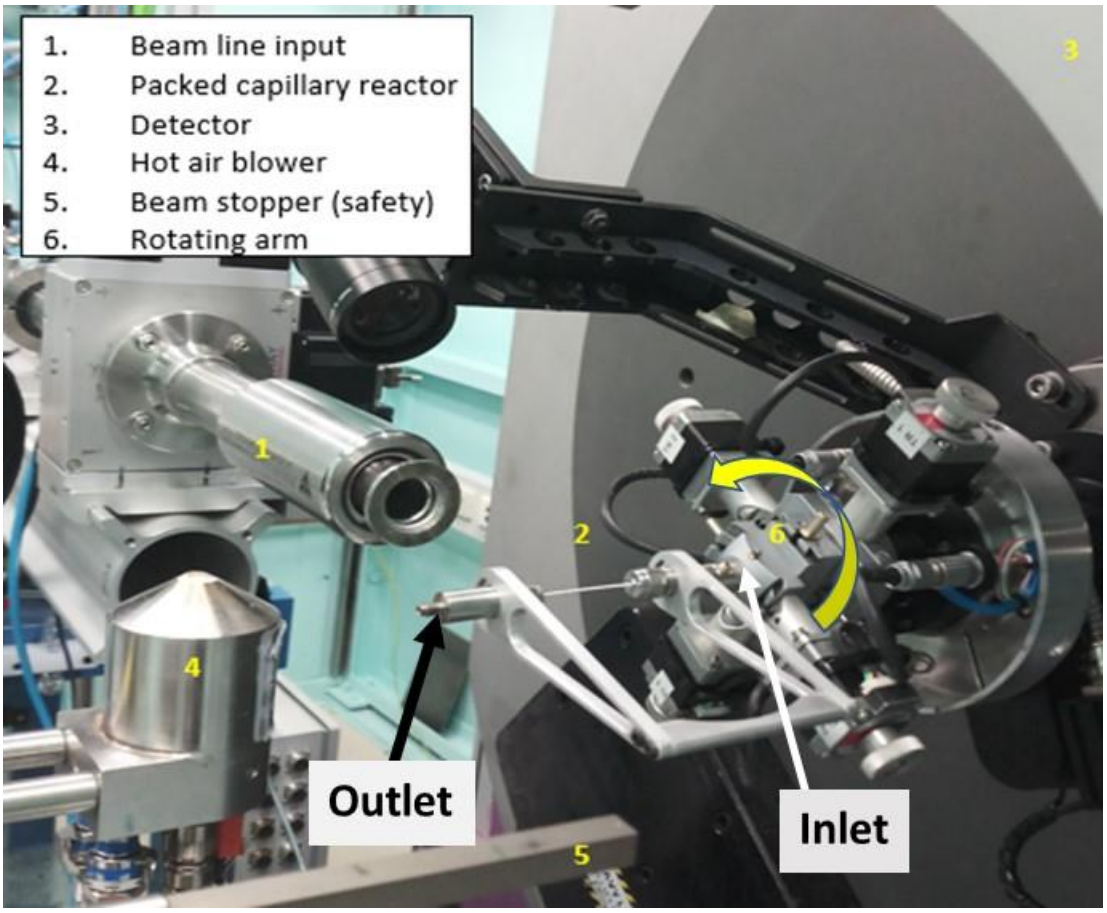

Figure 5-1: Experimental set up of in-situ flow reaction cell at the Australian Synchrotron powder XRD beamline

The energy of the X-ray beam used was 17 keV (λ = 0.74 Å). The diffraction patterns were recorded from 2θ = 2-80° using a high-resolution Mythen detector. The sample-filled capillary oscillated from 0-60º during the analysis. The diffraction patterns were collected in

pairs, with a difference of $2\theta = 0.5^{o}$ to eliminate the gap in the Mythen detector. Each pair of scans was carried out for 600 sec.

The high-resolution diffraction patterns were recorded simultaneously during the heating, carburization, reaction, and regeneration of the catalyst as detailed by scheme depicted in Figure 5-2. 11 diffraction patterns were collected during the ramp heating of the sample from room temperature to 775ºC at a rate of 6ºC/min in the flow of nitrogen. Upon reaching 775ºC, the gas flow was switched to a 1:9 mixture of methane and hydrogen for carburization of the sample. The flow of gas was 90 ml/min (gas hourly space velocity between 1080-2700 µl/(g.h)). The carburization was performed for 1 h and 6 diffraction patterns (scan number 12-17) were recorded. Following to the carburization, 100% methane at the rate of 10-15 ml/min (gas hourly space velocity between 180-300 µl/(g.h)) was passed for 1 h and another six diffraction patterns (scan number 18-23) were recorded. After the reaction, the capillary was cooled to 600ºC in a flow of nitrogen at 5 ml/min. Upon reaching 600ºC, the gas flow was switched to dry compressed air at about 5 ml/min for regenerating the catalyst. The regeneration was performed from 600-900ºC by heating at 6ºC/min along the way. Isothermal periods of 10 min each were programmed at 600ºC, 700ºC, 800ºC, and 900ºC. 14 diffraction patterns (scan number 24-37) were collected during the regeneration stage.

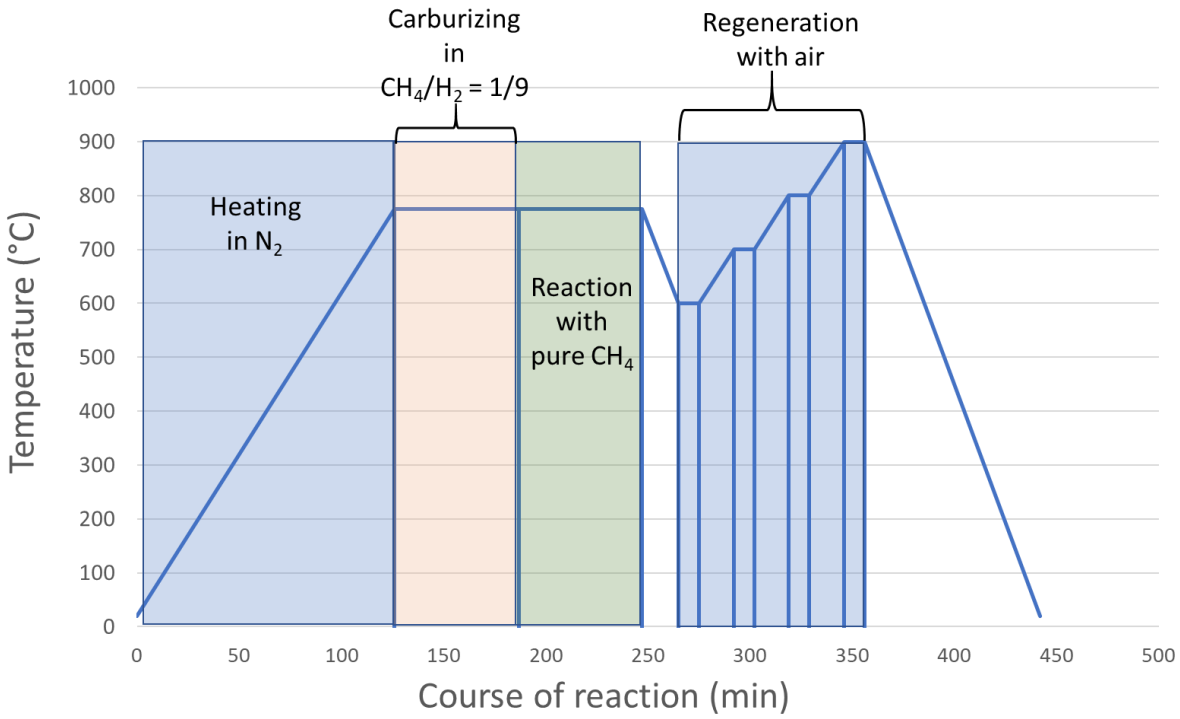

Figure 5-2: Flow sequence of the conducted in-situ reaction-regeneration studies on 5% Mo/HZSM-5.

The recorded data were merged using PDViper software [169] and were converted to the equivalent of Cu Kα wavelength (λ = 1.54 Å) using CMPR toolbox [136]. The database of zeolite structures, the Inorganic Crystal Structure Database (ICSD) and International center for diffraction data (ICDD) were used to identify the planes of different crystalline phases.

5.3 Results and Discussion

Powder X-ray diffraction was used to probe the catalyst's structure and identify changes through the reaction sequence. The diffraction patterns collected during the study are reported in the form of a 3D contour plot as shown in Figure 5-4. The 2D surface of the 3D contour is also shown in Figure 5-4 at the top of each 3D contour to more clearly show any changes in

the peak position. The patterns were matched with phases of orthorhombic ZSM-5 (PDF card 00-048-0135 [36]), MoO_3 (PDF card 00-005-0508 [36]), MoO_2 (PDF card 00-032-0671 [36]), Mo_4O_{11} (PDF card 01-089-8980 [36]), Mo_8O_{23} (PDF card00-005-0339 [36]), Mo_9O_{26} (PDF card 00-012-0753 [36]), $Mo_{13}O_{33}$ (PDF card 01-082-1930 [36]), $Mo_{17}O_{47}$ (PDF card 00-013-0345 [36]), $MoO_{2.8}$ (PDF card 00-012-0517 [36]), MoOC (PDF card 00-035-0787 [36]), $Mo_{2.25}O_{0.75}$ (PDF card 04-004-3020 [36]), and Mo_2C (PDF card 00-035-0787 [36]) reported in the ICDD database (given in supporting information) [36]. The diffraction pattern is represented by different two theta regions as shown Figure 5-4 to present peaks of varied intensity which was necessary to distinguish the planes of respective phases.

5.3.1 Structure of fresh Mo/HZSM-5 catalyst

The diffraction pattern of fresh Mo/HZSM-5 sample at room temperature is reported as the 1st scan. The pattern suggests the presence of crystalline ZSM-5, MoO_2, and MoO_3 phases, similar to our earlier study (ex-situ study reported in Chapter 2) and published reports [41,50,51]. The presence of MoO_2 and MoO_3 phases confirms that the molybdenum precursor, i.e. AHM, underwent dissociation to distribute over the surface of ZSM-5.

5.3.2 Structural changing of Mo/HZSM-5 catalyst with heating

The changes to Mo/HZSM-5 sample with heating can be categorized in two stages, viz. between 25-200ºC and 200-775ºC. The diffraction patterns at scan numbers 1, 2, 3, and 4 which correspond to a temperature range spanning 25-200ºC show that the peak intensity resulting from several of the ZSM-5 planes are affected with increasing temperature. Specifically, the peak intensity of (011), and (200) planes of HZSM-5 increased whereas the peak intensity of (251), (322), and (024) planes of HZSM-5 decreased. As relative intensity

reflects the relative abundance of a particular plane of the crystal [170] or crystal's morphology [171], it can be suggested that there is an increased presence of few planes in the beam pathway. It was however observed that the position of these peaks did not change with heating to 200°C, so, the structure of HZSM-5 and Mo-oxides are intact in this heating range. Heating to a temperature of 200°C removes moisture and volatile compounds that occupied spaces in the HZSM-5 pores (TGA study reported in Chapter 4), therefore, there is possibility that the removal of these compounds might lead to interference in the analysis and consequent peak intensity changes.

Upon heating between 200-775ºC, it can be noted that the peak intensity of (011), (200), (012, (031), (301) and several other planes of ZSM-5 increases but their ratios remained similar. Such a behavior suggests that there could be an increased packing density of HZSM-5 crystal [172] possibly by crystal structure rearrangement and expansion with heating. Thomas et al. [132] suggest partial dealumination with heating, which was not observed in the present study as the 2theta position did not vary.

It was observed that the diffraction peaks related to molybdenum oxide phases (MoO_3 and MoO_2) had a stable intensity upon heating till 300ºC. But, it then appears that a certain fraction of MoO_3 transforms to a lower oxidation state of molybdenum oxide (highlighted as transition phase in Figure 5-4), which causes reduction of the peak intensity of the (020), (040), and (021) planes of MoO_3 species. These low oxidation state molybdenum oxide phases may possibly include $MoO_{2.5}$ or Mo-oxo dimer as suggested in published literature [41,160] A comparison of the diffraction patterns with XRD database [149] it can be suggested that these phases can be either be individual or a mixture Mo_4O_{11}, Mo_8O_{23}, $Mo_{17}O_{47}$, $MoO_{2.8}$,

crystals. Thus, the lower oxidation state molybdenum oxide can be generalized as Mo_yO_x, where x/y=2.5-2.8.

5.3.3 Structural changes of Mo/HZSM-5 catalyst with carburization

The diffraction patterns collected during carburization are reported in Figure 5-4, between scan number 12 to 17 (the start of carburization is indicated by a blue arrow). The carburization was confirmed by a reduction in the peak intensity of (020), (040), (021), (130), (211), and (171) planes of MoO_3 and peaks associated with Mo_yO_x, phasewith subsequent formation of (020) and (101) plane of Mo_2C phase [144]. Interestingly, while the (021), (130), and (211) planes of MoO_3 disappear completely, the (040) and (171) planes do not. This could indicate a partial transformation of MoO_3 to Mo_2C. This phase transformation was however observed from scan number 15, i.e. after a delay, which was due to the gas hold-up (dead volume) in the gas flow line. The 15th diffraction pattern displayed peaks associated with MoOC, $Mo_{17}O_{47}$, Mo_9O_{26} and other similar molybdenum oxide forms which are probably short-lived transition phases [45,161,173]. (XRD patterns of these phases are provided in the supporting information for this chapter). Thereby, suggesting a possible route for Mo_2C formation from Mo_yO_x and MoO_3 species via intermediate molybdenum oxycarbide species.

This diffraction pattern also displayed broad peaks which are an indicating of amorphous coke species [174], as can be seen by an increase in the background intensity (Figure 5-4.A) and at $2\theta = 44.5^{o}$. The broad peaks decrease with the progress of carburization (scan numbers 16 and 17) as graphitic coke formation takes place leading to the growth of (100), (101), and (004) planes of graphitic carbon. This transformation progressed possibly with the addition

of cyclic and aromatic compounds, rearrangement and dehydrogenation of coke structure (our studies, [91,100]).

5.3.4 Structural changes of Mo/HZSM-5 catalyst with reaction

The diffraction patterns which were collected during the reaction stage with pure methane at 775ºC under atmospheric pressure are shown in Figure 5-4 (scan numbers 18-23). The patterns suggest that ZSM-5 and MoO_2 phases remained stable during the reaction. From earlier studies (chapter 3), it was shown that high temperature and high methane feed rate promote the formation of graphitic coke content and the same was been observed from the diffraction patterns which show peaks related to graphitic coke. The graphitic coke formation stops after a particular time-on-stream as can be seen from stable peak intensity of (100) plane. This could possibly mean that the catalyst is completely deactivated and ethylene and benzene which drives the coke growth have stopped (our study, [99]).

5.3.5 Structural changes of Mo/HZSM-5 catalyst with coke removal by oxidation

The diffraction patterns upon catalyst regeneration by oxidation were collected and are represented by scan numbers 24-37. The coke formed (amorphous and graphitic) was successfully removed upon oxidation before 700ºC, as their respective diffraction peaks disappeared. Further evidence of the coke removal was observed through the camera's footage as shown in Figure 5-3, which shows the change of color due to oxidative removal of the coke (black).

However, the formation of (004) plane of graphite was observed between scan number 22-26. This was however interesting, as the formation of (004) plane also influenced the (024) plane of ZSM-5.

The diffraction patterns show that Mo_2C was oxidized during regeneration below 700ºC, as peak representing molybdenum carbide phase disappeared. The molybdenum carbide was substituted by MoO_3 and MoyOx phases. The formation of MoO_3 is well discussed in the literature [49,146,175] , but, the formation of other molybdenum phases was observed for the first time. This indicates that the form(s) of molybdenum in the regenerated catalyst are not the same as in the fresh catalyst.

Oxidation above 700ºC oxidizes these Mo_yO_x, forms of molybdenum oxide to MoO_3. However, as indicated by our earlier studies, such conditions can cause agglomeration of molybdenum which is not desired. Upon oxidation to high temperature (900ºC), the crystallinity of MoO_3 phase changes across the (130) and (171) planes, which could be due to the smearing of molybdenum as discussed in earlier studies (chapter 3) or could be an effect of enhanced dispersion of MoO_3 within the HZSM-5 structure.

The diffraction pattern of the HZSM-5 phase showed a rapid decrease in the intensity of (011) and (200) planes. This could be related to the effect of cooling or air flow rate and/or the possible adsorption of air. In all cases, ZSM-5 was stable during oxidation until 900ºC, as no major changes to the structure were observed. This includes no formation of aluminum molybdate and no dealumination as observed in literature [161,167,174]. possibly due to sublimation of the molybdenum oxide [176]. Thus, it can be inferred that Mo/HZSM-5 catalyst

has high structural stability even at high oxidation temperature (till 900ºC) and is suitable for regeneration and re-use.

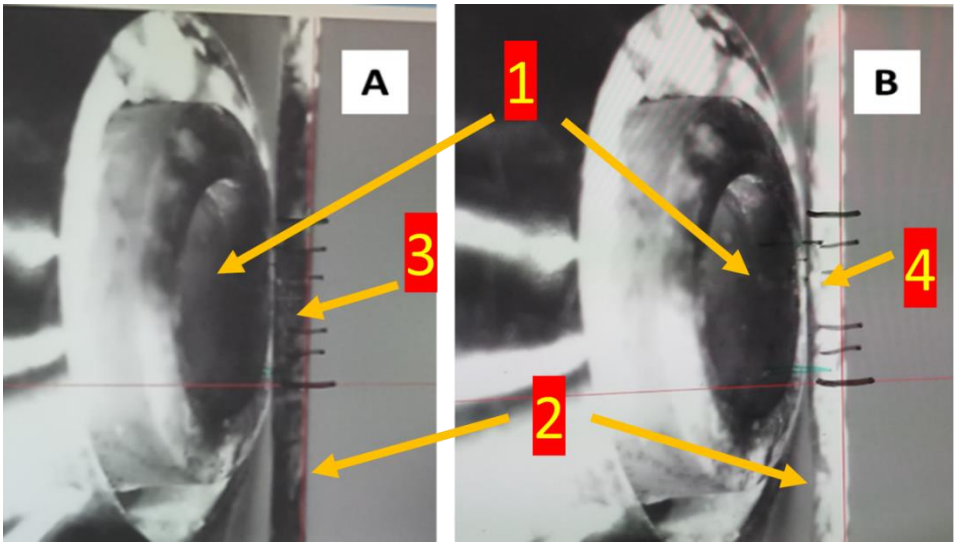

Figure 5-3: Image of the capillary reactor over hot air blower with 5% Mo/HZSM-5 filled A) during reaction B) during regeneration. 1. Opening of hot air blower, 2. The capillary reactor, 3. Coke Mo/HZSM-5 after the reaction, and 4. Regenerated Mo/HZSM-5 after coke removal.

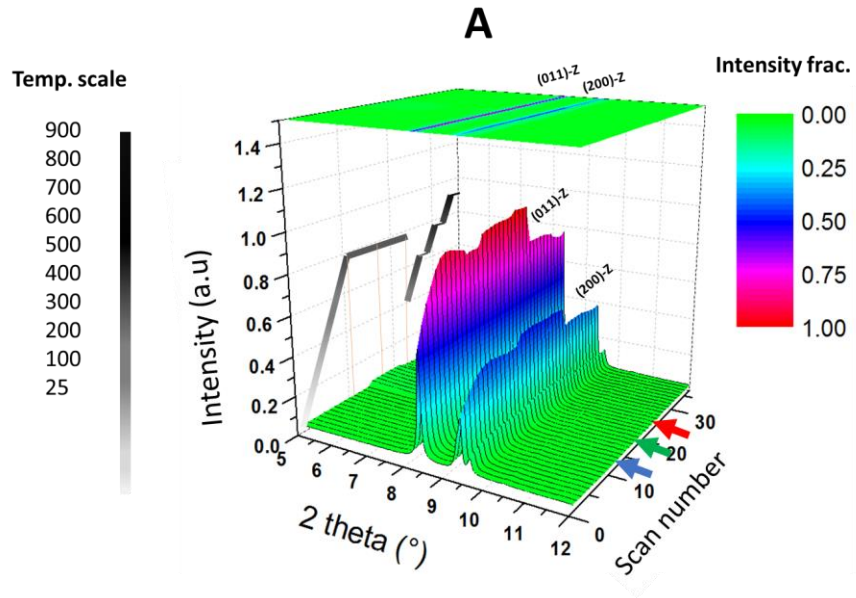

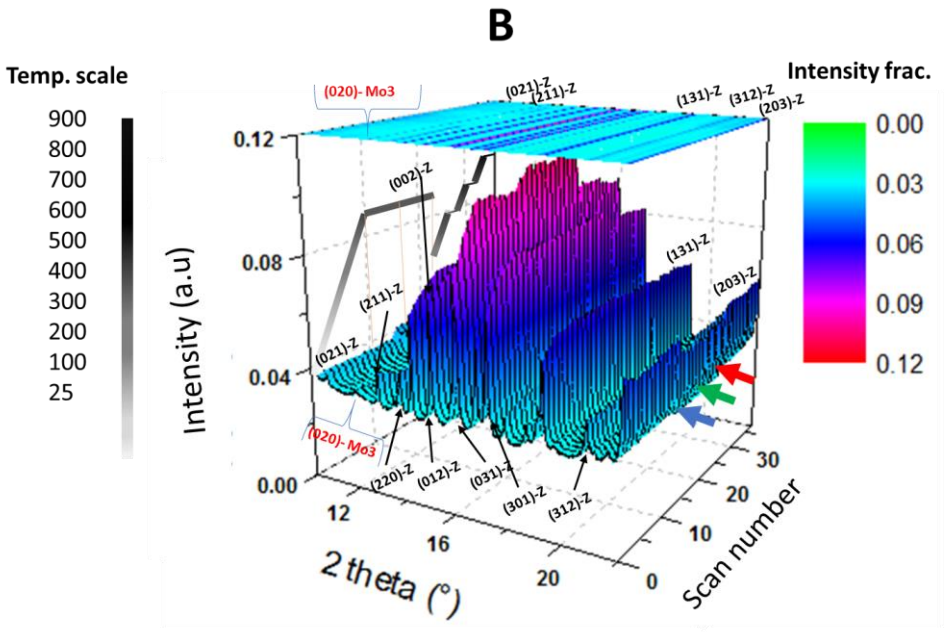
B
Temp. scale
900
800
700
600
500
400
300
200
100
25
Intensity frac.
0.00
0.03
0.06
0.09
0.12
Intensity (a.u)
0.12
0.08
0.04
0.00
(020)- Mo3
(021)-Z
(211)-Z
(002)-Z
(131)-Z
(312)-Z
(203)-Z
(220)-Z
(012)-Z
(031)-Z
(301)-Z
12
16
20
2 theta (°)
0
10
20
30
Scan number

1

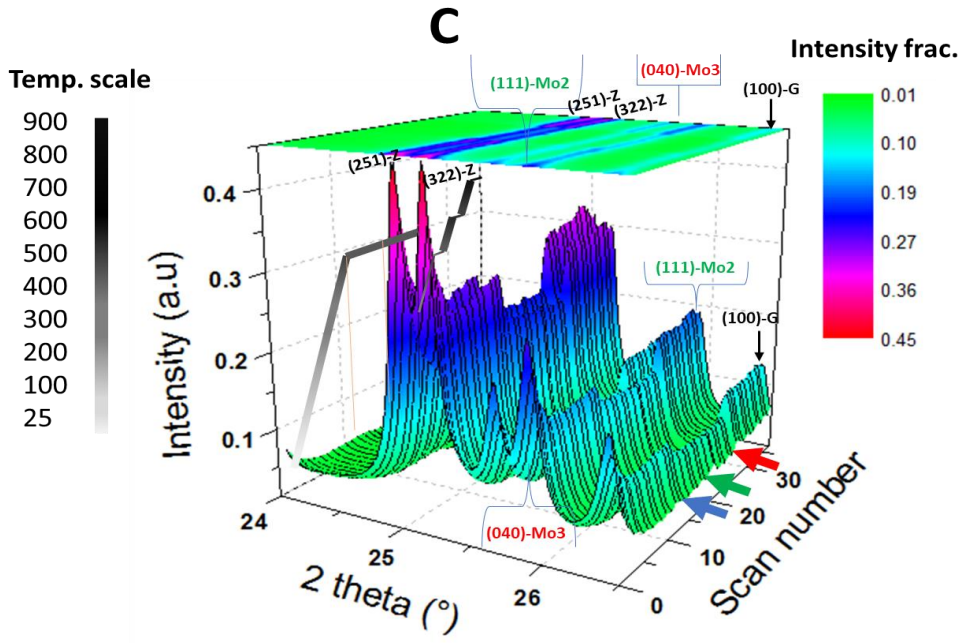
C
Temp. scale
900
800
700
600
500
400
300
200
100
25
Intensity frac.
0.01
0.10
0.19
0.27
0.36
0.45
Intensity (a.u)
0.4
0.3
0.2
0.1
(111)-Mo2
(040)-Mo3
(251)-Z
(322)-Z
(100)-G
24
25
26
2 theta (°)
0
10
20
30
Scan number

2

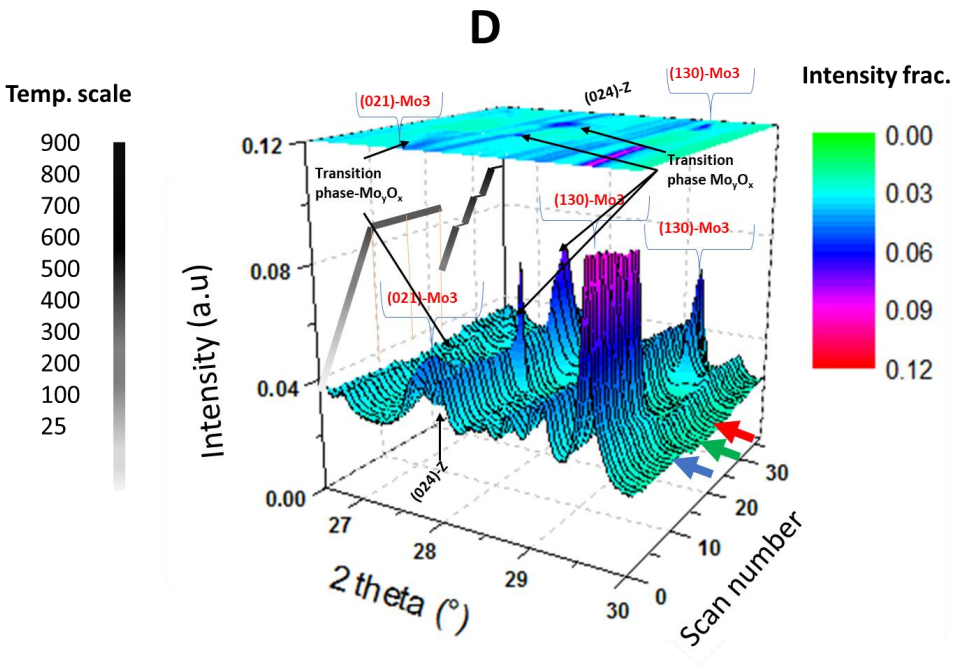
D
Temp. scale
900
800
700
600
500
400
300
200
100
25
Intensity frac.
0.00
0.03
0.06
0.09
0.12
(021)-Mo3
(024)-Z
(130)-Mo3
Transition phase-Mo$_y$O$_x$
Transition phase Mo$_y$O$_x$
(130)-Mo3
(130)-Mo3
(021)-Mo3
(024)-Z
Intensity (a.u)
0.12
0.08
0.04
0.00
27
28
29
30
2 theta (°)
0
10
20
30
Scan number

1

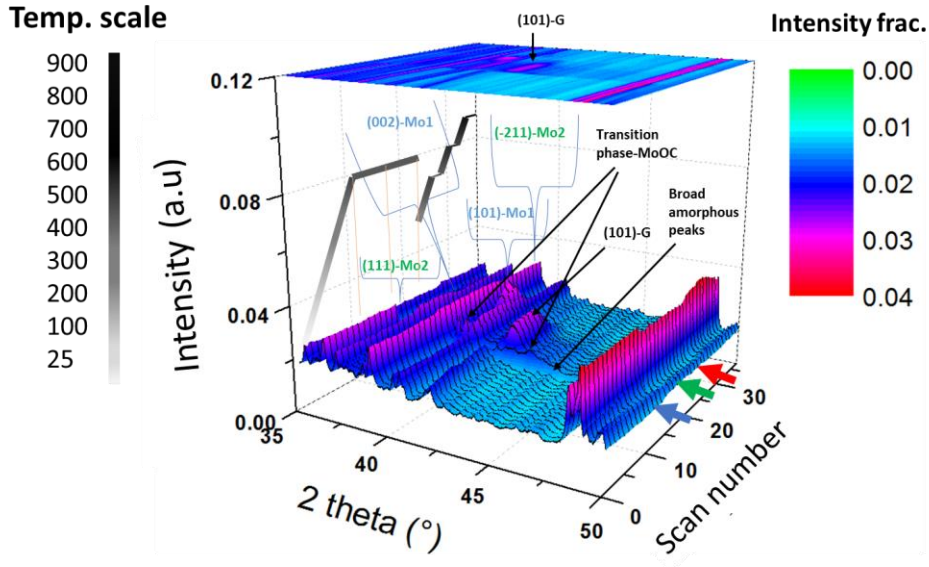
E
Temp. scale
900
800
700
600
500
400
300
200
100
25
Intensity frac.
0.00
0.01
0.02
0.03
0.04
(101)-G
(002)-Mo1
(-211)-Mo2
Transition phase-MoOC
Broad amorphous peaks
(101)-Mo1
(101)-G
(111)-Mo2
Intensity (a.u)
0.12
0.08
0.04
0.00
35
40
45
50
2 theta (°)
0
10
20
30
Scan number

2

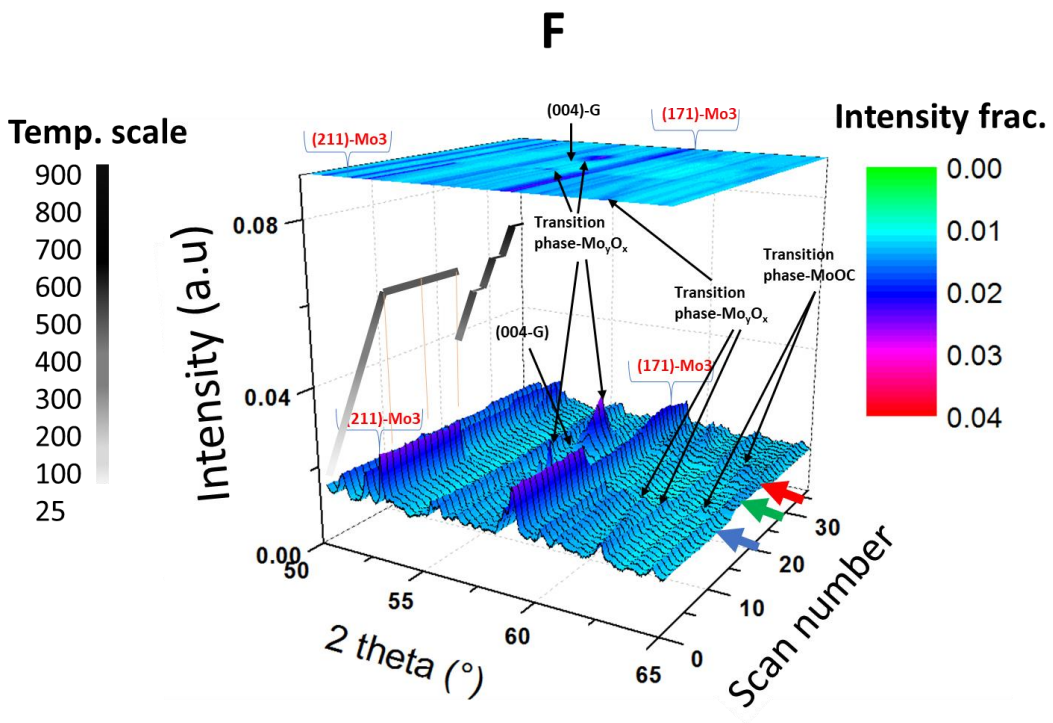

Figure 5-4 (A-F): Powder X-ray diffraction patterns of the Mo/HZSM-5 catalyst during an in-situ reaction and regeneration studies. The 3D contour plot highlights the peak intensity changes and the 2D top surface highlights the peak position changes. The planes are marked as Z for ZSM-5, Mo3 for MoO_3, Mo2 for MoO_2, Mo1 for Mo_2C, and G for graphite phases, respectively. Scan number 1-11 were collected during preheating, 12-17 during carburization, 18-23 during reaction, and 24-37 during regeneration by oxidation. The blue arrow marks the initiation of carburization, the green arrow marks the initiation of the reaction, and the red arrow marks the initiation of regeneration.

5.4 Conclusion:

The study has confirmed the presence of HZSM-5, MoO_3, and MoO_2 crystalline phases in the fresh catalyst sample at room temperature, which suggests that AHM dissociated to

two forms of molybdenum oxide. Upon heating (300-775°C), additional molybdenum oxidic phases (Mo_yO_x, x/y=2.5-2.8) forms, in conformity with literature [41]. These Mo_yO_x, and MoO_3 phase transform to molybdenum carbide (Mo_2C) via a possible transition state of molybdenum oxy-carbide (MoOC). This transformation to molybdenum carbide species increases steadily with carburization. Coke formation happens parallel to molybdenum carburization. The amorphous form of coke was observed before the graphitic form, which confirms that coke transforms into graphitic carbon with reaction progression. These coke structures were removed by oxidation at high temperatures. Further, the molybdenum oxide phases of MoO_3,were revived during the oxidation process. But, treatment at a high oxidation temperature above 800ºC can induce MoO_3 smearing and must be avoided.

The study confirmed that ZSM-5 phase was stable during the course of reaction and regeneration. ZSM-5 did not show any structural features that could be related to dealumination or aluminum molybdate formation, and therefore, it can be inferred from the study that HZSM-5 support should be reusable with proper regeneration. Also, MoO_2 phase did not change throughout the reaction, and therefore, its concentration should be minimized as it does not take part in the MTB reaction. Many other subtle changes in the XRD patterns can be noticed, but these are difficult to interpret. Therefore, a fuller understanding could be achieved with a comprehensive Rietveld analysis of the XRD patterns.

Supporting information:

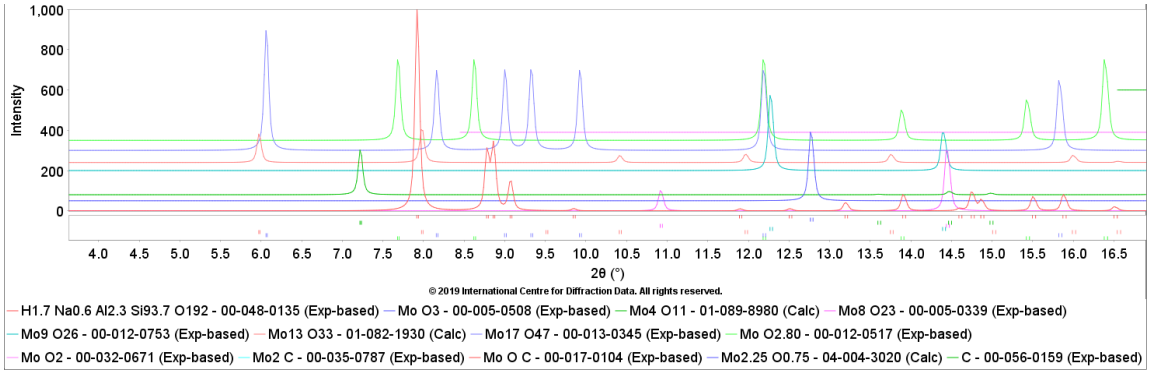

2

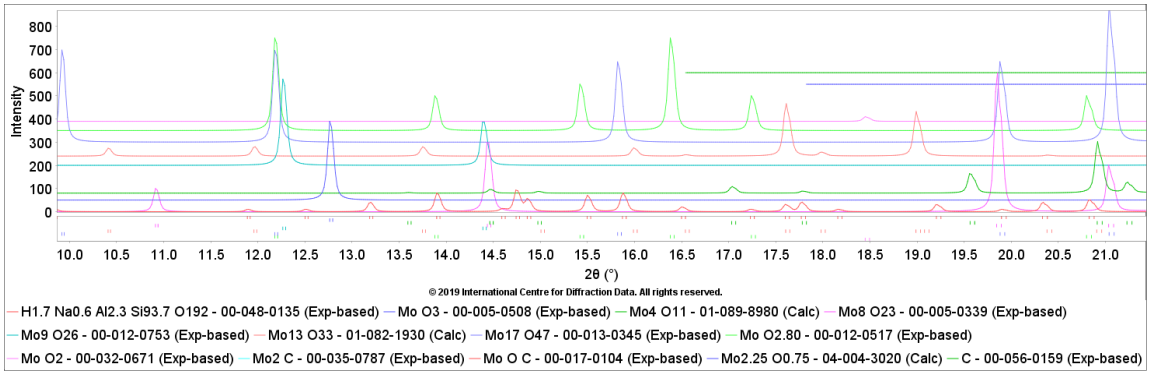

3

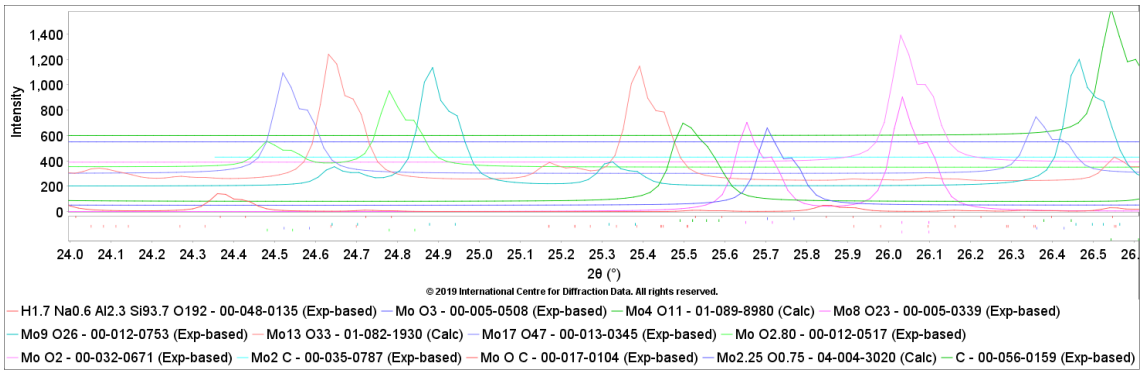

4

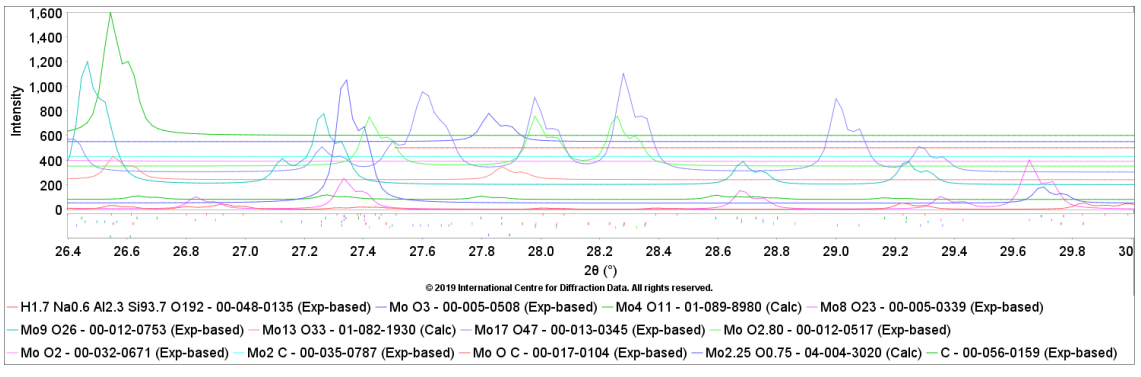

5

1

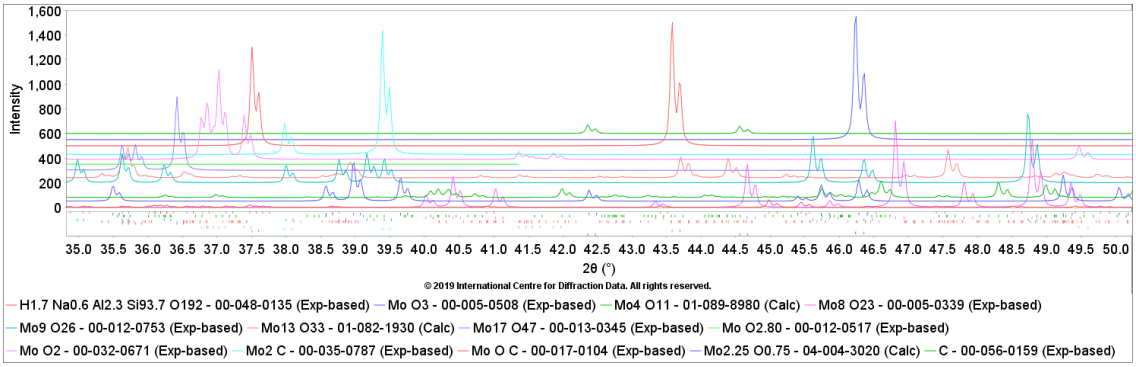
Intensity
2θ (°)
© 2019 International Centre for Diffraction Data. All rights reserved.
H1.7 Na0.6 Al2.3 Si93.7 O192 - 00-048-0135 (Exp-based)
Mo O3 - 00-005-0508 (Exp-based)
Mo4 O11 - 01-089-8980 (Calc)
Mo8 O23 - 00-005-0339 (Exp-based)
Mo9 O26 - 00-012-0753 (Exp-based)
Mo13 O33 - 01-082-1930 (Calc)
Mo17 O47 - 00-013-0345 (Exp-based)
Mo O2.80 - 00-012-0517 (Exp-based)
Mo O2 - 00-032-0671 (Exp-based)
Mo2 C - 00-035-0787 (Exp-based)
Mo O C - 00-017-0104 (Exp-based)
Mo2.25 O0.75 - 04-004-3020 (Calc)
C - 00-056-0159 (Exp-based)

2

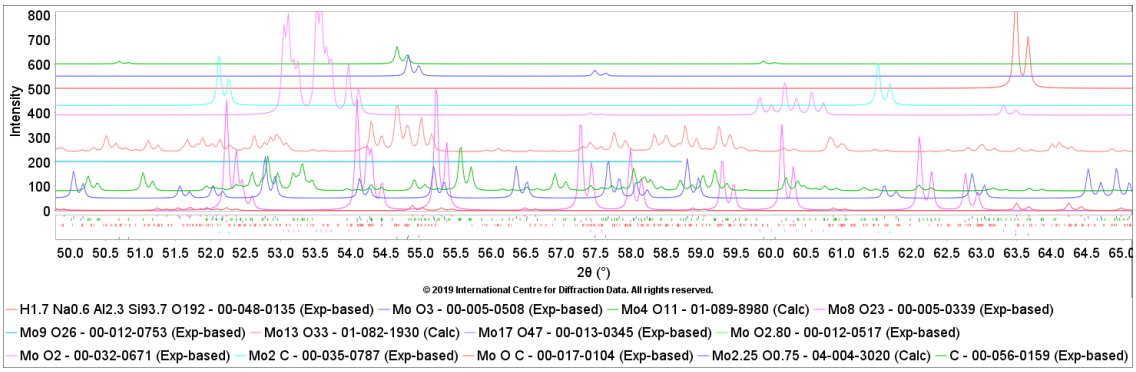
Intensity
2θ (°)
© 2019 International Centre for Diffraction Data. All rights reserved.
H1.7 Na0.6 Al2.3 Si93.7 O192 - 00-048-0135 (Exp-based)
Mo O3 - 00-005-0508 (Exp-based)
Mo4 O11 - 01-089-8980 (Calc)
Mo8 O23 - 00-005-0339 (Exp-based)
Mo9 O26 - 00-012-0753 (Exp-based)
Mo13 O33 - 01-082-1930 (Calc)
Mo17 O47 - 00-013-0345 (Exp-based)
Mo O2.80 - 00-012-0517 (Exp-based)
Mo O2 - 00-032-0671 (Exp-based)
Mo2 C - 00-035-0787 (Exp-based)
Mo O C - 00-017-0104 (Exp-based)
Mo2.25 O0.75 - 04-004-3020 (Calc)
C - 00-056-0159 (Exp-based)

Chapter 6 Overall Summary

In this thesis, the MDA process was investigated on Mo/HZSM-5 catalyst. The mechanistic pathway for methane to ethylene, benzene and coke, the role of the active components in their formation, and changes to the catalyst during the course of reaction were addressed in this work following a systematic approach. The work is presented in four main chapters, of which, each chapter was dedicated to a specific objective. The work undertaken was important in defining reaction-regeneration strategies for possible commercial application of this catalyst with repeated use.

Chapter 2 deals with understanding the role of ethylene in coke formation during its aromatization on HZSM-5 support. Chapter 3 provided insight into the active form of catalyst (Mo/HZSM-5) and highlighted the changes to the state of molybdenum in the catalyst upon use. Chapter 4 complements the findings from chapter 2 and 3 and adds understanding to the overall coke formation mechanism starting with methane feed. This chapter interrogated physical and chemical changes to the coke at varied reaction conditions. Chapter 5 describes further attempts to observe the transition of molybdenum species, ZSM-5 support, and coke species during carburization, reaction and regeneration stages by means of an in-situ capillary flow reactor set-up with synchrotron powder X-ray diffraction recording capability. The results of each stage have been written up in the thesis and have been either drafted or submitted for publication in peer-reviewed journals.

In the first stage of the study (chapter 2), a comprehensive spent HZSM-5 catalyst characterization was conducted, i.e. following to its use in the catalytic conversion of

ethylene into aromatics to observe the nature, structure, and morphology features of the resultant coke that was deposited on it. The study demonstrated the formation of aromatic compounds, preferentially benzene, from ethylene using HZSM-5 catalyst. The build-up of amorphous and graphitic coke, and its influence on the acid sites density and micropores of HZSM-5 was correlated.

A mechanistic insight on coke development was provided with catalyst time-on-stream, ethylene concentration, and HZSM-5's acid sites and micropores. The rate of coking was dependent on the ethylene concentration and the availability of the Brønsted acid sites and the micropores of HZSM-5, as high ethylene feed and fresh HZSM-5 catalyst was more active for reaction and coking. The coke formation started with the formation of amorphous carbon structures which transform to more condensed graphitic structures upon prolonged reaction times. As this graphitic coke structure was much more stable to oxidation, thus, the study advises it should be removed, thus regenerating the catalyst, in a timely manner, i.e. before the formation of extensive graphitic coke, for improved catalyst life-span.

In the second stage of the research (chapter 3), the catalytic testing of molybdenum supported on HZSM-5 (proven support) and SiO_2 (relatively inert support) was conducted to understand the active form of catalyst that is responsible for activating and dimerizing methane to ethylene. Several characterization techniques were used to evaluate changes to the structural, morphological, and chemical state of molybdenum in the samples during different stages of the reaction.

The catalytic study showed conclusively that only a combination of molybdenum carbide with HZSM-5 enabled the methane activation to ethylene and benzene. The characterization

revealed that molybdenum was strongly bonded to HZSM-5 and transitioned from its precursors to MoO_2 and MoO_3 forms, of which, MoO_3 carburized to Mo_2C and molybdenum oxy-carbide phases. Upon oxidation (regeneration), the molybdenum carbide phase was reverted to MoO_3 below 400ºC. Oxidation at high temperatures (600-800ºC) causes the MoO_3 phase to agglomerate and smear over the surface of HZSM-5. Thus, the study highlighted the importance of preserving the Mo and ZSM-5 bonding for the reaction and advises on the potential threat to the catalyst life-span if were to be oxidized under severe conditions.

Chapter 4 of the thesis highlights attempts to identify possible coke structures and to understand the coking mechanism with methane feed on the proven Mo/HZSM-5 catalyst at varying reaction temperatures, catalyst time-on-streams, and methane flow rates. The nature of the resultant coke, changes to its physical and chemical nature, and its impact on the catalyst and consequently, the reaction conversion were studied by comprehensively characterizing the used catalyst. It was shown that higher reaction temperature and methane feed rates promote the formation of coke structures which are more stable and less readily oxidized.

The catalyst activity study agreed with prior reports showing that methane transformed into benzene, naphthalene, and p-xylene via ethylene as an intermediate. Reaction time-on-stream, reaction temperature, and methane feed rate were observed to influence the catalyst's reaction performance and its deactivation. It was observed that high reaction temperatures and high methane feed rate triggered the formation of a relatively higher amount of graphitic coke which displayed high oxidizing stability as well. Thus, the study implies that the choice of reaction conditions can potentially define the life-span of the catalyst. In other words, there are advantages in conducting reaction at lower temperature and lower methane feed rate,

since this leads to lower graphitic coke content that can also be regenerated under milder conditions.

The fourth part of the study (chapter 5) strove to understand the changes Mo/HZSM-5 catalyst undergoes via an in-situ study. This was achieved by using a high-energy X-ray beam to map the catalyst structure while simultaneously conducting the reaction in a flow capillary reactor set-up at the Australian Synchrotron powder X-ray beamline.

The study observed that ZSM-5 and MoO_2 phases were stable throughout the course of the reaction, but, MoO_3, along with molybdenum oxidic phase ($MoO_{2.5}$) transitions to molybdenum carbide (Mo_2C) via an intermediate Mo-oxycarbide phase. Also, the study showed that amorphous coke forms prior to graphitic coke, and oxidation seems to be the ideal approach for the removal of both forms of coke species. During oxidation, the molybdenum carbide oxidizes to MoO_3 and $MoO_{2.5}$ species (below 700ºC) and extensively MoO_3 (below 800ºC). However, changes to the structure of the MoO_3 phase were also observed above 800ºC, which could be due to improved dispersion within HZSM-5 pores, smearing, or loss due to sublimation. The study found that no dealumination or aluminum molybdate formation takes place until 900ºC in air, and therefore, advises that Mo/HZSM-5 support can be reused with proper regeneration.

Chapter 7 Recommendations and Future work

These following opportunities as identified through this research work should be a part of future studies:

The work carried in this thesis indicates that oxidative regeneration, the agglomeration and smearing behaviour of molybdenum oxide (happens >600ºC) are likely to impact the catalyst performance upon reuse. Thus, reaction-regeneration studies with spent catalyst characterization should form part of future investigation.

The study suggest that the MoO_2 phase remains almost inert (unchanged) during the course of the reaction. Therefore, Mo/HZSM-5 catalyst without MoO_2 or minimum MoO_2 phase should be tested for its performance to validate this interpretation.

The impact of ethylene in coke formation was elaborated to an extent in this study. Similarly, experiments involving the co-addition of hydrocarbons will assist in developing an understanding of the coking mechanism, as they may identify new transformation routes for the coke formation and identify other precursors associated with them.

Chapter 8 References

1. Taifan, W. & Baltrusaitis, J. CH4 conversion to value added products: Potential, limitations and extensions of a single step heterogeneous catalysis. *Appl. Catal. B Environ.* **198**, 525–547 (2016).

2. Ojijiagwo, E., Oduoza, C. F. & Emekwuru, N. Economics of gas to wire technology applied in gas flare management. *Eng. Sci. Technol. an Int. J.* **19**, 2109–2118 (2016).

3. Corredor, E. C., Chitta, P. & Deo, M. D. Techno-economic evaluation of a process for direct conversion of methane to aromatics. *Fuel Process. Technol.* **183**, 55–61 (2019).

4. Company, B. P. BP Statistical Review of World Energy 2015. 1–45 (2015). doi:10.2307/3324639

5. Company, B. P. BP Statistical Review of World Energy 2016. *Stat. Rev. World Energy* **65th editi**, 1–45 (2016).

6. Company, B. P. BP Statistical Review of World Energy June 2017. **66th editi**, 1–48 (2017).

7. Company, B. P. BP statistical review of world energy 2018. **67th editi**, 1–56 (2018).

8. Company, B. P. BP Statistical Review of World Energy 2019. 1–61 (2019). doi:10.2307/3324639

9. Bahadori, A. & Bahadori, A. Overview of Natural Gas Resources. *Nat. Gas Process.* 1–22 (2014). doi:10.1016/B978-0-08-099971-5.00001-5

10. Elvidge, C. D. *et al.* The potential role of natural gas flaring in meeting greenhouse gas mitigation targets. *Energy Strateg. Rev.* **20**, 156–162 (2018).

11. Soltanieh, M., Zohrabian, A., Gholipour, M. J. & Kalnay, E. A review of global gas flaring and venting and impact on the environment: Case study of Iran. *Int. J. Greenh. Gas Control* **49**, 488–509 (2016).

12. Buzcu-Guven, B. & Harriss, R. Extent, impacts and remedies of global gas flaring and venting. *Carbon Manag.* **3**, 95–108 (2012).

13. News & Broadcast - Global Gas Flaring Reduction. Available at: http://web.worldbank.org/archive/website01363/WEB/0__CO-48.HTM. (Accessed: 21st May 2019)

14. Wang, B., Albarracín-Suazo, S., Pagán-Torres, Y. & Nikolla, E. Advances in methane conversion processes. *Catal. Today* **285**, 147–158 (2017).

15. Boyano, A., Morosuk, T., Blanco-Marigorta, A. M. & Tsatsaronis, G. Conventional and advanced exergoenvironmental analysis of a steam methane reforming reactor for hydrogen production. *J. Clean. Prod.* **20**, 152–160 (2012).

16. Kaiwen, L., Bin, Y. & Tao, Z. Economic analysis of hydrogen production from steam reforming process: A literature review. *Energy Sources, Part B Econ. Planning, Policy* **13**, 109–115 (2018).

17. Aramouni, N. A. K., Touma, J. G., Tarboush, B. A., Zeaiter, J. & Ahmad, M. N. Catalyst design for dry reforming of methane: Analysis review. *Renewable and Sustainable Energy Reviews* **82**, 2570–2585 (2018).

18. Keller, G. E. & Bhasin, M. M. Synthesis of ethylene via oxidative coupling of methane. I. Determination of active catalysts. *J. Catal.* **73**, 9–19 (1982).

19. Lunsford, J. H. The catalytic oxidative coupling of methane.pdf. (1995).

20. Gambo, Y., Jalil, A. A., Triwahyono, S. & Abdulrasheed, A. A. Recent advances and future prospect in catalysts for oxidative coupling of methane to ethylene: A review. *J. Ind. Eng. Chem.* **59**, 218–229 (2018).

21. Cruellas, A., Bakker, J. J., van Sint Annaland, M., Medrano, J. A. & Gallucci, F. Techno-economic analysis of oxidative coupling of methane: Current state of the art and future perspectives. *Energy Convers. Manag.* **198**, 111789 (2019).

22. Linsheng, W. *et al.* Dehydrogenation and aromatization of methane under non oxidizing conditions. - *Catal. Lett.* **21**, 35–41 (1993).

23. Dumesic, J. A. The Microkinetics of heterogeneous catalysis. *ACS Prof. Ref. B.* **40**, xii, 315 p. (1993).

24. Xu, Y., Liu, S., Guo, X., Wang, L. & Xie, M. Methane activation without using oxidants over Mo/HZSM-5 zeolite catalysts. *Catal. Letters* **30**, 135–149 (1994).

25. Chen, L. Dehydro-oligomerization of methane to ethylene and aromatics over molybdenum/HZSM-5 catalyst. *Journal of Catalysis* **157**, 190–200 (1995).

26. Solymosi, F., Erdöhelyi, A. & Szöke, A. Dehydrogenation of methane on supported molybdenum oxides. Formation of benzene from methane. *Catal. Letters* **32**, 43–53 (1995).

27. Karakaya, C. & Kee, R. J. Progress in the direct catalytic conversion of methane to fuels and chemicals. *Prog. Energy Combust. Sci.* **55**, 60–97 (2016).

28. Moghimpour Bijani, P., Sohrabi, M. & Sahebdelfar, S. Thermodynamic analysis of nonoxidative dehydroaromatization of methane. *Chem. Eng. Technol.* **35**, 1825–1832 (2012).

29. Weckhuysen, B. M., Wang, D., Rosynek, M. P. & Lunsford, J. H. Conversion of methane to benzene over transition metal ion ZSM-5 zeolites: I. Catalytic characterization. *J. Catal.* **175**, 338–346 (1998).

30. Miodrag Belosevic, M. G. E. D. Z. S. J. R. B. Zn-HZSM-5 Catalysts for Methane Dehydroaromatization. *Environ. Sci. Technol.* **33**, 482–489 (2014).

31. Mir, R. A., Sharma, P. & Pandey, O. P. Thermal and structural studies of carbon coated Mo 2 C synthesized via in-situ single step reduction-carburization. *Sci. Rep.* **7**, 1–12 (2017).

32. Zhang, C. *et al.* Aromatization of methane in the absence of oxygen over Mo-based catalysts supported on different types of zeolites. *Catal. Letters* **56**, 207–213 (1998).

33. Liu, S., Wang, L., Ohnishi, R. & Ichikawa, M. Bifunctional catalysis of Mo/HZSM-5 in the dehydroaromatization of methane to benzene and naphthalene XAFS/TG/DTA/MASS/FTIR characterization and supporting effects. *J. Catal.* **181**, 175–188 (1999).

34. Solymosi, F., Cserényi, J., Szöke, A., Bánsági, T. & Oszkó, A. Aromatization of methane over supported and unsupported Mo-based catalysts. *J. Catal.* **165**, 150–161

(1997).

35. Olson, D. H., Kokotailo, G. T., Lawton, S. L. & Meier, W. M. Crystal structure and structure-related properties of ZSM-5. *J. Phys. Chem.* **85**, 2238–2243 (1981).

36. The International Centre for Diffraction Data - ICDD. Available at: http://www.icdd.com/. (Accessed: 16th June 2019)

37. Mas, H. Solid state 13 C NMR studies of methane dehydroaromatization reaction on Mo / HZSM-5 and W / HZSM-5 catalysts. *Society* 3046–3047 (2002).

38. Zhang, J.-Z., Long, M. a. & Howe, R. F. Molybdenum ZSM-5 zeolite catalysts for the conversion of methane to benzene. *Catal. Today* **44**, 293–300 (1998).

39. Liu, S., Wang, L. & Ohnishi, R. Bifunctional Catalysis of Mo / HZSM-5 in the Dehydroaromatization of Methane with CO / CO2 to Benzene and Naphthalene 1 , 2. *J. Catal.* 175–188 (1999).

40. Sun, C., Yao, S., Shen, W. & Lin, L. Highly dispersed molybdenum oxide supported on hzsm-5 for methane dehydroaromatization. *Catal. Letters* **122**, 84–90 (2008).

41. Chithambararaj, A., Bhagya Mathi, D., Rajeswari Yogamalar, N. & Chandra Bose, A. Structural evolution and phase transition of [NH4]6Mo7O24.4H2O to 2D layered MoO3-x. *Mater. Res. Express* **2**, 055004 (2015).

42. Wienold, J., Jentoft, R. E. & Ressler, T. Structural investigation of the thermal decomposition of ammonium heptamolybdate by in situ XAFS and XRD. *Eur. J. Inorg. Chem.* 1058–1071 (2003). doi:10.1002/ejic.200390138

43. Campbell, S. ., Bibby, D. ., Coddington, J. . & Howe, R. . Dealumination of HZSM-5 Zeolites. *J. Catal.* **161**, 350–358 (1996).

44. Matsumoto, Y. & Shimanouchi, R. Synthesis of Al2(MoO4)3 by Two Distinct Processes, Hydrothermal Reaction and Solid-State Reaction. *Procedia Eng.* **148**, 158–162 (2016).

45. Vollmer, I. *et al.* On the dynamic nature of Mo sites for methane dehydroaromatization. *Chem. Sci.* **9**, 4801–4807 (2018).

46. Wang, L., Xu, Y., Wong, S. T., Cui, W. & Guo, X. Activity and stability enhancement of Mo/HZSM-5-based catalysts for methane non-oxidative transformation to aromatics and C2 hydrocarbons: Effect of additives and pretreatment conditions. *Appl. Catal. A Gen.* **152**, 173–182 (1997).

47. Shu, J., Adnot, A. & Grandjean, B. P. a. Bifunctional Behavior of Mo/HZSM-5 Catalysts in Methane Aromatization. *Ind. Eng. Chem. Res.* **38**, 3860–3867 (1999).

48. Solymosi, F., Cserényi, J., Szöke, A., Bánsági, T. & Oszkó, A. Aromatization of methane over supported and unsupported Mo-based catalysts. *J. Catal.* **165**, 150–161 (1997).

49. Solymosi, F., Szöke, A. & Cserényi, J. Conversion of methane to benzene over Mo2C and Mo2C/ZSM-5 catalysts. *Catal. Letters* **39**, 157–161 (1996).

50. Dang, J., Zhang, G. H. & Chou, K. C. Phase transitions and morphology evolutions during hydrogen reduction of MoO3 to MoO2. *High Temp. Mater. Process.* **33**, 305–312 (2014).

51. Enneti, R. K. & Wolfe, T. A. Agglomeration during reduction of MoO 3. *Int. J. Refract. Met. Hard Mater.* **31**, 47–50 (2012).

52. Ma, D., Shu, Y., Cheng, M., Xu, Y. & Bao, X. On the induction period of methane aromatization over Mo-based catalysts. *J. Catal.* **194**, 105–114 (2000).

53. Schuurman, Y., Decamp, T., Pantazidis, A., Xu, Y.-D. & Mirodatos, C. Transient kinetics of methane dehydrogenation and aromatisation: experiments and modelling. 351–360 (2007). doi:10.1016/s0167-2991(97)80422-3

54. Honda, K., Yoshida, T. & Zhang, Z. Methane dehydroaromatization over Mo / HZSM-5 in periodic CH 4 – H 2 switching operation mode. **4**, 21–26 (2003).

55. Wang, D., Lunsford, J. H. & Rosynek, M. P. Characterization of a Mo/ZSM-5 Catalyst for the Conversion of Methane to Benzene. *J. Catal.* **169**, 347–358 (1997).

56. Wang, D., Lunsford, J. H. & Rosynek, M. P. Catalytic conversion of methane to benzene over M o / Z S M - 5. *Top. Catal.* **3**, 289–297 (1996).

57. Xu, Y., Liu, S., Wang, L. & Xie, M. Methane activation without using oxidants over Mo / HZSM-5 zeolite catalysts. *Science (80-.).* **30**, 135–149 (1995).

58. Solymosi, F., Bugyi, L., Osz, A. & Hor, I. Generation and Reactions of CH 2 and C 2 H 5 Species on Mo 2 C/Mo(111) Surface. *J. Catal.* **185**, 160–169 (1999).

59. Solymosi, F., Bugyi, L. & Oszkó, A. Formation and reactions of CH3 species over Mo2C/Mo(111) surface. *Catal. Letters* **57**, 103–107 (1999).

60. Zhou, D., Zuo, S. & Xing, S. Methane dehydrogenation and coupling to ethylene over

a Mo/HZSM-5 catalyst: A density functional theory study. *J. Phys. Chem. C* **116**, 4060–4070 (2012).

61. Karakaya, C., Zhu, H. & Kee, R. J. Kinetic modeling of methane dehydroaromatization chemistry on Mo/Zeolite catalysts in packed-bed reactors. *Chem. Eng. Sci.* **123**, 474–486 (2015).

62. Hansen, A. G., Well, W. J. M. & Stoltze, P. Microkinetic modeling as a tool in catalyst discovery. *Top. Catal.* **45**, 219–222 (2007).

63. Iliuta, M. C., Iliuta, I., Grandjean, B. P. A. & Larachi, F. Kinetics of Methane Nonoxidative Aromatization over Ru−Mo/HZSM-5 Catalyst. *Ind. Eng. Chem. Res.* **42**, 3203–3209 (2003).

64. Li, Z., Kjø, C., Morejudo, S. H. & Haugsrud, R. Numerical Simulations of Methane Aromatization with and without a Ceramic Hydrogen Separation Membrane. *Proc. 2012 COMSOL* (2012).

65. Yao, B., Chen, J., Liu, D. & Fang, D. Intrinsic kinetics of methane aromatization under non-oxidative conditions over modified Mo/HZSM-5 catalysts. *J. Nat. Gas Chem.* **17**, 64–68 (2008).

66. Zhu, Y., Al-ebbinni, N., Henney, R., Yi, C. & Barat, R. Extension to multiple temperatures of a three-reaction global kinetic model for methane dehydroaromatization. *Chem. Eng. Sci.* **177**, 132–138 (2018).

67. Bhan, A. *et al.* Microkinetic modeling of propane aromatization over HZSM-5. *J. Catal.* **235**, 35–51 (2005).

68. Dean, A. Detailed kinetic modeling of autocatalysis in methane pyrolysis. *J. Phys. Chem.* **145**, 16–37 (1990).

69. Lukyanov, D. B., Gnep, N. S. & Guisnet, M. R. Kinetic Modeling of Ethene and Propene Aromatization over HZSM-5 and GaHZSM-5. *Ind. Eng. Chem. Res.* **33**, 223–234 (1994).

70. Narbeshuber, T. F., Vinek, H. & Lercher, J. A. Monomolecular Conversion of Light Alkanes over H-ZSM-5. *J. Catal.* **157**, 388–395 (1995).

71. Guisnet, M. & Gnep, N. S. Mechanism of short-chain alkane transformation over protonic zeolites. Alkylation, disproportionation and aromatization. *Appl. Catal. A Gen.* **146**, 33–64 (1996).

72. Wang, H. & Frenklach, M. A detailed kinetic modeling study of aromatics formation in laminar premixed acetylene and ethylene flames. *Combust. Flame* **110**, 173–221 (1997).

73. Froment, G. Kinetic modeling of acid-catalyzed oil refining processes. *Catal. Today* **52**, 153–163 (1999).

74. Buchanan, J. S., Santiesteban, J. G. & Haag, W. O. Mechanistic considerations in acid-catalyzed cracking of olefins. *J. Catal.* **158**, 279–287 (1996).

75. Yaluris, G. Isobutane Cracking Over Y-Zeolites I. Development of A Kinetic Model. *Journal of Catalysis* **153**, 54–64 (1995).

76. Liang, T., Toghiani, H. & Xiang, Y. Transient kinetic study of ethane and ethylene aromatization over zinc exchanged HZSM-5 catalyst. *Ind. Eng. Chem. Res.*

acs.iecr.8b03735 (2018). doi:10.1021/acs.iecr.8b03735

77. Kazansky, V. B., Senchenya, I. N., Frash, M. & van Santen, R. A. A quantum-chemical study of adsorbed nonclassical carbonium ions as active intermediates in catalytic transformations of paraffins. I. Protolytic cracking of ethane on high silica zeolites. *Catal. Letters* **27**, 345–354 (1994).

78. Joshi, Y. V, Bhan, A. & Thomson, K. T. DFT-Based Reaction Pathway Analysis of Hexadiene Cyclization via Carbenium Ion Intermediates : Mechanistic Study of Light Alkane Aromatization Catalysis. 971–980 (2004). doi:10.1021/jp036205m

79. Broclawik, E. *et al.* Density functional theory calculations of the reaction pathway for methane activation on a gallium site in metal exchanged ZSM-5. *J. Chem. Phys.* **103**, 2102–2108 (1995).

80. Xing, S., Zhou, D., Cao, L. & Li, X. Density functional theory study on structure of molybdenum carbide and catalytic mechanism for methane activation over ZSM-5 zeolite. *Chinese J. Catal.* **31**, 415–422 (2010).

81. Huang, Y., Dong, X., Li, M. & Yu, Y. A density functional theory study on ethylene formation and conversion over P modified ZSM-5. *Catal. Sci. Technol.* **5**, 1093–1105 (2015).

82. Wong, K. S., Thybaut, J. W., Tangstad, E., Stöcker, M. W. & Marin, G. B. Methane aromatisation based upon elementary steps: Kinetic and catalyst descriptors. *Microporous Mesoporous Mater.* **164**, 302–312 (2012).

83. Karakaya, C., Morejudo, S. H., Zhu, H. & Kee, R. J. Catalytic Chemistry for Methane

Dehydroaromatization (MDA) on a Bifunctional Mo/HZSM-5 Catalyst in a Packed Bed. *Ind. Eng. Chem. Res.* **55**, 9895–9906 (2016).

84. Gerceker, D. *et al.* Methane Conversion to Ethylene and Aromatics on PtSn Catalysts. *ACS Catal.* acscatal.6b02724 (2017). doi:10.1021/acscatal.6b02724

85. Weckhuysen, B. M., Rosynek, M. P. & Lunsford, J. H. Characterization of surface carbon formed during the conversion of methane to benzene over Mo / H-ZSM-5 catalysts. *Science (80-.).* **52**, 31–36 (1998).

86. Ma, D. *et al.* Carbonaceous Deposition on Mo/HMCM-22 Catalysts for Methane Aromatization: A TP Technique Investigation. *J. Catal.* **208**, 260–269 (2002).

87. Liu, B. S., Jiang, L., Sun, H. & Au, C. T. XPS, XAES, and TG/DTA characterization of deposited carbon in methane dehydroaromatization over Ga-Mo/ZSM-5 catalyst. *Appl. Surf. Sci.* **253**, 5092–5100 (2007).

88. He, S. *et al.* Characterization of coke deposited on spent catalysts for long-chain-paraffin dehydrogenation. *Chem. Eng. J.* **163**, 389–394 (2010).

89. Jiang, H., Wang, L. S., Cui, W. & Xu, Y. D. Study on the induction period of methane aromatization over Mo/HZSM-5: partial reduction of Mo species and formation of carbonaceous deposit. *Catal. Letters* **57**, 95–102 (1999).

90. Burns, S., Gallagher, J. G., Hargreaves, J. S. J. & Harris, P. J. F. Direct observation of carbon nanotube formation in Pd/H-ZSM-5 and MoO 3/H-ZSM-5 based methane activation catalysts. *Catal. Letters* **116**, 122–127 (2007).

91. Tempelman, C. H. L. & Hensen, E. J. M. On the deactivation of Mo/HZSM-5 in the

methane dehydroaromatization reaction. *Appl. Catal. B Environ.* **176**–**177**, 731–739 (2015).

92. Hu, Z. J. & Hüttinger, K. J. Mechanisms of carbon deposition—a kinetic approach. *Carbon N. Y.* **40**, 624–628 (2002).

93. Querini, C. a. & Fung, S. C. Temperature-programmed oxidation technique: kinetics of coke-O2 reaction on supported metal catalysts. *Appl. Catal. A Gen.* **117**, 53–74 (1994).

94. Liu, H., Li, T., Tian, B. & Xu, Y. Study of the carbonaceous deposits formed on a Mo/HZSM-5 catalyst in methane dehydro-aromatization by using TG and temperature-programmed techniques. *Appl. Catal. A Gen.* **213**, 103–112 (2001).

95. Shu, Y., Ohnishi, R. & Ichikawa, M. A Highly Selective and Coking-Resistant Catalyst for Methane Dehydrocondensation. *Chem. Lett.* **31**, 418–418 (2002).

96. Lu, Y. *et al.* A high coking-resistance catalyst for methane aromatization. *Chem. Commun. (Camb).* 2048–2049 (2001). doi:10.1039/b105853n

97. Dong, G. L. & Huttinger, K. J. Consideration of reaction mechanisms leading to pyrolytic carbon of different textures. *Carbon N. Y.* **40**, 2515–2528 (2002).

98. Van Speybroeck, V., Reyniers, M. F., Marin, G. B. & Waroquier, M. Modeling elementary reactions in coke formation from first principles. *ACS Div. Fuel Chem. Prepr.* **49**, 781–784 (2004).

99. Song, Y., Xu, Y., Suzuki, Y., Nakagome, H. & Zhang, Z.-G. A clue to exploration of the pathway of coke formation on Mo/HZSM-5 catalyst in the non-oxidative methane

dehydroaromatization at 1073K. *Appl. Catal. A Gen.* **482**, 387–396 (2014).

100. Song, Y. *et al.* The distribution of coke formed over a multilayer Mo/HZSM-5 fixed bed in H2 co-fed methane aromatization at 1073K: Exploration of the coking pathway. *J. Catal.* **330**, 261–272 (2015).

101. Kopinke, F. D., Zimmermann, G., Reyniers, G. C. & Froment, G. F. Relative Rates of Coke Formation from Hydrocarbons in Steam Cracking of Naphtha. 2. Paraffins, Naphthenes, Mono-, Di-, and Cycloolefins, and Acetylenes. *Ind. Eng. Chem. Res.* **32**, 56–61 (1993).

102. Spivey, J. J. & Hutchings, G. Catalytic aromatization of methane. *Chem. Soc. Rev.* **43**, 792–803 (2014).

103. Brunauer, S., Emmett, P. H. & Teller, E. Adsorption of gases in multimolecular layers. *J. Am. Chem. Soc.* **60**, 309–319 (1938).

104. Barrett, E. P., Joyner, L. G. & Halenda, P. P. The determination of pore volume and area distributions in porous substances. I. computations from nitrogen isotherms. *J. Am. Chem. Soc.* **73**, 373–380 (1951).

105. Radwan, A. M., Kyotani, T. & Tomita, A. Characterization of coke deposited from cracking of benzene over USY zeolite catalyst. *Appl. Catal. A Gen.* **192**, 43–50 (2000).

106. Kikuchi, S., Kojima, R., Ma, H., Bai, J. & Ichikawa, M. Study on Mo/HZSM-5 catalysts modified by bulky aminoalkyl-substituted silyl compounds for the selective methane-to-benzene (MTB) reaction. *J. Catal.* **242**, 349–356 (2006).

107. Emeis, C. A. Determination of integrated molar extinction coefficients for infrared

absorption bands of pyridine adsorbed on solid acid catalysts. *J. Catal.* **141**, 347–354 (1993).

108. Ferrari, A. C., Rodil, S. E. & Robertson, J. Resonant Raman spectra of amorphous carbon nitrides: The G peak dispersion. *Diam. Relat. Mater.* **12**, 905–910 (2003).

109. Pradhan, A., Wu, J., Jong, S., Tsai, T. & Liu, S. An ex situ methodology for characterization of coke by TGA and 13 C CP-MAS NMR spectroscopy. *Appl. Catal. A …* **165**, 489–497 (1997).

110. Choudhary, V. R., Devadas, P., Banerjee, S. & Kinage, A. K. Aromatization of dilute ethylene over Ga-modified ZSM-5 type zeolite catalysts. *Microporous Mesoporous Mater.* **47**, 253–267 (2001).

111. The irreversible formation of methane in the system ethane-ethylene-hydrogen. *Proc. R. Soc. London. Ser. A. Math. Phys. Sci.* **218**, 450–464 (1953).

112. Fila, V., Bernauer, M., Bernauer, B. & Sobalik, Z. Effect of addition of a second metal in Mo/ZSM-5 catalyst for methane aromatization reaction under elevated pressures. *Catal. Today* **256**, 269–275 (2015).

113. Tempelman, C. H. L., Zhu, X. & Hensen, E. J. M. Activation of Mo/HZSM-5 for methane aromatization. *Cuihua Xuebao/Chinese J. Catal.* **36**, 829–837 (2015).

114. Kosinov, N. *et al.* Structure and Evolution of Confined Carbon Species during Methane Dehydroaromatization over Mo/ZSM-5. *ACS Catal.* **8**, 8459–8467 (2018).

115. Martínez, A. & Peris, E. Non-oxidative methane dehydroaromatization on Mo/HZSM-5 catalysts: Tuning the acidic and catalytic properties through partial exchange of

zeolite protons with alkali and alkaline-earth cations. *Appl. Catal. A Gen.* **515**, 32–44 (2016).

116. Sedel'nikova, O. V., Stepanov, A. A., Zaikovskii, V. I., Korobitsyna, L. L. & Vosmerikov, A. V. Preparation method effect on the physicochemical and catalytic properties of a methane dehydroaromatization catalyst. *Kinet. Catal.* **58**, 51–57 (2017).

117. Manoj, B. & Kunjomana, A. G. Study of stacking structure of amorphous carbon by X-ray diffraction technique. *Int. J. Electrochem. Sci.* **7**, 3127–3134 (2012).

118. Gotoh, Y. Interlayer structure changes of graphite after hydrogen ion irradiation. *J. Nucl. Mater.* **248**, 46–51 (1997).

119. Börrnert, F. *et al.* Amorphous carbon under 80 kV electron irradiation: A means to make or break graphene. *Adv. Mater.* **24**, 5630–5635 (2012).

120. Schwan, J., Ulrich, S., Batori, V., Ehrhardt, H. & Silva, S. R. P. Raman spectroscopy on amorphous carbon films. *J. Appl. Phys.* **80**, 440 (1996).

121. Li, X., Hayashi, J. ichiro & Li, C. Z. FT-Raman spectroscopic study of the evolution of char structure during the pyrolysis of a Victorian brown coal. *Fuel* **85**, 1700–1707 (2006).

122. Nemanich, R. J. & Solin, S. A. First- and second-order Raman scattering from finite-size crystals of graphite. *Phys. Rev. B* **20**, 392–401 (1979).

123. Singh, B., Murad, L., Laffir, F., Dickinson, C. & Dempsey, E. Pt based nanocomposites (mono/bi/tri-metallic) decorated using different carbon supports for

methanol electro-oxidation in acidic and basic media. *Nanoscale* **3**, 3334–3349 (2011).

124. A. C. Ferrari and J. Robertson. Resonant Raman spectroscopy of disordered, amorphous, and diamondlike carbon. *Phys. Rev. B* **64**, 138–139 (2001).

125. Lin-Vien, D., Colthup, N. B., Fateley, W. G. & Grasselli, J. G. (Professor). *The Handbook of infrared and raman characteristic frequencies of organic molecules*. (Academic Press, 1991).

126. Ferrari, A. C. & Robertson, J. Interpretation of Raman spectra of disordered and amorphous carbon. *Phys. Rev. B* **61**, 14095–14107 (2000).

127. Li, T. *et al.* Effects of gasification temperature and atmosphere on char structural evolution and AAEM retention during the gasification of Loy Yang brown coal. *Fuel Process. Technol.* **159**, 48–54 (2017).

128. Konno, H. X-ray Photoelectron Spectroscopy. in *Materials Science and Engineering of Carbon* 153–171 (Elsevier, 2016). doi:10.1016/B978-0-12-805256-3.00008-8

129. Barlow, A. J. *et al.* Chemically specific identification of carbon in XPS imaging using Multivariate Auger Feature Imaging (MAFI). *Carbon N. Y.* **107**, 190–197 (2016).

130. Kim, K. C., Yoon, T. U. & Bae, Y. S. Applicability of using CO2 adsorption isotherms to determine BET surface areas of microporous materials. *Microporous Mesoporous Mater.* **224**, 294–301 (2016).

131. Ch. Baerlocher and L.B. McCusker. Database of Zeolite Structures. Available at: http://www.iza-structure.org/databases/. (Accessed: 7th June 2019)

132. Hoff, T. C., Thilakaratne, R., Gardner, D. W., Brown, R. C. & Tessonnier, J. P. Thermal Stability of Aluminum-Rich ZSM-5 Zeolites and Consequences on Aromatization Reactions. *J. Phys. Chem. C* **120**, 20103–20113 (2016).

133. Wang, L. *et al.* Dehydrogenation and aromatization of methane under non-oxidizing conditions. *Catal. Letters* **21**, 35–41 (1993).

134. Borry, R. W., Kim, Y. H., Huffsmith, A., Reimer, J. a. & Iglesia, E. Structure and Density of Mo and Acid Sites in Mo-Exchanged H-ZSM5 Catalysts for Nonoxidative Methane Conversion. *J. Phys. Chem. B* **103**, 5787–5796 (1999).

135. Technical information. Available at: http://archive.synchrotron.org.au/aussyncbeamlines/powder-diffraction/technical-information. (Accessed: 24th July 2019)

136. CMPR. Available at: https://subversion.xray.aps.anl.gov/CMPR/trunk/doc/cmprdoc.html. (Accessed: 16th June 2019)

137. Belsky, A., Hellenbrandt, M., Karen, V. L., Luksch, P. & IUCr. New developments in the Inorganic Crystal Structure Database (ICSD): accessibility in support of materials research and design. *Acta Crystallogr. Sect. B Struct. Sci.* **58**, 364–369 (2002).

138. Ha, V. T. T., Tiep, L. V., Meriaudeau, P. & Naccache, C. Aromatization of methane over zeolite supported molybdenum: Active sites and reaction mechanism. *J. Mol. Catal. A Chem.* **181**, 283–290 (2002).

139. Ramasubramanian, V., Ramsurn, H. & Price, G. L. Methane dehydroaromatization –

A study on hydrogen use for catalyst reduction, role of molybdenum, the nature of catalyst support and significance of Bronsted acid sites. *J. Energy Chem.* **34**, 20–32 (2019).

140. Kosinov, N. *et al.* Methane Dehydroaromatization by Mo/HZSM-5: Mono- or Bifunctional Catalysis? *ACS Catal.* **7**, 520–529 (2017).

141. Woolery, G. L., Kuehl, G. H., Timken, H. C., Chester, A. W. & Vartuli, J. C. On the nature of framework Brønsted and Lewis acid sites in ZSM-5. *Zeolites* **19**, 288–296 (1997).

142. Kosinov, N., Coumans, F. J. A. G., Uslamin, E., Kapteijn, F. & Hensen, E. J. M. Selective Coke Combustion by Oxygen Pulsing During Mo/ZSM-5-Catalyzed Methane Dehydroaromatization. *Angew. Chemie - Int. Ed.* **55**, 15086–15090 (2016).

143. Tan, P. L., Wong, K. W., Au, C. T. & Lai, S. Y. Effects of Co-fed O2 and CO2 on the deactivation of Mo/HZSM-5 for methane aromatization. *Appl. Catal. A Gen.* **253**, 305–316 (2003).

144. Weckhuysen, B. M., Wang, D., Rosynek, M. P. & Lunsford, J. H. Conversion of Methane to Benzene over Transition Metal Ion ZSM-5 Zeolites. *J. Catal.* **175**, 347–351 (1998).

145. Li, Y. *et al.* Enhanced performance of methane dehydro-aromatization on Mo-based HZSM-5 zeolite pretreated by NH4F. *Catal. Commun.* **8**, 1567–1572 (2007).

146. Óvári, L., Kiss, J., Farkas, A. P. & Solymosi, F. Surface and subsurface oxidation of Mo2C/Mo(100): Low-energy ion-scattering, auger electron, angle-resolved X-ray

photoelectron, and mass spectroscopy studies. *J. Phys. Chem. B* **109**, 4638–4645 (2005).

147. Likith, S. R. J. *et al.* Thermodynamic Stability of Molybdenum Oxycarbides Formed from Orthorhombic Mo2C in Oxygen-Rich Environments. *J. Phys. Chem. C* **122**, 1223–1233 (2018).

148. Hu, J. *et al.* Effect of the particle size of MoO3 on the catalytic activity of Mo/ZSM-5 in methane non-oxidative aromatization. *New J. Chem.* **39**, 5459–5469 (2015).

149. The International Centre for Diffraction Data - ICDD. Available at: http://www.icdd.com/. (Accessed: 25th July 2019)

150. Cho, S. Y., Kim, J. Y., Kwon, O., Kim, J. & Jung, H. T. Molybdenum carbide chemical sensors with ultrahigh signal-to-noise ratios and ambient stability. *J. Mater. Chem. A* **6**, 23408–23416 (2018).

151. Lili He,a Yu Qin,a Hui Lou, a and P. C. High dispersed molybdenum carbide nanoparticles supported on activated carbon as an efficient catalyst for the hydrodeoxygenation of vanillin. *R. Soc. Chem.* **5**, 43141–43147 (2015).

152. Hyeon, T., Fang, M. & Suslick, K. S. Nanostructured molybdenum carbide: Sonochemical synthesis and catalytic properties. *J. Am. Chem. Soc.* **118**, 5492–5493 (1996).

153. Tang, P., Zhu, Q., Wu, Z. & Ma, D. Methane activation: the past and future. *Energy Environ. Sci.* **7**, 2580 (2014).

154. D.M Bibby, N. B. Milestone, J E. Patterson, L. P. A. Coke formation in zeolite ZSM-

5. *J. Catal.* **97**, 493–502 (1986).

155. Urata, K., Furukawa, S. & Komatsu, T. Location of coke on H-ZSM-5 zeolite formed in the cracking of n-hexane. *Appl. Catal. A Gen.* **475**, 335–340 (2014).

156. Liu, B. *et al.* Microwaves effectively examine the extent and type of coking over acid zeolite catalysts. *Nat. Commun.* **8**, 1–7 (2017).

157. Li, C. & Stair, P. C. Coke formation in zeolites studied by a new technique : ultraviolet resonance Raman spectroscopy. **105**, 599–606 (1997).

158. Weckhuysen, B. M., Rosynek, M. P. & Lunsford, J. H. Characterization of surface carbon formed during the conversion of methane to benzene over Mo / H-ZSM-5 catalysts. *Catal. Letters* **52**, 31–36 (1998).

159. Pérez-Uresti, S., Adrián-Mendiola, J., El-Halwagi, M. & Jiménez-Gutiérrez, A. Techno-Economic Assessment of Benzene Production from Shale Gas. *Processes* **5**, 33 (2017).

160. Ding, W., Li, S., Meitzner, G. D. & Iglesia, E. Methane Conversion to Aromatics on Mo/H-ZSM5: Structure of Molybdenum Species in Working Catalysts. *J. Phys. Chem. B* **105**, 506–513 (2001).

161. Kosinov, N. *et al.* Stable Mo/HZSM-5 methane dehydroaromatization catalysts optimized for high-temperature calcination-regeneration. *J. Catal.* **346**, 125–133 (2017).

162. Shu, Y., Ohnishi, R. & Ichikawa, M. Pressurized dehydrocondensation of methane toward benzene and naphthalene on Mo/HZSM-5 catalyst: Optimization of reaction

parameters and promotion by CO2addition. *J. Catal.* **206**, 134–142 (2002).

163. Moulijn, J. A., Van Diepen, A. E. & Kapteijn, F. Catalyst deactivation: Is it predictable? What to do? *Appl. Catal. A Gen.* **212**, 3–16 (2001).

164. Kuvshinov, G. G., Mogilnykh, Y. I. & Kuvshinov, D. G. Kinetics of carbon formation from CH4–H2 mixtures over a nickel containing catalyst. *Catal. Today* **42**, 357–360 (1998).

165. Dong, X., Song, Y. & Lin, W. A new way to enhance the coke-resistance of Mo/HZSM-5 catalyst for methane dehydroaromatization. *Catal. Commun.* **8**, 539–542 (2007).

166. Tan, P. L., Leung, Y. L., Lai, S. Y. & Au, C. T. The effect of calcination temperature on the catalytic performance of 2 wt .% Mo / HZSM-5 in methane aromatization. *Appl. Catal. A Gen.* **228**, 115–125 (2002).

167. Ha, V. T. T., Sarioğlan, A., Erdem-Şenatalar, A. & Taârit, Y. Ben. An EPR and NMR study on Mo/HZSM-5 catalysts for the aromatization of methane: Investigation of the location of the pentavalent molybdenum. *J. Mol. Catal. A Chem.* **378**, 279–284 (2013).

168. Xu, Y., Shu, Y., Liu, S., Huang, J. & Guo, X. Interaction between ammonium heptamolybdate and NH4ZSM-5 zeolite: the location of Mo species and the acidity of Mo/HZSM-5. *Catal. Letters* **35**, 233–243 (1995).

169. Welcome to PDViPeR's documentation! — PDViPeR 1.2 documentation. Available at: https://pdviper.readthedocs.io/en/latest/#pdviper-url. (Accessed: 16th June 2019)

170. Holder, C. F. & Schaak, R. E. Tutorial on Powder X-ray Diffraction for Characterizing

Nanoscale Materials. *ACS Nano* **13**, 7359–7365 (2019).

171. Inoue, M. & Hirasawa, I. The relationship between crystal morphology and XRD peak intensity on CaSO4·2H2O. *J. Cryst. Growth* **380**, 169–175 (2013).

172. Esenli, F. & Kumbasar, I. X-ray diffraction intensity ratios I(111)/I(311) of natural heulandites and clinoptilolites. *Clays Clay Miner.* **46**, 679–686 (1998).

173. Aritani, H. *et al.* Mo LIII-edge XANES study of catalytically active Mo species on silica-alumina supports for methane dehydroaromatization. *Chem. Lett.* **35**, 416–417 (2006).

174. Pérez-Page, M. *et al.* Gas adsorption properties of ZSM-5 zeolites heated to extreme temperatures. *Ceram. Int.* **42**, 15423–15431 (2016).

175. Oshikawa, K., Nagai, M. & Omi, S. Characterization of molybdenum carbides for methane reforming by TPR, XRD, and XPS. *J. Phys. Chem. B* **105**, 9124–9131 (2001).

176. Kosinov, N. *et al.* Stable Mo/HZSM-5 methane dehydroaromatization catalysts optimized for high-temperature calcination-regeneration. *J. Catal.* **346**, 125–133 (2017).

Chapter 9 Appendices

9.1 Appendix 1

9.1.1 The formulae used for calculation of reaction conversion and product selectivity are given below.

The overall conversion of methane was calculated based on [65,66,76]:

$$X_{CH_4} = \frac{(F_{CH_{4,i}} - F_{CH_{4,o}})}{F_{CH_{4,i}}} * 100\ \% \qquad [A.1.9\text{-}1]$$

The carbon-based selectivity (with respect to methane) of each product was calculated based on [65,66,76]:

$$S_i = \frac{F_{i,o}\ n_i}{(F_{CH_{4,i}} - F_{CH_{4,o}})} * 100\ \% \qquad [A.1.9\text{-}2]$$

The aromatic selectivity of benzene was calculated based on [65,66,76]:

$$S_{aro,benzene} = \frac{y_{benzene}}{\sum y_i} * 100\ \% \qquad [A.1.9\text{-}3]$$

Where, $F_{CH_{4,i}}$ = inlet flowrate of methane, $F_{CH_{4,o}}$ = outlet flowrate of methane, $F_{i,o}$ = outlet flowrate of component 'i', n_i = no. of carbon number in component 'i'.

1